INSTRUCTION MANUAL

EASYFLUX DL CR3000OP
For CR3000 and Open-Path Eddy-Covariance System
Revision: 3/18

WARRANTY AND ASSISTANCE

This equipment is warranted by CAMPBELL SCIENTIFIC (CANADA) CORP. ("CSC") to be free from defects in materials and workmanship under normal use and service for **twelve (12) months** from date of shipment unless specified otherwise. ***** **Batteries are not warranted.** ***** CSC's obligation under this warranty is limited to repairing or replacing (at CSC's option) defective products. The customer shall assume all costs of removing, reinstalling, and shipping defective products to CSC. CSC will return such products by surface carrier prepaid. This warranty shall not apply to any CSC products which have been subjected to modification, misuse, neglect, accidents of nature, or shipping damage. This warranty is in lieu of all other warranties, expressed or implied, including warranties of merchantability or fitness for a particular purpose. CSC is not liable for special, indirect, incidental, or consequential damages.

Products may not be returned without prior authorization. To obtain a Return Merchandise Authorization (RMA), contact CAMPBELL SCIENTIFIC (CANADA) CORP., at (780) 454-2505. An RMA number will be issued in order to facilitate Repair Personnel in identifying an instrument upon arrival. Please write this number clearly on the outside of the shipping container. Include description of symptoms and all pertinent details.

CAMPBELL SCIENTIFIC (CANADA) CORP. does not accept collect calls.

Non-warranty products returned for repair should be accompanied by a purchase order to cover repair costs.

CAMPBELL® SCIENTIFIC

Campbell Scientific (Canada) Corp.
14532 131 Avenue NW | Edmonton AB T5L 4X4
780.454.2505 | fax 780.454.2655 | campbellsci.ca

Assistance

Products may not be returned without prior authorization. The following contact information is for Canadian and international clients residing in countries served by Campbell Scientific (Canada) Corp. directly. Affiliate companies handle repairs for clients within their territories. Please visit *www.campbellsci.ca* to determine which Campbell Scientific company serves your country.

To obtain a Returned Materials Authorization (RMA), contact CAMPBELL SCIENTIFIC (CANADA) CORP., phone (780) 454-2505. After a measurement consultant determines the nature of the problem, an RMA number will be issued. Please write this number clearly on the outside of the shipping container. Campbell Scientific's shipping address is:

CAMPBELL SCIENTIFIC (CANADA) CORP.
RMA#_____
14532 131 Avenue NW
Edmonton, Alberta T5L 4X4
Canada

For all returns, the client must fill out a "Statement of Product Cleanliness and Decontamination" form and comply with the requirements specified in it. The form is available from our web site at *www.campbellsci.ca/repair*. A completed form must be either emailed to *repair@campbellsci.ca* or faxed to (780) 454-2655. Campbell Scientific (Canada) Corp. is unable to process any returns until we receive this form. If the form is not received within three days of product receipt or is incomplete, the product will be returned to the client at the client's expense. Campbell Scientific (Canada) Corp.f reserves the right to refuse service on products that were exposed to contaminants that may cause health or safety concerns for our employees.

Precautions

DANGER — MANY HAZARDS ARE ASSOCIATED WITH INSTALLING, USING, MAINTAINING, AND WORKING ON OR AROUND **TRIPODS, TOWERS, AND ANY ATTACHMENTS TO TRIPODS AND TOWERS SUCH AS SENSORS, CROSSARMS, ENCLOSURES, ANTENNAS, ETC**. FAILURE TO PROPERLY AND COMPLETELY ASSEMBLE, INSTALL, OPERATE, USE, AND MAINTAIN TRIPODS, TOWERS, AND ATTACHMENTS, AND FAILURE TO HEED WARNINGS, INCREASES THE RISK OF DEATH, ACCIDENT, SERIOUS INJURY, PROPERTY DAMAGE, AND PRODUCT FAILURE. TAKE ALL REASONABLE PRECAUTIONS TO AVOID THESE HAZARDS. CHECK WITH YOUR ORGANIZATION'S SAFETY COORDINATOR (OR POLICY) FOR PROCEDURES AND REQUIRED PROTECTIVE EQUIPMENT PRIOR TO PERFORMING ANY WORK.

Use tripods, towers, and attachments to tripods and towers only for purposes for which they are designed. Do not exceed design limits. Be familiar and comply with all instructions provided in product manuals. Manuals are available at www.campbellsci.ca or by telephoning (780) 454-2505 (Canada). You are responsible for conformance with governing codes and regulations, including safety regulations, and the integrity and location of structures or land to which towers, tripods, and any attachments are attached. Installation sites should be evaluated and approved by a qualified personnel (e.g. engineer). If questions or concerns arise regarding installation, use, or maintenance of tripods, towers, attachments, or electrical connections, consult with a licensed and qualified engineer or electrician.

General

- Prior to performing site or installation work, obtain required approvals and permits.
- Use only qualified personnel for installation, use, and maintenance of tripods and towers, and any attachments to tripods and towers. The use of licensed and qualified contractors is highly recommended.
- Read all applicable instructions carefully and understand procedures thoroughly before beginning work.
- Wear a **hardhat** and **eye protection**, and take **other appropriate safety precautions** while working on or around tripods and towers.
- **Do not climb** tripods or towers at any time, and prohibit climbing by other persons. Take reasonable precautions to secure tripod and tower sites from trespassers.
- Use only manufacturer recommended parts, materials, and tools.

Utility and Electrical

- **You can be killed** or sustain serious bodily injury if the tripod, tower, or attachments you are installing, constructing, using, or maintaining, or a tool, stake, or anchor, come in **contact with overhead or underground utility lines**.
- Maintain a distance of at least one-and-one-half times structure height, 6 meters (20 feet), or the distance required by applicable law, **whichever is greater**, between overhead utility lines and the structure (tripod, tower, attachments, or tools).
- Prior to performing site or installation work, inform all utility companies and have all underground utilities marked.
- Comply with all electrical codes. Electrical equipment and related grounding devices should be installed by a licensed and qualified electrician.

Elevated Work and Weather

- Exercise extreme caution when performing elevated work.
- Use appropriate equipment and safety practices.
- During installation and maintenance, keep tower and tripod sites clear of un-trained or non-essential personnel. Take precautions to prevent elevated tools and objects from dropping.
- Do not perform any work in inclement weather, including wind, rain, snow, lightning, etc.

Maintenance

- Periodically (at least yearly) check for wear and damage, including corrosion, stress cracks, frayed cables, loose cable clamps, cable tightness, etc. and take necessary corrective actions.
- Periodically (at least yearly) check electrical ground connections.

WHILE EVERY ATTEMPT IS MADE TO EMBODY THE HIGHEST DEGREE OF SAFETY IN ALL CAMPBELL SCIENTIFIC PRODUCTS, THE CLIENT ASSUMES ALL RISK FROM ANY INJURY RESULTING FROM IMPROPER INSTALLATION, USE, OR MAINTENANCE OF TRIPODS, TOWERS, OR ATTACHMENTS TO TRIPODS AND TOWERS SUCH AS SENSORS, CROSSARMS, ENCLOSURES, ANTENNAS, ETC.

PLEASE READ FIRST

About this manual

Please note that this manual was originally produced by Campbell Scientific Inc. (CSI) primarily for the US market. Some spellings, weights and measures may reflect this origin.

Some useful conversion factors:

Area:	1 in^2 (square inch) = 645 mm^2
Length:	1 in. (inch) = 25.4 mm
	1 ft (foot) = 304.8 mm
	1 yard = 0.914 m
	1 mile = 1.609 km
Mass:	1 oz. (ounce) = 28.35 g
	1 lb (pound weight) = 0.454 kg
Pressure:	1 psi (lb/in2) = 68.95 mb
Volume:	1 US gallon = 3.785 litres

In addition, part ordering numbers may vary. For example, the CABLE5CBL is a CSI part number and known as a FIN5COND at Campbell Scientific Canada (CSC). CSC Technical Support will be pleased to assist with any questions.

About sensor wiring

Please note that certain sensor configurations may require a user supplied jumper wire. It is recommended to review the sensor configuration requirements for your application and supply the jumper wire is necessary.

Table of Contents

PDF viewers: These page numbers refer to the printed version of this document. Use the PDF reader bookmarks tab for links to specific sections.

Figures

Tables

EasyFlux™ DL

1. Introduction

EasyFlux™ DL is a CRBasic program that enables a CR3000 datalogger to collect fully corrected fluxes of CO_2, latent heat (H_2O), sensible heat, ground surface heat flux (optional), and momentum from a Campbell Scientific open-path eddy-covariance (EC) system with optional energy balance sensors. The program processes the EC data using commonly used corrections in the scientific literature. Specifically, the program supports data collection and processing from the following sensors.

Gas analyzer and sonic anemometer (qty 1)
Supports one combination of gas analyzer and sonic anemometer.

- EC150 with CSAT3A
- IRGASON

Fine-wire thermocouple (optional, qty 0 to 1)

- FW05
- FW1
- FW3

Biometeorology (biomet) and energy balance sensors (optional)

- Temperature/Relativity Humidity (RH) Probe (qty 0 to 1)
  - HC2S3
  - HMP155A
- Radiation measurements
  - Option 1
    - NR-LITE2 Net Radiometer (qty 0 to 1)
    - CS300 or LI200X Pyranometer (qty 0 to 1)
    - LI190SB Quantum Sensor (qty 0 to 1)
    - SI-111 Infrared Radiometer (qty 0 to 1)
  - Option 2
    - NR01 or CNR4 4-Way Radiometers (qty 0 to 1)
- TE525MM Rain Gage (qty 0 to 1)
- TCAV Soil Thermocouple Probe (qty 0 to 2)
- Soil Water Content Reflectometer (qty 0 to 2)
  - CS616
  - CS650
  - CS655
- Soil Heat Flux Plates
  - Option 1: HFP01 plates (qty 0 to 4)
  - Option 2: HFP01SC self-calibrating plates (qty 0 to 4)

NOTE It may be possible to customize the program for other sensors or quantities that are not described here. Contact an application engineer at Campbell Scientific for more information.

EasyFlux is a trademark of Campbell Scientific, Inc.

NOTE In this manual, "IRGA" refers to either the EC150 or the IRGASON gas analyzer, "sonic anemometer" refers to either the CSAT3A or IRGASON sonic anemometer, and "FW" refers to a FW05, FW1, or FW3 fine-wire thermocouple.

2. Precautions

- *EasyFlux DL* requires the CR3000 to have operating system version 28.0 or newer.
- The program applies the most common open-path EC corrections to fluxes. However, the user should determine the appropriateness of the corrections for their site.
- Campbell Scientific®, Inc. always recommends saving time-series data in the event reprocessing of raw data is warranted. Furthermore, the user should determine the quality and fitness of any and all data for publication, regardless of whether said data were processed by *EasyFlux DL* or another tool.
- As *EasyFlux DL* is not encrypted, users have the ability to view and edit the code. Campbell Scientific®, Inc. does not guarantee the function of a program that has been altered.

3. Installation

3.1 Wiring

Installation of sensors and system components should be done according to the respective product manuals. When wiring the sensors to the datalogger, the default wiring schemes, along with the number of instruments *EasyFlux DL* supports, should be followed if the standard version of the program is being used. TABLES 3-1 through 3-10 present the wiring schemes.

An IRGA with an associated sonic anemometer are the only required sensors for the program. The additional sensors described in the following tables are optional. If one or more of the optional sensors are not used, the datalogger terminals assigned to those sensor wires should be left unwired.

NOTE If the standard datalogger program is modified, the wiring presented in TABLE 3-1 may no longer apply. In such cases, refer directly to the program code to determine proper wiring.

3.1.1 IRGA and Sonic Anemometer

An open-path IRGA and sonic anemometer must be connected to the EC100 electronics, and the EC100 must be wired to a CR3000 datalogger for *EasyFlux DL* to be functional. The default wiring for these sensors is shown in TABLE 3-1.

TABLE 3-1. Default Wiring for IRGA and Sonic Anemometer				
Sensor	**Quantity**	**Wire Description**	**Color**	**Datalogger Terminal**
IRGASON or EC150/CSAT3A (from EC100)	1	SDM Data	Green	SDM-C1
		SDM Clock	White	SDM-C2
		SDM Enable	Red / Brown	SDM-C3
		Signal Ground	Black	G
		Shield	Clear	⏚

3.1.2 Fine-Wire Thermocouple

Several fine-wire thermocouple sensors are available that can be integrated with the IRGA and sonic anemometer. The *EasyFlux DL* can support from zero to one fine-wire thermocouple along with the IRGA and sonic anemometer. Shown in TABLE 3-2 are the available types and default wiring for adding a fine-wire thermocouple.

TABLE 3-2. Default Wiring for Fine-Wire Thermocouple				
Sensor	**Quantity**	**Wire Description**	**Color**	**Datalogger Terminal**
FW05, FW1, or FW3	0 or 1	Signal	Purple	Diff 5H
		Signal Reference	Red	Diff 5L
		Shield	Clear	⏚

3.1.3 Temperature and Relative Humidity Probe

The *EasyFlux DL* can support from zero to one temperature and relative humidity probe with the IRGA and sonic anemometer. The default wiring for the HC2S3/HMP155A is shown in TABLE 3-3.

NOTE

There are two options for a temperature and relative humidity probe, the HC2S3 and the HMP155A. For details and specifications of these probes, visit *www.campbellsci.com*. The physical wiring to the CR3000 datalogger is the same for each sensor. The colors of the wires, however, are different. The wire colors for the HMP155A sensor are noted by an * in TABLE 3-3.

TABLE 3-3. Default Wiring for Temperature and Relative Humidity Probe				
Sensor	**Quantity**	**Wire Description**	**Color**	**Datalogger Terminal**
HC2S3 / HMP155A	0 or 1	Temp Signal	Brown / Yellow*	SE 27 (Diff 14H)
		RH Signal	White / Blue*	SE 28 (Diff 14L)
		Signal Reference	Yellow / White*	G
		Shield	Clear / Clear*	⏚
		Power	Green / Red*	+12 V
		Power Ground	Grey / Black*	G

3.1.4 Radiation Measurements Option 1

There are two options for making radiation measurements with *EasyFlux DL*. The program can support any combination of the four sensors described in TABLE 3-4. Or it can support one of the two types of four-way radiometers described in TABLE 3-5. The default wiring for Option 1 is detailed in TABLE 3-4. The default wiring for Option 2 is detailed in TABLE 3-5.

TABLE 3-4. Default Wiring for Radiation Measurements Option 1

Sensor	Quantity	Wire Description	Color	Datalogger Terminal
NR-LITE2 Net Radiometer	0 or 1	Radiation Signal	Red	Diff 6H
		Signal Reference	Blue[1]	Diff 6L[1]
		Shield	Black	⏚
CS300 or LI200X Pyranometer	0 or 1	Signal	Red	Diff 7H
		Signal Reference	Black	Diff 7L[1]
		Signal Ground	White (no white for CS300)	⏚
		Shield	Clear	⏚
LI190SB Quantum Sensor	0 or 1	Signal	Red	Diff 8H
		Signal Reference	Black	Diff 8L[1]
		Shield	Clear	⏚
SI-111 Infrared Radiometer	0 or 1	Target Temp Signal	Red	Diff 9H
		Target Temp Reference	Black	Diff 9L
		Shield	Clear	⏚
		Sensor Temp Signal	Green	SE 19 (Diff 10L)
		Sensor Temp Reference	Blue	⏚
		Voltage Excitation	White	VX1

[1] Jumper to ⏚ with user-supplied wire.

3.1.5 Radiation Measurements Option 2

There are two models of four-way radiometers that are compatible with the program, however, only one can be used at a time due to channel limitations. The default wiring for each of the four-way radiometers is shown in TABLE 3-5.

TABLE 3-5. Default Wiring for Radiation Measurements Option 2				
Sensor	**Quantity**	**Wire Description**	**Color**	**Datalogger Terminal**
NR01 4-Way Radiometer	0 or 1	Pyranometer Up Signal	Red	Diff 6H
		Pyranometer Up Reference	Blue[1]	Diff 6L[1]
		Pyranometer Down Signal	White	Diff 7H
		Pyranometer Down Reference	Green[1]	Diff 7L[1]
		Pyrgeometer Up Signal	Brown	Diff 8H
		Pyrgeometer Up Reference	Yellow[1]	Diff 8L[1]
		Pyrgeometer Down Signal	Purple	Diff 9H
		Pyrgeometer Down Reference	Grey[1]	Diff 9L[1]
		PT100 Signal	White	Diff 10H
		PT100 Reference	Green	Diff 10L
		Current Excite	Red	IX1
		Current Return	Blue	IXR
		Shields	Clear	⏚
CNR4 4-Way Radiometer	0 or 1	Pyranometer Up Signal	Red	Diff 6H
		Pyranometer Up Reference	Blue[1]	Diff 6L[1]
		Pyranometer Down Signal	White	Diff 7H
		Pyranometer Down Reference	Black[1]	Diff 7L[1]
		Pyrgeometer Up Signal	Grey	Diff 8H
		Pyrgeometer Up Reference	Yellow[1]	Diff 8L[1]
		Pyrgeometer Down Signal	Brown	Diff 9H
		Pyrgeometer Down Reference	Green[1]	Diff 9L[1]
		Thermistor Signal	White	SE 19 (Diff 10H)
		Thermistor V Excite	Red	VX1
		Thermistor Reference	Black	⏚
		Shields	Clear	⏚
[1] Jumper to ⏚ with user-supplied wire.				

3.1.6 Precipitation Gage

EasyFlux DL can support a single TE525MM tipping rain gage, or a precipitation gage can be omitted. The default wiring for the precipitation gage is shown in TABLE 3-6.

TABLE 3-6. Default Wiring for Precipitation Gage				
Sensor	**Quantity**	**Wire Description**	**Color**	**Datalogger Terminal**
TE525MM Tipping Rain Gage	0 or 1	Pulse Output	Black	P1
		Signal Ground	White	⏚
		Shield	Clear	⏚

3.1.7 Soil Temperature

The TCAV is an Averaging Soil Thermocouple Probe used for measuring soil temperature. *EasyFlux DL* can support up to two TCAV probes. The order of wiring, however, is important. If only one TCAV sensor is used, it must be wired as described for TCAV #1 in TABLE 3-7. An additional TCAV sensor would be wired according to TCAV #2 in TABLE 3-7.

CAUTION If only one TCAV is being used and it is wired to terminals 12H and 12L (leaving terminals 11H and 11L empty), the datalogger will not record any TCAV measurements.

TABLE 3-7. Default Wiring for Soil Thermocouple Probes

Sensor	Quantity	Wire Description	Color	Datalogger Terminal
TCAV #1	1	Signal	Purple	Diff 11H
		Signal Reference	Red	Diff 11L
		Shield	Clear	⏚
TCAV #2	1	Signal	Purple	Diff 12H
		Signal Reference	Red	Diff 12L
		Shield	Clear	⏚

NOTE The CS650 or CS655 sensors also measure soil temperature. If the CS650 or CS655 sensors are used but no TCAV probes are used, *EasyFlux DL* will use soil temperature from the CS650 or CS655 to compute ground surface heat flux. If available, soil temperature from the TCAV probe is preferred since it provides a better spatial average. See wiring details for these sensors in TABLE 3-8.

3.1.8 Soil Water Content

EasyFlux DL supports one of three models of soil water content sensors: CS616, CS650, or CS655; up to two of the model used are supported. A soil water content sensor can also be omitted. The default wiring for each is shown in TABLE 3-8.

CAUTION If only one soil water content sensor is being used, wire it according to the first probe as described in TABLE 3-8. If only one sensor is being used and it is wired according to the second sensor, *EasyFlux DL* will not record any measurements from the soil water content sensor.

TABLE 3-8. Default Wiring for Soil Water Content Probes				
Sensor	**Quantity**	**Wire Description**	**Color**	**Datalogger Terminal**
CS616 #1	1	Power	Red	+12 V
		Signal Output	Green	SE 25 (Diff 13H)
		Enable	Orange	C4
		Signal Ground	Black	⏚
		Power Ground	Clear	G
CS616 #2	1	Power	Red	+12 V
		Signal Output	Green	SE 26 (Diff 13L)
		Enable	Orange	C4
		Signal Ground	Black	⏚
		Power Ground	Clear	G
CS650/CS655 #1	1	SDI-12 Data	Green	C5
		SDI-12 Power	Red	+12 V
		SDI-12 Reference	Black	G
		Shield	Clear	G
		Not Used	Orange	G
CS650/CS655 #2	1	SDI-12 Data	Green	C5
		SDI-12 Power	Red	+12 V
		SDI-12 Reference	Black	G
		Shield	Clear	G
		Not Used	Orange	G

3.1.9 Soil Heat Flux Plates

EasyFlux DL can support from zero to four standard (non-self-calibrating) soil heat flux plates. The default wiring for the standard soil heat flux plates is shown in TABLE 3-9.

TABLE 3-9. Default Wiring for Non-Calibrating Soil Heat Flux Plates				
Sensor	**Quantity**	**Wire Description**	**Color**	**Datalogger Terminal**
HFP01 #1	1	Signal	White	Diff 1H
		Signal Reference	Green	Diff 1L
		Shield	Clear	⏚
HFP01 #2	1	Signal	White	Diff 2H
		Signal Reference	Green	Diff 2L
		Shield	Clear	⏚
HFP01 #3	1	Signal	White	Diff 3H
		Signal Reference	Green	Diff 3L
		Shield	Clear	⏚

TABLE 3-9. Default Wiring for Non-Calibrating Soil Heat Flux Plates				
Sensor	**Quantity**	**Wire Description**	**Color**	**Datalogger Terminal**
HFP01 #4	1	Signal	White	Diff 4H
		Signal Reference	Green	Diff 4L
		Shield	Clear	⏚

3.1.10 Self-Calibrating Soil Heat Flux Plates

A user can also choose from zero to four of the self-calibrating soil heat flux plates described in TABLE 3-10. However, due to channel limits of the CR3000, if choosing the self-calibrating heat plates, the measurements will be made in a single-ended mode. The default wiring for the self-calibrating soil heat flux plates is shown in TABLE 3-10.

TABLE 3-10. Default Wiring for Soil Heat Flux Plates (Self Calibrating)				
Sensor	**Quantity**	**Wire Description**	**Color**	**Datalogger Terminal**
HFP01SC #1	1	Signal	White	SE 1 (Diff 1H)
		Signal Reference	Green	⏚
		Shield	Clear	⏚
		Heater Signal	Yellow	SE 5 (Diff 3H)
		Heater Reference	Purple	⏚
		Shield	Clear	⏚
		Heater Power	Red	SW12-1
		Power Reference	Black	G
HFP01SC #2	1	Signal	White	SE 2 (Diff 1L)
		Signal Reference	Green	⏚
		Shield	Clear	⏚
		Heater Signal	Yellow	SE 6 (Diff 3L)
		Heater Reference	Purple	⏚
		Shield	Clear	⏚
		Heater Power	Red	SW12-1
		Power Reference	Black	G
HFP01SC #3	1	Signal	White	SE 3 (Diff 2H)
		Signal Reference	Green	⏚
		Shield	Clear	⏚
		Heater Signal	Yellow	SE 7 (Diff 4H)
		Heater Reference	Purple	⏚
		Shield	Clear	⏚
		Heater Power	Red	SW12-1
		Power Reference	Black	G

TABLE 3-10. Default Wiring for Soil Heat Flux Plates (Self Calibrating)				
Sensor	**Quantity**	**Wire Description**	**Color**	**Datalogger Terminal**
HFP01SC #4	1	Signal	White	SE 4 (Diff 2L)
		Signal Reference	Green	⏚
		Shield	Clear	⏚
		Heater Signal	Yellow	SE 8 (Diff 4L)
		Heater Reference	Purple	⏚
		Shield	Clear	⏚
		Heater Power	Red	SW12-1
		Power Reference	Black	G

4. Operation

4.1 Set Constants in *CRBasic Editor* and Load Program

Before operating the station, the values for some configuration constants should be verified in the program code.

Open the program in *CRBasic Editor* or another text editor. Search the program for the word "unique". This will locate all lines of code containing constants that need to be verified. Constants can also be identified by text that is all capitalized. Look for the text comments on the right side of the code for more explanation of each constant. Generally, the constants fall into four categories:

1. **Sensor Selection Constants**
   The value for these constants is set to **TRUE** if the system includes the sensor. For example, if a system has a fine-wire thermocouple, the constant **SENSOR_FW** should be set to **TRUE**. When set to **TRUE**, the wiring in TABLE 3-10 will apply to the sensor and the data from that sensor will be included in the data output tables.

   If a sensor is not used, make sure the constant is set to **FALSE**.

2. **Sensor Quantity Constants**
   The value for these constants indicates the number of each type of sensor in the system. For example, if four soil heat flux (SHF) plates were being used, the constant **NMBR_SHF** would be set to **4**.

3. **Sensor Calibration Constants**
   Some sensors have unique multipliers or offsets that should be applied to their raw measurements. Typically, these values are found on the calibration sheet from the sensor's original manufacturer. For example, if an NR-LITE2 net radiometer is being used, a unique multiplier is set in the following line of code: Const **NRLITE_CAL = 1000/16**. The comments in the code explain that the number in the denominator (in this example: 16) is the sensor sensitivity value provided in the NR-LITE2 calibration sheet.

4. **Program Function Constants**
   These are constants that determine the timing of code execution, frequency of writing to output tables, memory allocation, etc. In most cases, these constants may be left with their default values.

   One program function constant that should be mentioned specifically is the **ONE_FULL_TABLE** constant. If this is set to **TRUE**, all of the intermediate and auxiliary measurements will be included as data fields in the main **FLUX** output table, rather than being in a separate output table called **FLUX_NOTES**. For more information, see Section 4.4, *Output Tables* *(p. 16)*.

After all constants are verified, the program should be saved. It is suggested to save the program under a new or modified file name to keep track of different program versions. Finally, send the program to the CR3000 using *LoggerNet*, *PC400*, or *PC200W* user-interface software.

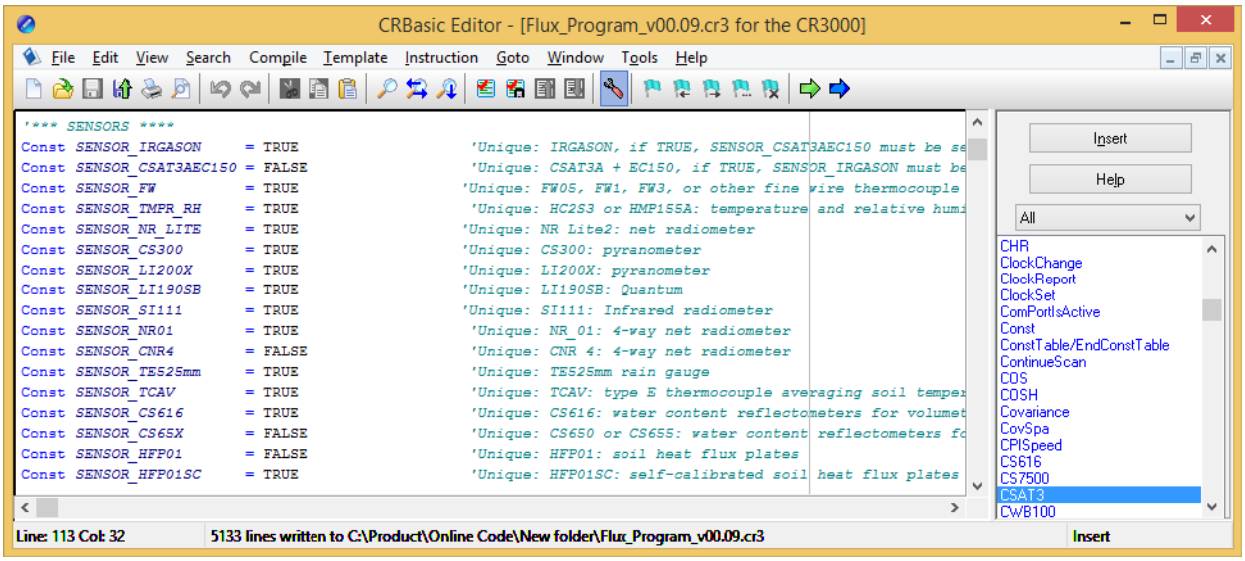

FIGURE 4-1. Example screen from CRBasic Editor showing sensor selection constants

4.2 Enter Site-Specific Variables with Datalogger Keypad

After the eddy-covariance station is installed and the datalogger is running the program, a custom menu for the CR3000 keyboard display is displayed (FIGURE 4-2). Use this menu to enter and view station-specific variables. Use the up and down arrow buttons to navigate to different variables. Press **Enter** to select a variable or to set a new value after typing it. Press **Esc** to return to the previous menu.

FIGURE 4-2 depicts the structure of the custom menu. The custom menu can be bypassed such that the user can interact directly with the datalogger through the datalogger default menus. To bypass the custom menus, select <**System Menu**>.

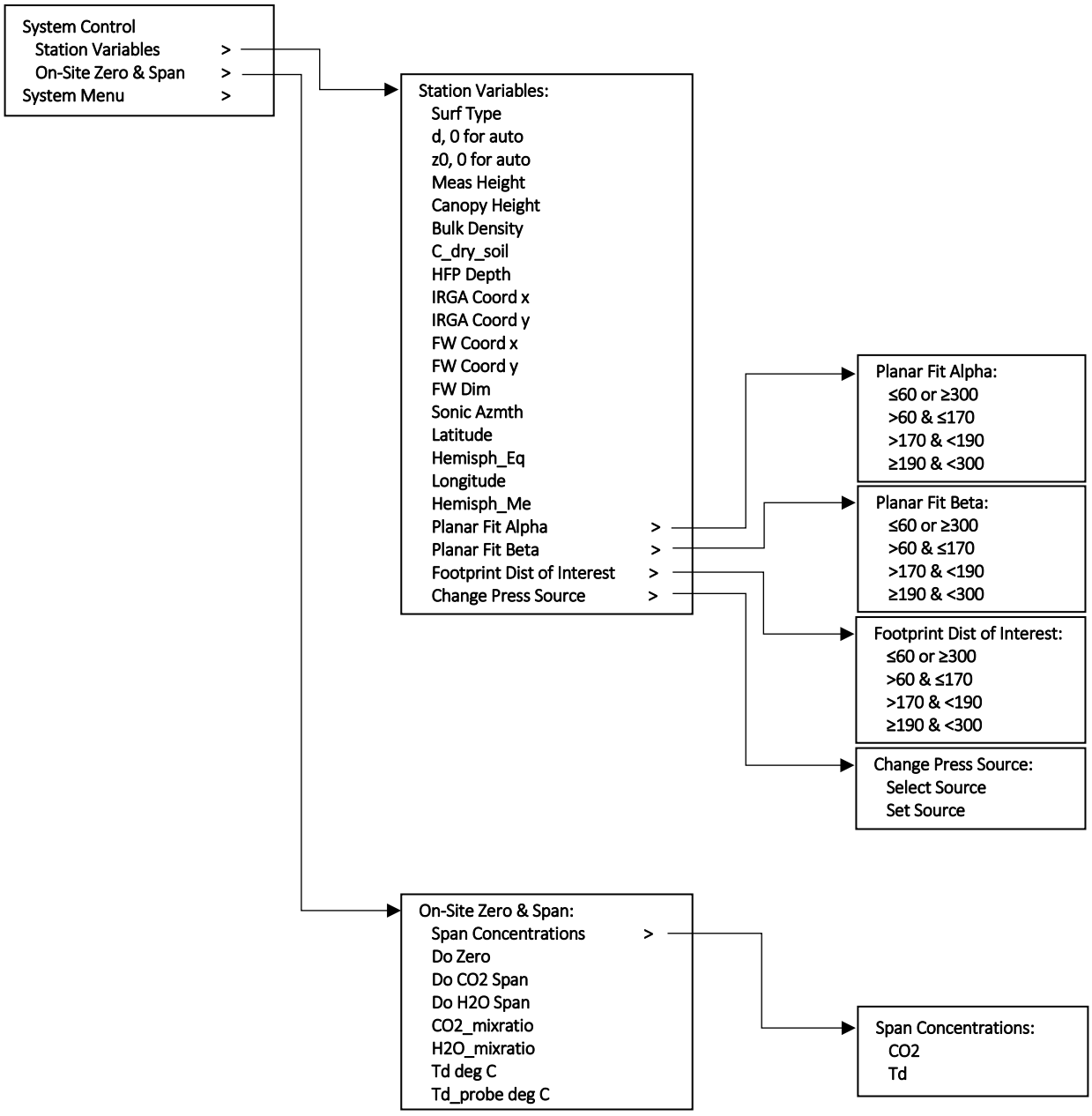

FIGURE 4-2. Custom keypad menu; arrows indicate submenus

Before fluxes are processed correctly, the user must go through each of the station variables and set or confirm the assigned values. TABLE 4-1 gives short descriptions of each station variable.

TABLE 4-1. Station Variables with Descriptions			
Station Variable	**Units**	**Default**	**Description**
Surf Type	unitless	BARELAND	Type of surface at the measurement site. Options are CROP, GRASS, FOREST, SHRUB, BARELAND, and WATER. This is used to estimate displacement height (see Appendix D.6.1, *Aerodynamic Height* ***(p. D-8)***) and roughness length (see Appendix G.1.3, *Programmatic Approach* ***(p. G-6)***).
d	m	0 (Auto)	Displacement height. Set to zero (0) for program to auto-calculate. See Appendix D.6.1, *Aerodynamic Height* ***(p. D-8)***, for details.
z0	m	0 (Auto)	Roughness length. Set to zero (0) for program to auto-calculate. See Appendix G.1.3, *Programmatic Approach* ***(p. G-6)***, for details.
Meas Height	m	3	The height of the center of the eddy-covariance sensors measurement volumes above ground.
Canopy Height	m	0	The average height of the canopy.
Bulk Density	$kg \cdot m^{-3}$	1300	Average bulk density of soil. If energy balance sensors are not used, this variable is omitted.
C_dry_soil	$J \cdot kg^{-1} \cdot K^{-1}$	870	Specific heat of dry mineral soil. If energy balance sensors are not used, this variable is omitted.
HFP Depth	m	0.08	Depth of the soil heat flux plates. If energy balance sensors are not used, this variable is omitted.
IRGA Coord x	m	0 for IRGASON; 0.04066 for EC150	Distance along the sonic x-axis between the sonic sampling volume and the gas analyzer sampling volume. If an IRGASON is used, this should be set to 0. If an EC150 with CSAT3A is used, this defaults to 0.04066, which corresponds to the EC150 mounting position closest to the CSAT3A sonic measurement volume.
IRGA Coord y	m	0 for IRGASON; 0.02905 for EC150	Distance along the sonic y-axis between the sonic sampling volume and the gas analyzer sampling volume. If an IRGASON is used, this should be set to 0. If an EC150 with CSAT3A is used, this defaults to 0.02905, which corresponds to the EC150 mounting position closest to the CSAT3A sonic measurement volume.
FW Coord x	m	0.005870	Distance along the sonic x-axis between the sonic sampling volume and fine-wire thermocouple. If no fine-wire thermocouple is being used, this variable is omitted.
FW Coord y	m	0.03259	Distance along the sonic y-axis between the sonic sampling volume and the fine-wire thermocouple. If no fine-wire thermocouple is being used, this variable is omitted.

TABLE 4-1. Station Variables with Descriptions

Station Variable		Units	Default	Description
FW Dim		m	FW05_DIA	Identifies which fine-wire thermocouple is being used and loads the appropriate diameter. For FW05_DIA, FW1_DIA and FW3_DIA, the diameters are 1.27 x 10^{-5}, 2.54 x 10^{-5}, and 7.62 x 10^{-5} m, respectively. If no fine-wire thermocouple is being used, this variable is omitted.
Sonic Azmth		deg	0	The compass direction in which the sonic negative x-axis points (the compass direction in which the sonic head is pointing).
Latitude		deg	41.8	The site latitude in degrees North or South.
Hemisph_Eq		unitless	NORTH	The site latitudinal hemisphere. Options are NORTH or SOUTH.
Longitude		unitless	111.9	The site longitude in degrees East or West.
Hemisph_Me		unitless	WEST	The site longitudinal hemisphere. Options are EAST or WEST.
Planar Fit Alpha	≤ 60 or ≥ 300	deg	0	Alpha angle used to rotate the wind when the mean horizontal wind is blowing from the sector of 0 to 60 and 300 to 360 degrees in the sonic coordinate system (wind blowing into sonic head).[1]
Planar Fit Alpha	> 60 & ≤ 170	deg	0	Alpha angle used to rotate the wind when the mean horizontal wind is blowing from the sector of 60 to 170 degrees in the sonic coordinate system (wind blowing from the sector left and behind sonic head).[1]
Planar Fit Alpha	> 170 & < 190	deg	0	Alpha angle used to rotate the wind when the mean horizontal wind is blowing from the sector of 170 to 190 degrees in the sonic coordinate system (wind blowing from behind sonic head).[1]
Planar Fit Alpha	≥ 190 & < 300	deg	0	Alpha angle used to rotate the wind when the mean horizontal wind is blowing from the sector of 190 to 300 degrees in the sonic coordinate system (wind blowing from the sector right and behind sonic head).[1]
Planar Fit Beta	≤ 60 or ≥ 300	deg	0	Beta angle used to rotate the wind when the mean horizontal wind is blowing from the sector of 0 to 60 and 300 to 360 degrees in the sonic coordinate system (wind blowing into sonic head).[1]
Planar Fit Beta	> 60 & ≤ 170	deg	0	Beta angle used to rotate the wind when the mean horizontal wind is blowing from the sector of 60 to 170 degrees in the sonic coordinate system (wind blowing from left and behind sonic head).[1]
Planar Fit Beta	> 170 & < 190	deg	0	Beta angle used to rotate the wind when the mean horizontal wind is blowing from the sector of 170 to 190 degrees in the sonic coordinate system (wind blowing from behind sonic head).[1]
Planar Fit Beta	≥ 190 & < 300	deg	0	Beta angle used to rotate the wind when the mean horizontal wind is blowing from the sector of 190 to 300 degrees in the sonic coordinate system (wind blowing from right and behind sonic head).[1]

TABLE 4-1. Station Variables with Descriptions

Station Variable		Units	Default	Description
Footprint Dist of Interest	≤ 60 or ≥ 300	m	100*z*	The upwind distance of interest from the station when the mean horizontal wind is blowing from the sector of 0 to 60 and 300 to 360 degrees in the sonic coordinate system (wind blowing into sonic head). Note: The program will report the percentage of cumulative footprint from within this distance. The default value is 100 times the aerodynamic height, *z*. Recall that *z* is the difference between the measurement height and displacement height.
Footprint Dist of Interest	> 60 & ≤ 170	m	100*z*	The upwind distance of interest from the station when the mean horizontal wind is blowing from the sector of 60 to 170 degrees in the sonic coordinate system (wind blowing from left and behind sonic head).
Footprint Dist of Interest	> 170 & < 190	m	100*z*	The upwind distance of interest from the station when the mean horizontal wind is blowing from the sector of 170 to 190 degrees in the sonic coordinate system (wind blowing from behind sonic head).
Footprint Dist of Interest	≥ 190 & < 300	m	100*z*	The upwind distance of interest from the station when the mean horizontal wind is blowing from the sector of 190 to 300 degrees in the sonic coordinate system (wind blowing from right and behind sonic head).
Pressure Source	Select Source	unitless	EB	Used to select the barometer to use for meausrements of ambient pressure. Set to "EB" for EC100 enhanced barometer. Set to "BB" for the EC100 on-board basic barometer.
Pressure Source	Set Source	unitless	FALSE	If the variable "Select Source" has been changed, this variable must be set to "TRUE" to enable the change. The program will return "Set Source" to "FALSE" once the change has been applied.

[1] Leave *all* planar fit alpha and beta angles set to 0 to use Tanner and Thurtell (1969) method of double coordinate rotations.

Planar fit alpha and beta angles must be determined by post-processing time series data with an appropriate PC software package. Once the angles are determined, they can be entered into *EasyFlux DL*, and then the planar-fit coordinate rotations will be automatically applied. In contrast, the angles for Tanner and Thurtell (1969) double coordinate rotations can be determined automatically by *EasyFlux DL* for each averaging interval (e.g., 30 minutes).

After all of the station variables have been verified, it is recommended to do an on-site zero and span of the gas analyzer before leaving the station. If a span is not possible, it is still strongly recommended to do a zero. Using the Zero Air Generator, pn 31022, is a convenient way to provide a portable source of zero air, especially for remote sites. Follow the zero and span procedure outlined in the IRGASON or EC150 manuals. TABLE 4-2 gives descriptions of the variables in the "On-Site Zero & Span" keypad menu, which may be used to carry out the zero-and-span procedure described in the manuals.

TABLE 4-2. On-Site Zero and Span Variables				
On-Site Zero & Span Variable		**Units**	**Default**	**Description**
Span Concentrations	CO_2	ppm	0	This is the concentration of span gas flowing through the zero/span shroud. It should be on a basis of dry air.
	Td	°C	0	This is the dewpoint temperature of the H_2O span gas generated from a dewpoint generator. It should match the dewpoint temperature setting on the generator.
Do Zero		unitless	FALSE	Set this to TRUE after flowing zero gas through the zero/span shround and reaching equilibrium.
Do CO_2 Span		unitless	FALSE	Set this to TRUE after flowing CO_2 span gas through the zero/span shroud and reaching equilibrium.
Do H_2O Span		unitless	FALSE	Set this to TRUE after flowing H_2O span gas through the zero/span shround and reaching equilibrium.
CO_2_mixratio		ppm	–	This is a real-time measurement of CO_2 molar mixing ratio (dry basis) as measured by the gas analyzer. This can be monitored to know when equilibrium has been reached.
H_2O_mixratio		ppth	–	This is a real-time measurement of H_2O molar mixing ratio (dry basis) as measured by the gas analyzer. This can be monitored to know when equilibrium has been reached.
Td deg C		°C	–	This is a real-time measurement of dewpoint temperature as measured by the gas analyzer.
Td_probe deg C		°C	–	This is a real-time measurement of dewpoint temperature derived from measurements by the temp/RH probe. It is ommitted if there is no temp/RH probe being used. This value could potentially be input for dewpoint temperature, Td above, if a dewpoint generator is unavailable and performing a rough H_2O span is helpful (for example, during troubleshooting).

4.3 Data Retrieval

The program stores a very limited amount of data to the internal CPU of the datalogger, so a CompactFlash® (CF) card, along with an NL115/NL116/CFM100 card module, should be used with the CR3000. TABLE 4-3 shows the number of days of data a 2 GB and 16 GB will typically hold before the memory is full and data starts to be overwritten. In cases where real-time remote monitoring is desired, various telemetry options (for example, cellular, radio, etc.) are available to transmit the processed flux data. Certain conditions may also allow remote transmittal of time series data. Contact Campbell Scientific for more details.

TABLE 4-3. CF Card Fill Times		
CompactFlash® card size	**Fill time with gas analyzer and sonic only**	**Fill time with gas analyzer, sonic, FW, and biomet/energy balance sensors)[1]**
2 GB	43 days	40 days
16 GB	353 days	327 days
[1] Biomet and energy balance sensors used for this fill time estimate include the following: HMP155A, NR-LITE2, CS300, LI200X, LI190SB, SI-111, TE525MM, TCAV (qty 2), CS616 (qty 2), and HFP01 (qty 4)		

NOTE CF cards from various manufacturers may have slightly different memory sizes on their 2 G and 16 G cards, respectively. Also, as a card ages some of its sectors may become unusable, decreasing the available memory. Fill time estimates given in TABLE 4-3 are approximations for new cards.

4.4 Output Tables

Besides the standard **Public**, **Status**, and **TableInfo** tables that every datalogger reports, the program has four output tables. TABLE 4-4 gives the names of these output tables, along with a short description, the frequency at which a record is written to the table, and the amount of memory allocated from the CPU and CF card for each table. Note that if the user would prefer to have the data fields contained in the **Flux_Notes** table appended to the end of the **Flux** table rather than being placed in a separate output table, this is possible by changing the constant **ONE_FULL_TABLE** from **FALSE** to **TRUE** (see Section 4.1, *Set Constants in CRBasic Editor and Load Program* *(p. 9)*, on changing constants).

TABLE 4-4. Data Output Tables				
Table Name	**Description**	**Recording Interval**	**Memory on CR3000 CPU**	**Memory on CF Card**
Time_Series	Time series data (aligned to account for electronic delays)	SCAN_INTERVAL (default 100 ms)	Auto-Allocate (typically less than 1 hour)	Time_Series is broken up into 1 day files (see TABLE 4-3)
Diagnostic	Reports most recent diagnostic flags from gas analyzer and sonic anemometer	SCAN_INTERVAL (default 100 ms)	1 record (most recent scan)	0 records
Flux	Processed flux and statistical data	OUTPUT_INTERVAL (default 30 minutes)	NUM_DAY_CPU (default 7 days)	The Flux table is broken up into 30-day files (see TABLE 4-3)
Flux_Notes	Intermediate variables, station constants, and correction variables used to generate results in Flux table	OUTPUT_INTERVAL (default 30 minutes)	NUM_DAY_CPU (default 7 days)	The Flux_Notes table is broken up into 30-day files (see TABLE 4-3)

TABLES 4-5 through 4-8 give a description of all data fields that are found in each data output table and when each data field is included in the table. Note that prior to coordinate rotations, the orthogonal wind components from the sonic anemometer are denoted as U_x, U_y, and U_z. Following coordinate rotations, the common denotation of u, v, and w is used, respectively.

NOTE

Variables with _R denote that the value was computed after coordinate rotations were done. Variables with a _F denote that the value was calculated after frequency corrections were applied. Similarly, _SND and _WPL refer to variables that have had the SND correction or the WPL correction applied, respectively.

TABLE 4-5. Data Fields in the Time_Series Data Output Table

Data Field Name	Units	Description	Data Field Included
Ux	$m \cdot s^{-1}$	Wind speed along sonic x-axis	Always
Uy	$m \cdot s^{-1}$	Wind speed along sonic y-axis	Always
Uz	$m \cdot s^{-1}$	Wind speed along sonic z-axis	Always
Ts	°C	Sonic temperature	Always
diag_sonic	unitless	Raw sonic diagnostic value (0 indicates no diagnostic flags set)	Always
CO2	$mg \cdot m^{-3}$	CO_2 density	Always
H2O	$g \cdot m^{-3}$	Water vapor density	Always
diag_irga	unitless	Raw gas analyzer diagnostic value (0 indicates no diagnostic flags set)	Always
Tc	°C	Air temperature derived from sonic temperature corrected for humidity and pressure	If IRGASON is used
amb_tmpr	°C	Air temperature measured by the EC100 temperature probe	Always
amb_press	kPa	Ambient pressure	Always
CO2_sig_strgth	ratio	CO_2 signal strength	Always
H2O_sig_strgth	ratio	H_2O signal strength	Always
FW	°C	Air temperature measured by fine-wire thermocouple	If FW05, FW1, or FW3 is used

TABLE 4-6. Data Fields in the Diagnostic Output Table

Data Field Name	Units	Description	Data Field Included
sonic_amp_l_f	unitless	Amplitude low diagnostic flag	Always
sonic_amp_h_f	unitless	Amplitude high diagnostic flag	Always
sonic_sig_lck_f	unitless	Signal lock diagnostic flag	Always
sonic_del_T_f_f	unitless	Delta Temp diagnostic flag	Always
sonic_aq_sig_f	unitless	Acquiring signal diagnostic flag	Always
sonic_cal_err_f	unitless	Calibration error diagnostic flag	Always

TABLE 4-6. Data Fields in the Diagnostic Output Table

Data Field Name	Units	Description	Data Field Included
irga_bad_data_f	unitless	Any gas analyzer diagnostic flag is set	Always
irga_gen_fault_f	unitless	General system fault diagnostic flag	Always
irga_startup_f	unitless	Startup diagnostic flag	Always
irga_motor_spd_f	unitless	Motor speed diagnostic flag	Always
irga_tec_tmpr_f	unitless	Thermoelectrical cooler (TEC) temperature diagnostic flag	Always
irga_src_pwr_f	unitless	Source power diagnostic flag	Always
irga_src_tmpr_f	unitless	Source temperature diagnostic flag	Always
irga_src_curr_f	unitless	Source current diagnostic flag	Always
irga_off_f	unitless	Gas head power down diagnostic flag	Always
irga_sync_f	unitless	Synchronization diagnostic flag	Always
irga_amb_tmpr_f	unitless	Ambient temperature probe diagnostic flag	Always
irga_amb_press_f	unitless	Ambient pressure diagnostic flag	Always
irga_CO2_I_f	unitless	CO_2 I signal diagnostic flag	Always
irga_CO2_Io_f	unitless	CO_2 Io signal diagnostic flag	Always
irga_H2O_I_f	unitless	H_2O I signal diagnostic flag	Always
irga_H2O_Io_f	unitless	H_2O Io signal diagnostic flag	Always
irga_CO2_Io_var_f	unitless	CO_2 Io variation diagnostic flag	Always
irga_H2O_Io_var_f	unitless	H_2O Io variation diagnostic flag	Always
irga_CO2_sig_strgth_f	unitless	CO_2 signal strength diagnostic flag	Always
irga_H2O_sig_strgth_f	unitless	H_2O signal strength diagnostic flag	Always
irga_cal_err_f	unitless	Calibration file read error flag	Always
irga_htr_ctrl_off_f	unitless	Heater control off diagnostic flag	Always

TABLE 4-7. Data Fields in the Flux Data Output Table

Data Field Name	Units	Description	Data Field Included
Fc_molar	$\mu mol \cdot m^{-2} \cdot s^{-1}$	Final corrected CO_2 flux	Always
Fc_mass	$mg \cdot m^{-2} \cdot s^{-1}$	Final corrected CO_2 flux	Always
Fc_qc_grade	grade	Overall quality grade for Fc_molar and Fc_mass following Foken et al. 2012	Always
Fc_samples_Tot	count	The total number of time series samples used in calculation of Fc	Always
LE	$W \cdot m^{-2}$	Final corrected latent heat flux	Always
LE_qc_grade	grade	Overall quality grade for LE following Foken et al. 2012	Always
LE_samples_Tot	count	The total number of time series samples used in calculation of LE	Always

TABLE 4-7. Data Fields in the Flux Data Output Table

Data Field Name	Units	Description	Data Field Included
H	$W \cdot m^{-2}$	Final corrected sensible heat flux derived from sonic sensible heat flux	Always
H_qc_grade	grade	Overall quality grade for Hs following Foken et al. 2012	Always
H_samples_Tot	count	The total number of time series samples used in calculation of H	Always
H_FW	$W \cdot m^{-2}$	Final corrected sensible heat flux derived from fine-wire thermocouple measurements	If FW05, FW1, or FW3 is used
H_FW_samples_Tot	count	The total number of time series samples used in calculation of H_FW	If FW05, FW1, or FW3 is used
Rn	$W \cdot m^{-2}$	Average net radiation (corrected for wind)	If NR-LITE2, NR01, or CNR4 is used
G_surface	$W \cdot m^{-2}$	Heat flux at the ground surface	If energy balance sensors are used
energy_closure	ratio	The ratio of sensible and latent heat fluxes over surface heat flux plus net radiation	If energy balance sensors are used
Bowen_ratio	ratio	The ratio of final sensible heat flux over final latent heat flux	Always
tau	$N \cdot s \cdot m^{-2} \cdot s^{-1}$	Final corrected momentum flux	Always
tau_qc_grade	grade	Overall quality grade for tau following Foken et al. 2012	Always
u_star	$m \cdot s^{-1}$	Friction velocity after coordinate rotations and frequency corrections	Always
T_star	°C	Scaling temperature after coordinate rotations, frequency corrections, and SDN correction	Always
TKE	$m^2 \cdot s^{-2}$	Specific turbulence kinetic energy after coordinate rotations	Always
amb_tmpr_Avg	°C	Average ambient temperature from EC100 temperature probe	Always
Tc_Avg	°C	Average air temperature derived from corrected sonic temperature	If IRGASON is used
Td	°C	Average dewpoint temperature derived from gas analyzer and sonic measurements	Always
RH_Avg	%	Average relative humidity derived from gas analyzer measurements	Always
e_sat_Avg	kPa	Average saturation vapor pressure derived from gas analyzer measurements	Always
e_Avg	kPa	Average vapor pressure derived from gas analyzer measurements	Always

TABLE 4-7. Data Fields in the Flux Data Output Table

Data Field Name	Units	Description	Data Field Included
amb_press_Avg	kPa	Average ambient air pressure	Always
VPD_air	kPa	Vapor pressure deficit	Always
Ux_Avg	$m \cdot s^{-1}$	Average U_x	Always
Ux_Std	$m \cdot s^{-1}$	Standard deviation of U_x	Always
Uy_Avg	$m \cdot s^{-1}$	Average U_y	Always
Uy_Std	$m \cdot s^{-1}$	Standard deviation of U_y	Always
Uz_Avg	$m \cdot s^{-1}$	Average U_z	Always
Uz_Std	$m \cdot s^{-1}$	Standard deviation of U_z	Always
Ts_Avg	°C	Average sonic temperature	Always
Ts_Std	°C	Standard deviation of sonic temperature	Always
sonic_azimuth	deg	Compass direction in which the sonic negative x-axis points	Always
wnd_spd	$m \cdot s^{-1}$	Average wind speed	Always
rslt_wnd_spd	$m \cdot s^{-1}$	Average horizontal wind speed	Always
wnd_dir_sonic	deg	Average wind direction in the sonic coordinate system	Always
wnd_dir_Std	deg	Standard deviation of wind direction	Always
wnd_dir_compass	deg	Average compass wind direction	Always
CO2_molfrac_Avg	$\mu mol \cdot mol^{-1}$	Average CO_2 mole fraction (wet basis)	Always
CO2_mixratio_Avg	$\mu mol \cdot mol^{-1}$	Average CO_2 dry molar mixing ratio	Always
CO2_Avg	$mg \cdot m^{-3}$	Average CO_2 mass density	Always
CO2_Std	$mg \cdot m^{-3}$	Standard deviation of CO_2 mass density	Always
H2O_molfrac_Avg	$mmol \cdot mol^{-1}$	Water vapor mole fraction (wet basis)	Always
H2O_mixratio_Avg	$mmol \cdot mol^{-1}$	Water vapor dry molar mixing ratio	Always
H2O_Avg	$mmol \cdot mol^{-1}$	Water vapor mass density	Always
H2O_Std	$mmol \cdot mol^{-1}$	Standard deviation of water vapor mass density	Always
CO2_sig_strgth_Min	ratio	Minimum CO_2 signal strength	Always
H2O_sig_strgth_Min	ratio	Minimum H_2O signal strength	Always
FW_Avg	°C	Average fine-wire thermocouple temperature	If FW05, FW1, or FW3 is used
FW_Std	°C	Standard deviation of fine-wire thermocouple temperature	If FW05, FW1, or FW3 is used
T_probe_Avg	°C	Average ambient temperature measured by temp/RH probe	If HC2S3 or HMP155A is used
e_probe_Avg	kPa	Average water vapor pressure derived from temp/RH probe	If HC2S3 or HMP155A is used

TABLE 4-7. Data Fields in the Flux Data Output Table

Data Field Name	Units	Description	Data Field Included
e_sat_probe_Avg	kPa	Average saturation water vapor pressure derived from temp/RH probe	If HC2S3 or HMP155A is used
Td_probe_Avg	°C	Average dewpoint temperature derived from temp/RH probe	If HC2S3 or HMP155A is used
H2O_probe _Avg	$g \cdot m^{-3}$	Average water vapor density derived from temp/RH probe measurements	If HC2S3 or HMP155A is used
RH_probe_Avg	%	Average relative humidity from temp/RH probe	If HC2S3 or HMP155A is used
rho_a_probe_Avg	$kg \cdot m^{-3}$	Average air density derived from temp/RH probe	If HC2S3 or HMP155A is used
rho_d_probe_Avg	$kg \cdot m^{-3}$	Average dry air density derived from temp/RH probe	If HC2S3 or HMP155A is used
Precipitation_Tot	mm	Total precipitation	If TE525MM is used
Rn_meas_Avg	$W \cdot m^{-2}$	Average net radiation (raw, not corrected for wind)	If NR-LITE2 is used
albedo_Avg	unitless	Average albedo	If CNR4 or NR01 is used
R_SW_in_Avg	$W \cdot m^{-2}$	Average incoming short wave radiation	If CNR4 or NR01 is used
R_SW_out_Avg	$W \cdot m^{-2}$	Average outgoing short wave radiation	If CNR4 or NR01 is used
R_LW_in_Avg	$W \cdot m^{-2}$	Average incoming long wave radiation	If CNR4 or NR01 is used
R_LW_out_Avg	$W \cdot m^{-2}$	Average outgoing long wave radiation	If CNR4 or NR01 is used
T_nr_Avg	K	Average sensor body temperature	If CNR4 or NR01 is used
R_LW_in_meas_Avg	$W \cdot m^{-2}$	Average raw incoming long wave radiation	If CNR4 or NR01 is used
R_LW_out_meas_Avg	$W \cdot m^{-2}$	Average raw outgoing long wave radiation	If CNR4 or NR01 is used
R_pyran_Avg	$W \cdot m^{-2}$	Average radiation measured by pyranometer	If LI200X or CS300 is used
PAR_density_Avg	$\mu mol \cdot s^{-1} \cdot m^{-2}$	Average density of photosynthetic active radiation	If LI190SB is used
T_SI111_targeted_Avg	°C	Average temperature of targeted object	If SI111 is used
T_SI111_body_Avg	°C	Average temperature of sensor body	If SI111 is used
Tsoil_Avg(i)	°C	Average soil temperature for each TCAV sensor; i identifies which TCAV sensor	If TCAV is used
soil_wtr_T_Avg(i)	ratio	Average volumetric soil water content with temperature correction for each CS616; i identifies which CS616 sensor	If CS616 and TCAV are used

TABLE 4-7. Data Fields in the Flux Data Output Table

Data Field Name	Units	Description	Data Field Included
soil_wtr_Avg(i)	ratio	Average volumetric soil water content without temperature correction	If CS616 is used without TCAV
CS616_wcr_Avg(i)	µs	Average water content reflectometer period for each CS616; i identifies which CS616 sensor	If CS616 is used
CS65x_wc_Avg(i)	ratio	Average volumetric soil water content for each sensor; i identifies which CS650 or CS655 sensor	If CS650 or CS655 is used
CS65x_ec_Avg(i)	$dS \cdot m^{-1}$	Average electrical conductivity for each sensor; i identifies which CS650 or CS655 sensor	If CS650 or CS655 is used
CS65x_tmpr_Avg(i)	°C	Average soil temperature for each sensor; i identifies which CS650 or CS655 sensor	If CS650 or CS655 is used
shf_plate_Avg(i)	$W \cdot m^{-2}$	Average soil heat flux; i identifies which sensor	If HFP01 or HFP01SC is used
shf_plate_cal(i)	unitless	Coefficients found from the HFP01SC self-calibration and used to calculate shf_plate_Avg(i); i indicates which sensor	If HFP01SC is used
upwnd_dist_interest	m	Upwind distance of interest for the average wind direction	Always
FP_dist_interest	%	Percentage of footprint from within the upwind range of interest	Always
FP_max	m	Distance upwind where the maximum contribution to the footprint is found	Always
FP_40	m	Upwind distance that contains 40% of cumulative footprint	Always
FP_55	m	Upwind distance that contains 55% of footprint	Always
FP_90	m	Upwind distance that contains 90% of footprint. If **NAN** is returned, integration of the model never reached 90% within the allowable distance of integration. See Appendix G, *Footprint (p. G-1)*, for more details.	Always
FP_equation	text	Returns either **Kljun** or **KormannMeixner**. The model of Kljun et al. (2004) is used for applicable atmospheric conditions, else the model of Kormann & Meixner (2001) is used.	Always

TABLE 4-8. Data fields in the Flux_Notes Output Table			
Data Field Name	**Units**	**Description**	**Data Field Included**
UxUy_cov	$m^2 \cdot s^{-2}$	Covariance of U_x and U_y	Always
UxUz_cov	$m^2 \cdot s^{-2}$	Covariance of U_x and U_z	Always
UyUz_cov	$m^2 \cdot s^{-2}$	Covariance of U_y and U_z	Always
TsUx_cov	$°C \cdot m \cdot s^{-1}$	Covariance of T_s and U_x	Always
TsUy_cov	$°C \cdot m \cdot s^{-1}$	Covariance of T_s and U_y	Always
TsUz_cov	$°C \cdot m \cdot s^{-1}$	Covariance of T_s and U_z	Always
u_star_R	$m \cdot s^{-1}$	Friction velocity after coordinate rotations	Always
u_Avg_R	$m \cdot s^{-1}$	Mean streamwise wind speed after coordinate rotations	Always
u_Std_R	$m \cdot s^{-1}$	Standard deviation of streamwise wind after coordinate rotations	Always
v_Avg_R	$m \cdot s^{-1}$	Average crosswind speed after coordinate rotations	Always
v_Std_R	$m \cdot s^{-1}$	Standard deviation of crosswind after coordinate rotations	Always
w_Avg_R	$m \cdot s^{-1}$	Average vertical wind speed after coordinate rotations	Always
w_Std_R	$m \cdot s^{-1}$	Standard deviation of vertical wind after coordinate rotations	Always
uv_cov_R	$m \cdot s^{-1}$	Covariance of streamwise and crosswind after coordinate rotations	Always
uw_cov_R	$m \cdot s^{-1}$	Covariance of streamwise and crosswind after coordinate rotations	Always
vw_cov_R	$m \cdot s^{-1}$	Covariance of crosswind and vertical wind after coordinate rotations	Always
uTs_Cov_R	$m \cdot °C \cdot s^{-1}$	Covariance of streamwise wind and sonic temperature after coordinate rotations	Always
vTs_Cov_R	$m \cdot °C \cdot s^{-1}$	Covariance of crosswind and sonic temperature after coordinate rotations	Always
wTs_Cov_R	$m \cdot °C \cdot s^{-1}$	Covariance of vertical wind (after coordinate rotations) and sonic temperature	Always
uw_Cov_R_F	$m^2 \cdot s^{-2}$	Covariance of streamwise and vertical wind after coordinate rotations and frequency corrections	Always
vw_Cov_R_F	$m^2 \cdot s^{-2}$	Covariance of cross and vertical wind after coordinate rotations and frequency corrections	Always
wTs_Cov_R_F	$m \cdot °C \cdot s^{-1}$	Covariance of vertical wind and sonic temperature after coordinate rotations and frequency corrections	Always

TABLE 4-8. Data fields in the Flux_Notes Output Table			
Data Field Name	**Units**	**Description**	**Data Field Included**
wTs_Cov_R_F_SND	$m \cdot °C \cdot s^{-1}$	Covariance of vertical wind and sonic temperature after coordinate rotations, frequency corrections, and SND correction	Always
sonic_samples_Tot	count	Number of raw sonic samples in averaging period without diagnostic flags	Always
no_sonic_head_Tot	count	Number of sonic samples where no sonic head was detected	Always
no_new_sonic_data_Tot	count	Number of scans where no sonic data were received	Always
sonic_amp_l_f_Tot	count	Number of sonic samples with amplitude low diagnostic flag	Always
sonic_amp_h_f_Tot	count	Number of sonic samples with amplitude high diagnostic flag	Always
sonic_sig_lck_f_Tot	count	Number of sonic samples with signal lock diagnostic flag	Always
sonic_del_T_f_f_Tot	count	Number of sonic samples with delta temp diagnostic flag	Always
sonic_aq_sig_f_Tot	count	Number of sonic samples with acquiring signal diagnostic flag	Always
sonic_cal_err_f_Tot	count	Number of sonic samples with calibration error diagnostic flag	Always
UxCO2_Cov	$mg \cdot m^{-2} \cdot s^{-1}$	Covariance of U_x and CO_2 density	Always
UyCO2_Cov	$mg \cdot m^{-2} \cdot s^{-1}$	Covariance of U_y and CO_2 density	Always
UzCO2_Cov	$mg \cdot m^{-2} \cdot s^{-1}$	Covariance of U_z and CO_2 density	Always
UxH2O_Cov	$g \cdot m^{-2} \cdot s^{-1}$	Covariance of U_x and water vapor density	Always
UyH2O_Cov	$g \cdot m^{-2} \cdot s^{-1}$	Covariance of U_y and water vapor density	Always
UzH2O_Cov	$g \cdot m^{-2} \cdot s^{-1}$	Covariance of U_z and water vapor density	Always
uCO2_Cov_R	$mg \cdot m^{-2} \cdot s^{-1}$	Covariance of streamwise wind and CO_2 density after coordinate rotations	Always
vCO2_Cov_R	$mg \cdot m^{-2} \cdot s^{-1}$	Covariance of crosswind and CO_2 density after coordinate rotations	Always
wCO2_Cov_R	$mg \cdot m^{-2} \cdot s^{-1}$	Covariance of vertical wind and CO_2 density after coordinate rotations	Always
uH2O_Cov_R	$g \cdot m^{-2} \cdot s^{-1}$	Covariance of streamwise wind and H_2O density after coordinate rotations	Always
vH2O_Cov_R	$g \cdot m^{-2} \cdot s^{-1}$	Covariance of crosswind and H_2O density after coordinate rotations	Always
wH2O_Cov_R	$g \cdot m^{-2} \cdot s^{-1}$	Covariance of vertical wind and H_2O density after coordinate rotations	Always

TABLE 4-8. Data fields in the Flux_Notes Output Table			
Data Field Name	**Units**	**Description**	**Data Field Included**
wCO2_Cov_R_F	$mg \cdot m^{-2} \cdot s^{-1}$	Covariance of vertical wind and CO_2 density after coordinate rotations and frequency corrections	Always
wH2O_Cov_R_F	$g \cdot m^{-2} \cdot s^{-1}$	Covariance of vertical wind and H_2O density after coordinate rotations and frequency corrections	Always
CO2_E_WPL_R_F	$mg \cdot m^{-2} \cdot s^{-1}$	CO_2 flux WPL correction term due to water vapor flux after coordinate rotations and frequency corrections	Always
CO2_T_WPL_R_F	$mg \cdot m^{-2} \cdot s^{-1}$	CO_2 flux WPL correction term due to sensible heat flux after coordinate rotations and frequency corrections	Always
H2O_E_WPL_R_F	$g \cdot m^{-2} \cdot s^{-1}$	H_2O flux WPL correction term due to water vapor flux after coordinate rotations and frequency corrections	Always
H2O_T_WPL_R_F	$g \cdot m^{-2} \cdot s^{-1}$	H_2O flux WPL correction term due to sensible heat flux after coordinate rotations and frequency corrections	Always
CO2_samples_Tot	count	Number of CO_2 samples without diagnostic flags and within thresholds for CO_2 signal strength (set in code to default of 0.6, see Section 4.1, *Set Constants in CRBasic Editor and Load Program (p. 9)*) and the factory calibrated CO_2 measurement range (0 to 1000 µmol/mol)	Always
H2O_samples_Tot	count	Number of H_2O samples without diagnostic flags and within thresholds for H_2O signal strength (set in code to default of 0.7, see Section 4.1, *Set Constants in CRBasic Editor and Load Program (p. 9)*) and the factory calibrated H_2O measurement range (0 to 72 mmol/mol)	Always
no_irga_head_Tot	count	Number of samples where no gas analyzer head was detected	Always
no_new_irga_data_Tot	count	Number of scans where no gas analyzer data were received	Always
irga_bad_data_f_Tot	count	Number of IRGA samples with any IRGA diagnostic flag set high	Always
irga_gen_fault_f_Tot	count	Number of gas analyzer samples with general system fault diagnostic flag	Always
irga_startup_f_Tot	count	Number of gas analyzer samples with startup diagnostic flag	Always
irga_motor_spd_f_Tot	count	Number of gas analyzer samples with motor speed diagnostic flag	Always

TABLE 4-8. Data fields in the Flux_Notes Output Table			
Data Field Name	**Units**	**Description**	**Data Field Included**
irga_tec_tmpr_f_Tot	count	Number of gas analyzer samples with TEC temperature diagnostic flag	Always
irga_src_pwr_f_Tot	count	Number of gas analyzer samples with source power diagnostic flag	Always
irga_src_tmpr_f_Tot	count	Number of gas analyzer samples with source temperature diagnostic flag	Always
irga_src_curr_f_Tot	count	Number of gas analyzer samples with source current diagnostic flag	Always
irga_off_f_Tot	count	Number of gas analyzer samples with gas head power down diagnostic flag	Always
irga_sync_f_Tot	count	Number of gas analyzer samples with synchronization diagnostic flag	Always
irga_amb_tmpr_f_Tot	count	Number of gas analyzer samples with ambient temperature probe diagnostic flag	Always
irga_amb_press_f_Tot	count	Number of gas analyzer samples with ambient pressure diagnostic flag	Always
irga_CO2_l_f_Tot	count	Number of gas analyzer samples with CO_2 l signal diagnostic flag	Always
irga_CO2_Io_f_Tot	count	Number of gas analyzer samples with CO_2 I_o signal diagnostic flag	Always
irga_H2O_I_f_Tot	count	Number of gas analyzer samples with H_2O I signal diagnostic flag	Always
irga_H2O_Io_f_Tot	count	Number of gas analyzer samples with H_2O I_o signal diagnostic flag	Always
irga_CO2_Io_var_f_Tot	count	Number of gas analyzer samples with CO_2 I_o variation diagnostic flag	Always
irga_H2O_Io_var_f_Tot	count	Number of gas analyzer samples with H_2O I_o variation diagnostic flag	Always
irga_CO2_sig_strgth_f_Tot	count	Number of gas analyzer samples with CO_2 signal strength diagnostic flag	Always
irga_H2O_sig_strgth_f_Tot	count	Number of gas analyzer samples with H_2O signal strength diagnostic flag	Always
irga_cal_err_f_Tot	count	Number of gas analyzer samples with calibration file read error flag	Always
irga_htr_ctrl_off_f_Tot	count	Number of gas analyzer samples with heater control off diagnostic flag	Always
UxFW_cov	$°C \cdot m \cdot s^{-1}$	Covariance of U_x and fine-wire thermocouple temperature	If FW05, FW1, or FW3 is used
UyFW_cov	$°C \cdot m \cdot s^{-1}$	Covariance of U_y and fine-wire thermocouple temperature	If FW05, FW1, or FW3 is used
UzFW_cov	$°C \cdot m \cdot s^{-1}$	Covariance of U_z and fine-wire thermocouple temperature	If FW05, FW1, or FW3 is used

TABLE 4-8. Data fields in the Flux_Notes Output Table			
Data Field Name	**Units**	**Description**	**Data Field Included**
uFW_cov_R	°C·m·s^{-1}	Covariance of streamwise wind and fine-wire thermocouple temperature after coordinate rotations	If FW05, FW1, or FW3 is used
vFW_cov_R	°C·m·s^{-1}	Covariance of crosswind and fine-wire thermocouple temperature after coordinate rotations	If FW05, FW1, or FW3 is used
wFW_cov_R	°C·m·s^{-1}	Covariance of vertical wind and fine-wire thermocouple temperature after coordinate rotations	If FW05, FW1, or FW3 is used
wFW_cov_R_F	°C·m·s^{-1}	Covariance of vertical wind and fine-wire thermocouple temperature after coordinate rotations and frequency corrections	If FW05, FW1, or FW3 is used
FW_samples_Tot	count	The number of valid fine-wire thermocouple measurements in the averaging period from which covariances may be calculated	If FW05, FW1, or FW3 is used
alpha	deg	Alpha angle used for coordinate rotations (regardless of planar fit or double rotation method, angle convention of Wilczak et al. 2001 used)	Always
beta	deg	Beta angle used for coordinate rotations (regardless of planar fit or double rotation method, angle convention of Wilczak et al. 2001 used)	Always
gamma	deg	Gamma angle used for coordinate rotations (regardless of planar fit or double rotation method, angle convention of Wilczak et al. 2001 used)	Always
height_measurement	m	User entered measurement height of EC sensors	Always
height_canopy	m	User entered canopy height	Always
surface_type_text	m	User entered surface type	Always
displacement_user	m	User entered displacement height; 0 for auto calculation	Always
d	m	Displacement height used in calculations; it will equal displacement_user if user entered a non-zero value; if displacement_user is zero, program will auto calculate	Always
z0	m	Roughness length	Always
z	m	Aerodynamic height	Always
L	m	Obukhov length	Always
stability_zL	m·m^{-1}	Atmospheric surface layer stability	Always

TABLE 4-8. Data fields in the Flux_Notes Output Table			
Data Field Name	**Units**	**Description**	**Data Field Included**
iteration_FreqFactor	count	Number of iterations for recalculating Obukhov length and frequency factors	Always
latitude	deg	Latitude; positive for Nothern hemisphere, negative for Southern hemisphere	Always
longitude	deg	Longitude; positive for Eastern hemisphere, negative for Western hemisphere	Always
separation_x_irga	m	Separation between sonic and gas analyzer with respect to sonic x-axis	Always
separation_y_irga	m	Separation between sonic and gas analyzer with respect to sonic y-axis	Always
separation_lat_dist_irga	m	Separation distance between sonic and gas analyzer along the axis perpendicular to oncoming wind	Always
separation_lag_dist_irga	m	Separation distance between sonic and gas analyzer along the axis parallel to oncoming wind	Always
separation_lag_scan_irga	scans	Number of scans to lag gas analyzer data relative to sonic data to account for separation along the axis of oncoming wind and wind velocity	Always
separation_x_FW	m	Separation between sonic and fine-wire thermocouple with respect to sonic x-axis	If FW05, FW1, or FW3 is used
separation_y_FW	m	Separation between sonic and fine-wire thermocouple with respect to sonic y-axis	If FW05, FW1, or FW3 is used
FW_diameter	m	Effective diameter of fine-wire thermocouple junction	If FW05, FW1, or FW3 is used
separation_lat_dist_FW	m	Separation distance between sonic and fine-wire thermocouple along axis perpendicular to oncoming wind	If FW05, FW1, or FW3 is used
separation_lag_dist_FW	m	Separation distance between sonic and fine-wire thermocouple along axis parallel to oncoming wind	If FW05, FW1, or FW3 is used
separation_lag_scan_FW	m	Number of scans to lag fine-wire thermocouple data relative to sonic data to account for separation along axis of oncoming wind and wind velocity	If FW05, FW1, or FW3 is used
time_const_FW	m	Calculated time constant of the fine-wire thermocouple	If FW05, FW1, or FW3 is used

TABLE 4-8. Data fields in the Flux_Notes Output Table			
Data Field Name	**Units**	**Description**	**Data Field Included**
MAX_LAG	scans	Maximum number of scans to lag gas analyzer or fine-wire thermocouple data with respect to sonic data when doing cross correlation for covariance maximization. For example, if MAX_LAG = 2, the program will consider lags of –2, –1, 0, +1, and +2.	Always
lag_irga	scans	The lag applied to gas analyzer data with respect to sonic data that maximizes covariance	Always
lag_FW	scans	The lag applied to fine-wire thermocouple data with respect to sonic data that maximizes covariance	Always
FreqFactor_uw_vw	number	Frequency correction factor applied to momentum fluxes	Always
FreqFactor_wTs	number	Frequency correction factor applied to wTs covariance	Always
FreqFactor_wCO2_wH2O	number	Frequency correction factor applied to wCO_2 and wH_2O covariances	Always
FreqFactor_wFW	number	Frequency correction factor applied to fine-wire thermocouple derived wFW covariance	Always
rho_d_Avg	$g \cdot m^{-3}$	Average density of dry air	Always
rho_a_Avg	$kg \cdot m^{-3}$	Average density of ambient (moist) air	Always
Cp	$J \cdot kg^{-1} \cdot K^{-1}$	Specific heat of ambient (moist) air at constant pressure	Always
Lv	$J \cdot g^{-1}$	Latent heat of vaporization	Always
panel_tmpr_Avg	°C	Average temperature of the datalogger wiring panel	Always
batt_volt_Avg	volt	Average battery voltage supplying power to the datalogger	Always
slowsequence_Tot	count	Number of slow sequences during the averaging interval (for example, the number of times biomet and energy balance sensors were measured)	Always
process_time_Avg	µs	Average processing time for each scan	Always
process_time_Max	µs	Maximum processing time for a scan	Always
buff_depth_Max	number	Maximum number of records stored in the buffer	Always

4.5 Program Sequence of Measurement and Corrections

The main correction procedures and algorithms implemented into the program are listed below. For more information on the sequence of measurements and corrections, refer to Appendix I, *EasyFlux DL Process Flow Diagram* *(p. I-1)*.

The appendices of this manual will give addition information on each major correction and its implementation in the program.

1. Despike and filter 10 Hz data using sonic and gas analyzer diagnostic codes and signal strength and measurement output range thresholds.

2. Coordinate rotations with an option to use the double rotation method (Tanner and Thurtell 1969), or planar fit method (Wilczak et al. 2001).

3. Lag CO_2 and H_2O measurements against sonic wind measurements for maximization of CO_2 and H_2O fluxes (Horst and Lenschow 2009; Foken et al. 2012), with additional constraints to ensure lags are physically possible.

4. Frequency corrections using commonly used cospectra (Moore 1986; van Dijk 2002a; Moncrieff et al. 1997) and transfer functions of block averaging (Kaimal et al. 1989), line/volume averaging (Moore 1986; Moncrieff et al. 1997; Foken et al. 2012; van Dijk 2002a), time constants (Montgomery 1947; Shapland et al. 2014; Geankoplis 1993), and sensor separation (Horst and Lenschow 2009; Foken et al. 2012).

5. A modified SND correction (Schotanus et al. 1983) to derive sensible heat flux from sonic sensible heat flux following the implementation as outlined in van Dijk 2002b. Additionally, fully corrected real sensible heat flux computed from fine-wire thermometry may be provided.

6. Correction for air density changes using WPL equations (Webb et al. 1980).

7. Data quality qualifications based on steady state conditions, surface layer turbulence characteristics, and wind directions following Foken et al. 2012.

8. If energy balance sensors are used, calculation of energy closure based on energy balance measurements and corrected sensible and latent heat fluxes.

5. References

Foken et al. (2012) ″Eddy Covariance: A Practical Guide to Measurement and Data Analysis” by Aubinet, Vesala, and Papale from Springer. This book consists of chapters that are written by specialists in the field. Chapter 4 titled “Corrections and Data Quality Control” is written by Foken et al.

Geankoplis, C.J. 1993. Transportation Processes and Unit Operation. 3rd Edition. PTR Prentice Hall, New Jersey. pp 114-131 and Appendix.

Horst, T.W., and D.H. Lenschow. 2009. Attenuation of scalar fluxes measured with spatially-displaced sensors. Boundary-Layer Meteorology 130:275-300.

Kaimal, J.C., S.F. Clifford, R.J. Lataitis. 1989. Effect of finite sampling on atmospheric spectra. Boundary-Layer Meteorology 7:827-837.

Moncrieff, J.B., J.M. Massheder, H. de Bruin, J.A. Elbers, T. Friborg, B. Heusinkveld, P. Kabat, S. Scott, H. Soegaard, A. Verhoef. 1997. A system to measure surface fluxes of momentum, sensible heat, water vapour and carbon dioxide. Journal of Hydrology 188-189:589-611.

Montgomery, R.B. 1947. Viscosity and thermal conductivity of air and diffusivity of water vapor in air. J. Meteor 4:193–196.

Moore, C.J. 1986. Frequency response corrections for eddy correlation systems. Boundary-Layer Meteorology 37:17-35.

Schotanus, P.S., F.T.M. Nieuwstadt, H.A.R. Debruin. 1983. Temperature measurement with a sonic anemometer and its application to heat and moisture flux. Boundary-Layer Meteorology 26:81-93.

Shapland, T.M., R.L. Snyder, K.T. Paw U, A.J. McElrone. 2014. Thermocouple frequency response compensation leads to convergence of the surface renewal alpha calibration. Agricultural and Forest Meteorology 189-190:36-47.

Tanner, C.B., and G.W. Thurtell. 1969. “Anemoclinometer measurements of Reynolds stress and heat transport in the atmospheric surface layer science lab”, US Army Electronics Command, Atmospheric Sciences Laboratory TR ECOM 66-G22-F. pp: R1-R10.

van Dijk, A. 2002a. Extension of 3D of “the effect of linear averaging on scalar flux measurements with a sonic anemometer near the surface” by Kristensen and Fitzjarrald. Journal of Atmospheric and Ocean Technology 19:80-19.

van Dijk, A. 2002b. The Principle of Surface Flux Physics. Research Group of the Royal Netherlands Meteorological Institute and Department of Meteorology and Air Quality with Agricultural University Wageningen. 65p.

Webb, E.K., G.I. Pearman, R. Leuning. 1980. Correction of flux measurements for density effects due to heat and water transfer. Quart. J. Met. Soc. 106:85-100.

Wilczak, J.M., S.P. Oncley, S.A. Stage. 2001. Sonic anemometer tilt correction algorithm. Boundary-Layer Meteorology 99:127-150.

Appendix A. Vapor Pressure and Dewpoint Temperature

IRGAs require an occasional span (i.e., field calibration) of water vapor. When doing a span, the humidity of the span gas must be known and entered using the On Site Zero & Span menu on the datalogger keypad (or alternatively, it is entered into ECMon, the IRGA's user-interface software). Although this humidity may be expressed in various units, dew point temperature is used since the H_2O span gas is typically generated with a dew point generator. Because dew point temperature is used, it is sometimes desirable to convert the water vapor density measurements of the IRGA to dew point temperature, especially as it provides comparability with the span gas before and after the span. Accordingly, the program converts water vapor density to dew point temperature using the algorithms described in this appendix.

A.1 Equations to Calculate Dewpoint Temperature from Water Vapor Density

An EC system measures and reports water vapor density (ρ_w in $g \cdot m^{-3}$), air temperature (T in °C), and total atmospheric pressure (P in kPa). Using the ideal gas equation, vapor pressure (e in kPa) can be calculated using:

$$e = \rho_w R_v (T + 273.15) \tag{A-1}$$

where:

R_v is the gas constant for water vapor ($4.61495 \cdot 10^{-4}$ $kPa \cdot m^3 \cdot K^{-1} \cdot g^{-1}$))

In this equation, if e were saturation water vapor pressure (e_s in kPa), T would be dew point temperature (T_d). However, since the air is unlikely to be saturated, other equations are needed to estimate the dew point temperature.

Buck (1981) developed equations to relate saturation water vapor pressure to dew point temperature in moist air. The equations were designed to be easily implemented in a computer program for conversion of saturation water vapor pressure to dew point temperature, or vice versa. The general model of equations was:

$$e_s = f_w(T_d, P) e_{ws}(T_d) \tag{A-2}$$

where:

e_s is saturation vapor pressure, and $e_{ws}(T_d)$ is saturation vapor pressure of pure water at pressure of the sea level, given by:

$$e_{ws} = a \exp\left(\frac{bT_d}{T_d + c}\right) \tag{A-3}$$

where: a, b, and c are parameters, and $f_w(T_d, P)$ is the enhancement factor that is the ratio of vapor pressure of moist air to that of pure water vapor, given by

$$f_w(T_d, P) = \frac{e_s}{e_{ws}} = A + P\left[B + C(T_d + D + EP)^2\right] \tag{A-4}$$

where:

A, B, C, D, and E are parameters. In Buck (1981), Figure 1 and Table 2 show results for $e_{ws}(T_d)$ from model (3), and Figure 3 and Table 3 show results for $f_w(T_d, P)$ from model (4). Combing the saturation water vapor pressure equation, which has an error of ± 0.05% in a temperature range of –40 to +50 °C and within a normal range of surface layer pressures, with the enhancement factor, which has an equivalent error of ±0.05% in the same temperature range, generates the following water vapor pressure equation for moist air:

$$e_s\left(T_d, P\right) = \begin{cases} 0.61121\exp\left(\frac{17.368T_d}{T_d + 238.88}\right) f_w(T_d, P) & T_d \geq 0 \\ 061121\exp\left(\frac{17.966T_d}{T_d + 247.15}\right) f_w(T_d, P) & T_d < 0 \end{cases} \tag{A-5}$$

where:

$$f_w(T_d, P) = 1.00041 + P\left[3.48 \times 10^{-5} + 7.4 \times 10^{-9}\left(T_d + 30.6 - 0.38P\right)^2\right] \tag{A-6}$$

Given measured water vapor pressure and total pressure from an EC system, the only unknown variable in equations (A-5) and (A-6) is dew point temperature. However, analytically solving the equations for T_d is not feasible due to complication from the quadratic term in equation (A-6). Fortunately, the enhancement factor is a very weak function of T_d, which is why Buck (1981) recommended that "a rough approximation of T_d will serve nicely in calculating $f_w(T_d, P)$". A question then emerges concerning what should be considered reasonable for a rough approximation. In the case that relative humidity is high, the air temperature measured by an EC system may be close enough to be a rough estimation of T_d, however this may be considered unreasonable in the sense of a numerical analysis because an error range is unknown. And in case when relative humidity is low, this approximation could differ from the true dew point temperature by more than 10 °C, making it even more unreasonable in terms of atmospheric physics. Thus another approach is proposed by Buck (1981) for calculating a more accurate approximation of T_d as described below.

A.2 Approach to Approximation of T_d for the Enhancement Factor

For general use to calculate dew point temperature (T_{d_gu} where subscript *gu* indicates general use), Buck (1981) recommended the following equation:

$$e_s\left(T_{d\_gu}, P\right) = 0.61121\exp\left(\frac{17.502T_{d\_gu}}{T_{d\_gu} + 240.97}\right) f_w(P) \tag{A-7}$$

Where:

$$f_w(P) = 1.0007 + 3.46 \times 10^{-5} P \tag{A-8}$$

Unlike $f_w(T_d, P)$ in equation (A-5), $f_w(P)$ in equation (A-7) does not include a quadratic term of dew point temperature, T_{d_gu} can be analytically expressed in terms of saturation water pressure and total pressure as

$$T_{d\_gu} = \frac{240.97\left\{\ln e_s - \ln\left[0.61121 f_w(P)\right]\right\}}{17.502 - \left\{\ln e_s - \ln\left[0.61121 f_w(P)\right]\right\}} \tag{A-9}$$

Because in equation (A-7) the saturation water vapor equation for pure water has an error limit of ±0.2% in a temperature range of –20 to +50 °C and a normal range of surface-layer pressures [see Figure 1 and Table 1 in Buck (1981)], and because the enhancement factor also has an error limit of ±0.2% in a temperature range of –40 to +50 °C [see Figure 3 and Table 3 in Buck (1981)], the dew point temperature for general use (T_{d_gu}) as calculated using equation (10) has known an error limit and can be considered a relatively accurate approximation for T_d in equation (A-6).

A.3 Dewpoint Temperature Equation

Now that a good approximation for T_d is found, *Td_gu* from equation (A-9) may be substituted for T_d into equation (A-6). The resulting enhancement factor can then be used along with measured water vapor pressure and total pressure to give a more accurate dew point temperature (T_d):

$$T_d = \begin{cases} \dfrac{238.88\left\{\ln e_s - \ln\left[0.61121 f_w(T_{d\_gu}, P)\right]\right\}}{17.368 - \left\{\ln e_s - \ln\left[0.61121 f_w(T_{d\_gu}, P)\right]\right\}} & T_{d\_gu} \geq 0 \\ \dfrac{247.15\left\{\ln e_s - \ln\left[0.61121 f_w(T_{d\_gu}, P)\right]\right\}}{17.966 - \left\{\ln e_s - \ln\left[0.61121 f_w(T_{d\_gu}, P)\right]\right\}} & T_{d\_gu} < 0 \end{cases} \tag{A-10}$$

Note that in this equation, the variable of T_{d_gu} instead of T_d in eq. 5 is used to judge the boundary for use of two sub-equations, although using either variable for the boundary should yield nearly the same result since according to Buck (1981), T_d and T_{d_gu} should be within 0.1 °C of each other as long as the magnitude of dew point temperature is less than 50 °C. Furthermore, the two sub-equations in equation (5) have the same accuracy around 0 °C dew point temperature for a range of –1 to +1 °C [see Figure 1 in Buck (1981)] and are effectively interchangeable from -1 to +1 °C. Because the two sub-equations in equation (A-10) are simply rearrangements of the two sub-equations in equation (A-5), respectively, the two sub-equations in equation (A-10) also must be interchangeable from –1 to 1 °C.

A.4 Online Flux Program

The datalogger program calculates T_d by first converting measured water vapor density to water vapor pressure, *e* (equation A-1). Because dew point temperature is the temperature at which *e* becomes the saturated vapor

pressure, e_s, we use the value of e from the IRGA in place of e_s in equation (A-10).

A.5 Reference

Buck, A. L.: 1981, "New equations for computing vapor pressure and enhancement factor", *J. Applied Meteorol*., **20**: 1527-1532.

Appendix B. Coordinate Rotations: Double Rotation Method

The covariance of vertical wind with a scalar (for example, heat, water vapor, or CO_2) yields a scalar flux. The covariance of vertical wind with horizontal wind along with air density, gives momentum flux. If the measured vertical wind is not truly normal to the surface of interest, the flux estimates are in error (Kaimal and Haugen 1969). Flow velocities measured by a three-dimensional anemometer are defined in an instrument coordinate system. Although the instrument coordinate system is defined accurately in the manufacturing process by precision machining, and field mounting may be done carefully to align the sensor's vertical axis (z_m-axis) to be perpendicular to the field surface, it is almost impossible for the z_m-axis to be aligned perfectly. Some degree of leveling errors will be present and surface undulation may occur. Tilts of the order of a degree could cause errors in excess of 100% for momentum flux (Kraus 1968). Kaimal and Haugen (1969) further confirmed that large errors can occur in the measurement of momentum flux unless the sensors are vertically aligned and horizontally leveled with a great accuracy (at least ±0.1°). The errors caused by tilt in estimates of flux can be corrected using the mathematical method of coordinate transforms based on the physical process of turbulent flows (mean vertical velocity of dry air is zero).

B.1 Matrix Transformation of Instrument to Flow Coordinate System

Let us define a 3D right-handed orthogonal instrument coordinate system where u_m, v_m, and w_m are the orthogonal components of the 3D wind vector reported by the sonic anemometer. Now suppose that it is more convenient to report the same vector but using components on another orthogonal coordinate system that we will call the flow coordinate system, where the u axis is parallel to the mean wind vector over some period of time (i.e., the streamwise vector), v is the mean crosswind component, and w is the vertical component. This is possible using the matrix transformation presented in B-1. This transformation performs the following functions: 1) the instrument coordinate system is rotated about the w_m-axis by a counterclockwise angle γ as viewed against the w_m direction to the 1st rotated coordinate system. If components are reported at this intermediary stage, u_1, v_1, w_1 are used, where subscript "1" indicates the value of variable after the 1st rotation; 2) next the coordinate system is rotated about the v_1-axis by a counterclockwise angle α as viewed down the v_1 axis. This results in the 2nd rotated system, where u_2, v_2, and w_2 are the components of the wind vector after the 2nd rotation; 3) finally the 2nd rotated system is rotated about the u_2-axis by a counterclockwise angle β as viewed against u_2 axis, resulting in the final flow coordinate system (u, v, w).

NOTE The angle rotations from the instrument coordinate system to natural flow coordinate system are used inconsistently in the literature. Tanner and Thurtell (1969) used counterclockwise rotations about vertical and stream-wise axes and clockwise rotation about lateral axis. Wilczak et al (2001) used clockwise rotations for all of the three axes. The online flux program uses the rotation convention of Wilzcak et al (2001) regardless of whether the double rotation or the planar fit method is used.

$$\begin{pmatrix} u \\ v \\ w \end{pmatrix} = \begin{pmatrix} 1 & 0 & 0 \\ 0 & \cos\beta & \sin\beta \\ 0 & -\sin\beta & \cos\beta \end{pmatrix} \begin{pmatrix} \cos\alpha & 0 & -\sin\alpha \\ 0 & 1 & 0 \\ \sin\alpha & 0 & \cos\alpha \end{pmatrix} \begin{pmatrix} \cos\gamma & \sin\gamma & 0 \\ -\sin\gamma & \cos\gamma & 0 \\ 0 & 0 & 1 \end{pmatrix} \begin{pmatrix} u_m \\ v_m \\ w_m \end{pmatrix}$$

$$= \mathbf{U}(\beta)\mathbf{V}(\alpha)\mathbf{W}(\gamma) \begin{pmatrix} u_m \\ v_m \\ w_m \end{pmatrix} = \mathbf{U}(\beta)\mathbf{V}(\alpha) \begin{pmatrix} u_1 \\ v_1 \\ w_1 \end{pmatrix} = \mathbf{U}(\beta) \begin{pmatrix} u_2 \\ v_2 \\ w_2 \end{pmatrix} \quad \text{(B-1)}$$

Where $\mathbf{U}(\beta)$, $\mathbf{V}(\alpha)$, and $\mathbf{W}(\gamma)$ are the three 3 x 3 matrices shown in the first equation of (B-1). The rotations are performed sequentially as shown in the second equation of (B-1). The 2nd and 3rd rotation angles are defined with respect to the coordinates after the preceding rotation.

B.2 Natural Wind Coordinated System

A 3D right-handed natural wind coordinate system has the u-axis parallel to the mean or streamwise flow; thus the mean wind components along v-axis ($\bar{v}$) and w-axis ($\bar{w}$) are zero, as shown in FIGURE B-1.

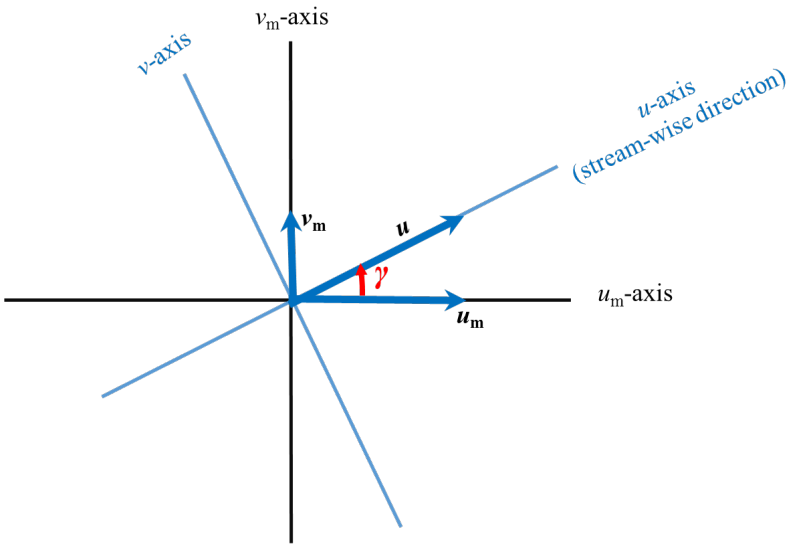

FIGURE B-1. As viewed down the z_m and z axes and assuming the vertical wind component is zero, horizontal wind components v_m and u_m are measured in the instrument coordinate system and then rotated by angle γ, yielding the streamwise wind velocity vector, u. The u and v axes of the flow coordinate system are also shown.

Because velocity in the *v* direction (orthogonal to *u* direction) is zero and flow is horizontally homogenous, the tilt in the *v* direction causes less error than in the *u* direction. Additionally, the calculation of the 3rd rotation angle assumes the following:

$$\overline{w_2' v_2'} = 0$$

which may not necessarily be true in field conditions and introduces more uncertainties; therefore, the third rotation is not recommended (Wilczak et al. 2001). The algorithm for the first two rotations is given as follows:

angle γ in FIGURE B-1 can be approximated by:

$$\gamma = \arctan\left(\frac{\overline{v}_m}{\overline{u}_m}\right) \tag{B-2}$$

This angle is the mean wind direction of 0 to 360° that is output from the CRBasic instruction of WindVector used in the datalogger. The anticlockwise angle α around the v_1-axis is given by:

$$\alpha = -\arctan\frac{\overline{w}_1}{\overline{u}_1} = -\arctan\frac{\overline{w}_m}{\overline{u}_m\cos\gamma + \overline{v}_m\sin\gamma} \tag{B-3}$$

The CRBasic function ATN2() is used to calculate (B-3) and return an angle in the range of ±180°. The result, however, must be further constrained to the range of ±90° since relative to γ, the range of this angle is narrower and should be within ±90°.

According to equation (B-1), the first two rotations are expressed as:

$$\begin{bmatrix} u_2 \\ v_2 \\ w_2 \end{bmatrix} = \begin{bmatrix} \cos\alpha\cos\gamma & \cos\alpha\sin\gamma & -\sin\alpha \\ -\sin\gamma & \cos\gamma & 0 \\ \sin\alpha\cos\gamma & \sin\alpha\sin\gamma & \cos\alpha \end{bmatrix} \begin{bmatrix} u_m \\ v_m \\ w_m \end{bmatrix} = \mathbf{R}_2 \begin{bmatrix} u_m \\ v_m \\ w_m \end{bmatrix} \tag{B-4}$$

B.2.1 Covariance of Momentum Variables after Coordinate Rotation

Using matrix operations, the covariance of the momentum variables can be reasonably found as follows:

From (B-4), the mean terms can be written as:

$$\begin{bmatrix} \overline{u}_2 \\ \overline{v}_2 \\ \overline{w}_2 \end{bmatrix} = \mathbf{R}_2 \begin{bmatrix} \overline{u}_m \\ \overline{v}_m \\ \overline{w}_m \end{bmatrix} = \begin{bmatrix} \cos\alpha\left(\overline{u}_m\cos\gamma + \overline{v}_m\sin\gamma\right) - \overline{w}_m\sin\alpha \\ 0 \\ \sin\alpha\left(\overline{u}_m\cos\gamma + \overline{v}_m\sin\gamma\right) + \overline{w}_m\cos\alpha \end{bmatrix} \tag{B-5}$$

And the fluctuation terms can be written as:

$$\begin{bmatrix} u_2' \\ v_2' \\ w_2' \end{bmatrix} = \mathbf{R}_2 \begin{bmatrix} u_m' \\ v_m' \\ w_m' \end{bmatrix} \tag{B-6}$$

Self-multiplication generates:

$$\begin{bmatrix} u_2' \\ v_2' \\ w_2' \end{bmatrix} \begin{bmatrix} u_2' & v_2' & w_2' \end{bmatrix} = \mathbf{R}_2 \begin{bmatrix} u_m' \\ v_m' \\ w_m' \end{bmatrix} \begin{bmatrix} u_m' & v_m' & w_m' \end{bmatrix} \mathbf{R}_2^{\mathsf{T}} \tag{B-7}$$

Applying Reynolds averaging yields:

$$\begin{bmatrix} \overline{u_2'^2} & \overline{u_2'v_2'} & \overline{u_2'w_2'} \\ \overline{u_2'v_2'} & \overline{v_2'^2} & \overline{v_2'w_2'} \\ \overline{u_2'w_2'} & \overline{v_2'w_2'} & \overline{w_2'^2} \end{bmatrix} = \mathbf{R}_2 \begin{bmatrix} \overline{u_m'^2} & \overline{u_m'v_m'} & \overline{u_m'w_m'} \\ \overline{u_m'v_m'} & \overline{v_m'^2} & \overline{v_m'w_m'} \\ \overline{u_m'w_m'} & \overline{v_m'w_m'} & \overline{w_m'^2} \end{bmatrix} \mathbf{R}_2^{\mathsf{T}} \tag{B-8}$$

See Appendix B.3, *Extended Equations* *(p. B-5)*, for the expansion of these matrix operations for CRBasic coding.

B.2.2 Covariance of a Scalar Variable and Momentum Variable After Second Coordinate Rotation

The covariance of a scalar variable, *Q,* and each rotated wind variable is found by multiplying the fluctuation of the scalar, *Q'*, to equation (B-6):

$$Q' \begin{bmatrix} u_2' \\ v_2' \\ w_2' \end{bmatrix} = \mathbf{R}_2 Q' \begin{bmatrix} u_m' \\ v_m' \\ w_m' \end{bmatrix} \tag{B-9}$$

Then by applying Reynolds averaging:

$$\begin{bmatrix} \overline{Q'u_2'} \\ \overline{Q'v_2'} \\ \overline{Q'w_2'} \end{bmatrix} = \mathbf{R}_2 \begin{bmatrix} \overline{Q'u_m'} \\ \overline{Q'v_m'} \\ \overline{Q'w_m'} \end{bmatrix} = \begin{bmatrix} \cos\alpha\left(\overline{Q'u_m'}\cos\gamma + \overline{Q'v_m'}\sin\gamma\right) - \overline{Q'w_m'}\sin\alpha \\ -\overline{Q'u_m'}\sin\gamma + \overline{Q'v_m'}\cos\gamma \\ \sin\alpha\left(\overline{Q'u_m'}\cos\gamma + \overline{Q'v_m'}\sin\gamma\right) + \overline{Q'w_m'}\cos\alpha \end{bmatrix} \tag{B-10}$$

B.3 Extended Equations

The extended form of Equation (B-8) is given by:

$$\begin{bmatrix} \overline{u_2'^2} & \overline{u_2'v_2'} & \overline{u_2'w_2'} \\ \overline{u_2'v_2'} & \overline{v_2'^2} & \overline{v_2'w_2'} \\ \overline{u_2'w_2'} & \overline{v_2'w_2'} & \overline{w_2'^2} \end{bmatrix} = \begin{bmatrix} \cos\alpha\cos\gamma & \cos\alpha\sin\gamma & -\sin\alpha \\ -\sin\gamma & \cos\gamma & 0 \\ \sin\alpha\cos\gamma & \sin\alpha\sin\gamma & \cos\alpha \end{bmatrix} \begin{bmatrix} \overline{u_m'^2} & \overline{u_m'v_m'} & \overline{u_m'w_m'} \\ \overline{u_m'v_m'} & \overline{v_m'^2} & \overline{v_m'w_m'} \\ \overline{u_m'w_m'} & \overline{v_m'w_m'} & \overline{w_m'^2} \end{bmatrix} \begin{bmatrix} \cos\alpha\cos\gamma & -\sin\gamma & \sin\alpha\cos\gamma \\ \cos\alpha\sin\gamma & \cos\gamma & \sin\alpha\sin\gamma \\ -\sin\alpha & 0 & \cos\alpha \end{bmatrix} \quad \text{(B-11)}$$

In Equation (B-11), the extended forms of variance terms in the matrix on the left hand side are, expressed in terms of the matrices on the right hand side:

$$\begin{cases} \overline{u_2'^2} = \cos^2\alpha\left(\overline{u_m'^2}\cos^2\gamma + \overline{v_m'^2}\sin^2\gamma\right) + \overline{w_m'^2}\sin^2\alpha + \overline{u_m'v_m'}\cos^2\alpha\sin 2\gamma - \sin 2\alpha\left(\overline{u_m'w_m'}\cos\gamma + \overline{v_m'w_m'}\sin\gamma\right) \\ \overline{v_2'^2} = \overline{u_m'^2}\sin^2\gamma + \overline{v_m'^2}\cos^2\gamma - \overline{u_m'v_m'}\sin 2\gamma \\ \overline{w_2'^2} = \sin^2\alpha\left(\overline{u_m'^2}\cos^2\gamma + \overline{v_m'^2}\sin^2\gamma\right) + \overline{w_m'^2}\cos^2\alpha + \overline{u_m'v_m'}\sin^2\alpha\sin 2\gamma + \sin 2\alpha\left(\overline{u_m'w_m'}\cos\gamma + \overline{v_m'w_m'}\sin\gamma\right) \end{cases} \quad \text{(B-12)}$$

In Equation (B-11), the extended forms of covariance terms in the matrix of left hand side are expressed in terms of the matrices on the right hand side

$$\begin{cases} \overline{u_2'v_2'} = -\frac{1}{2}\left(\overline{u_m'^2} - \overline{v_m'^2}\right)\cos\alpha\sin 2\gamma + \overline{u_m'v_m'}\cos\alpha\cos 2\gamma + \sin\alpha\left(\overline{u_m'w_m'}\sin\gamma - \overline{v_m'w_m'}\cos\gamma\right) \\ \overline{u_2'w_2'} = \frac{1}{2}\sin 2\alpha\left[\left(\overline{u_m'^2}\cos^2\gamma + \overline{v_m'^2}\sin^2\gamma\right) - \overline{w_m'^2} + \overline{u_m'v_m'}\sin 2\gamma\right] + \cos 2\alpha\left(\overline{u_m'w_m'}\cos\gamma + \overline{v_m'w_m'}\sin\gamma\right) \\ \overline{v_2'w_2'} = -\sin\alpha\left[\frac{1}{2}\left(\overline{u_m'^2} - \overline{v_m'^2}\right)\sin 2\gamma - \overline{u_m'v_m'}\cos 2\gamma\right] - \cos\alpha\left(\overline{u_m'w_m'}\sin\gamma - \overline{v_m'w_m'}\cos\gamma\right) \end{cases} \quad \text{(B-13)}$$

B.4 References

Kaimal, J. C. and Haugen, D. A.: 1969, "Some errors in the measurement of Reynolds stress", *J. Applied Meteorol.*, **8**, 460-462.

Kraus, E. B.: 1968, "What we do not know about the sea-surface wind stress", *Bull. Amer. Meteorol. Soc.*, **49**, 247-253.

Lettau, H. H.: 1968, "Three-dimensional turbulence in unidirectional mean flow", In studies of the effects of boundary modification in problems of small areas meteorology. US Army Electronics Command Technical Report ECOM66-624-A. pp: 127-156.

Sutton, O. G.: 1948, *Atmospheric turbulence*. Methuen & Co. Ltd., London.

Tanner, C. B., and Thurtell, G. W.: 1969, "Anemoclinometer measurements of Reynolds stress and heat transport in the atmospheric surface layer science lab", US Army Electronics Command, Atmospheric Sciences Laboratory TR ECOM 66-G22-F. pp: R1-R10.

Wilczak, J. M., S. P. Oncley, S. A. Stage.: 2001, "Sonic Anemometer tilt correction algorithm", *Boundary-Layer Meteorol.* **99**: 127-150.

Appendix C. Coordinate Rotations: Planar Fit Method

C.1 Planar Fit

The planar fit method of coordinate rotations is based on Wilczak et al. (2001). The method is used to transform the measured wind velocities in the right-handed measurement coordinate system of a sonic anemometer (u_m, v_m, w_m), where subscript m indicates measurement coordinate system, to the natural wind coordinate system (u, v, w) if the three rotations are performed.

The first and the second rotations in the planar fit are related to flux; that is, both rotations transform the measured wind velocities to a coordinate system with the horizontal coordinate plane parallel to the natural wind plane. The algorithm used for the planar fit rotations mathematically describes two counterclockwise coordinate rotations, first about the u_m-axis by an angle β, and second about the intermediate v_1-axis by an angle α, where the subscript 1 indicates the variable after the 1st rotation. The expression of measured fluxes in this coordinate system avoids the errors in fluxes due to the tilt of the sonic anemometer vertical axis away from the vertical axis of the natural wind flow coordinate system.

The angle α is the angle between the instrument u_m-axis and the u-v plane of natural wind (i.e., the tilt angle of the instrument vertical w_m-axis away from the natural wind vertical axis in the instrument u_m-w_m plane), where α increases clockwise in the 360° domain, which means a clockwise rotation for angle α is positive and a counterclockwise rotation is negative. The angle β is the angle between the instrument v_m-axis and the u-v plane (i.e., the tilt angle of the w_m-axis away from the natural wind vertical axis in the instrument v_m-w_m plane), where β increases counterclockwise in the 360° domain, which means a clockwise rotation for angle β is negative and a counterclockwise rotation is positive.

Even if the sonic anemometer is well secured and leveled in the field, wind may force the mounting structure and sonic anemometer to tilt, especially if the tower is tall (greater than 3 m, for example). The degree of the inclination depends on the momentum load determined mainly by wind speed. Furthermore, the natural u-v plain relative to a fixed plain varies if the field undulates and has a slope that varies from different directions. Therefore, in a given field station, the two coordinate rotation angles should be defined as a function of wind direction and wind speed. However, it is not practical to determine the angles for every possible wind direction and speed, so instead, the angles are defined for certain sectors of wind direction using data averaged over a time interval (for example, 30 min), and the dependence on wind speed is not considered.

For the online planar fit algorithm, four sectors or ranges of wind direction *in the instrument coordinate system* are used. The boundaries of sectors match the boundaries of sectors in "horizontal orientation of the sonic anemometer" for data quality classification by Foken et al. (2012). Using statistically sufficient data [see models (37) to (48) in Wilczak et al. (2001)] from the four direction sectors, a user can calculate the two angles for the four sectors, respectively.

The four ranges are given below along with the angle names used in the program:

Sector 1: [0, 60] and [300, 360]
α_60_300
β_60_300

Sector 2: (60, 170]
α_60_170
β_60_170

Sector 3: (170, 190)
α_170_190
β_170_190

Sector 4: [190, 300)
α_190_300
β_190_300

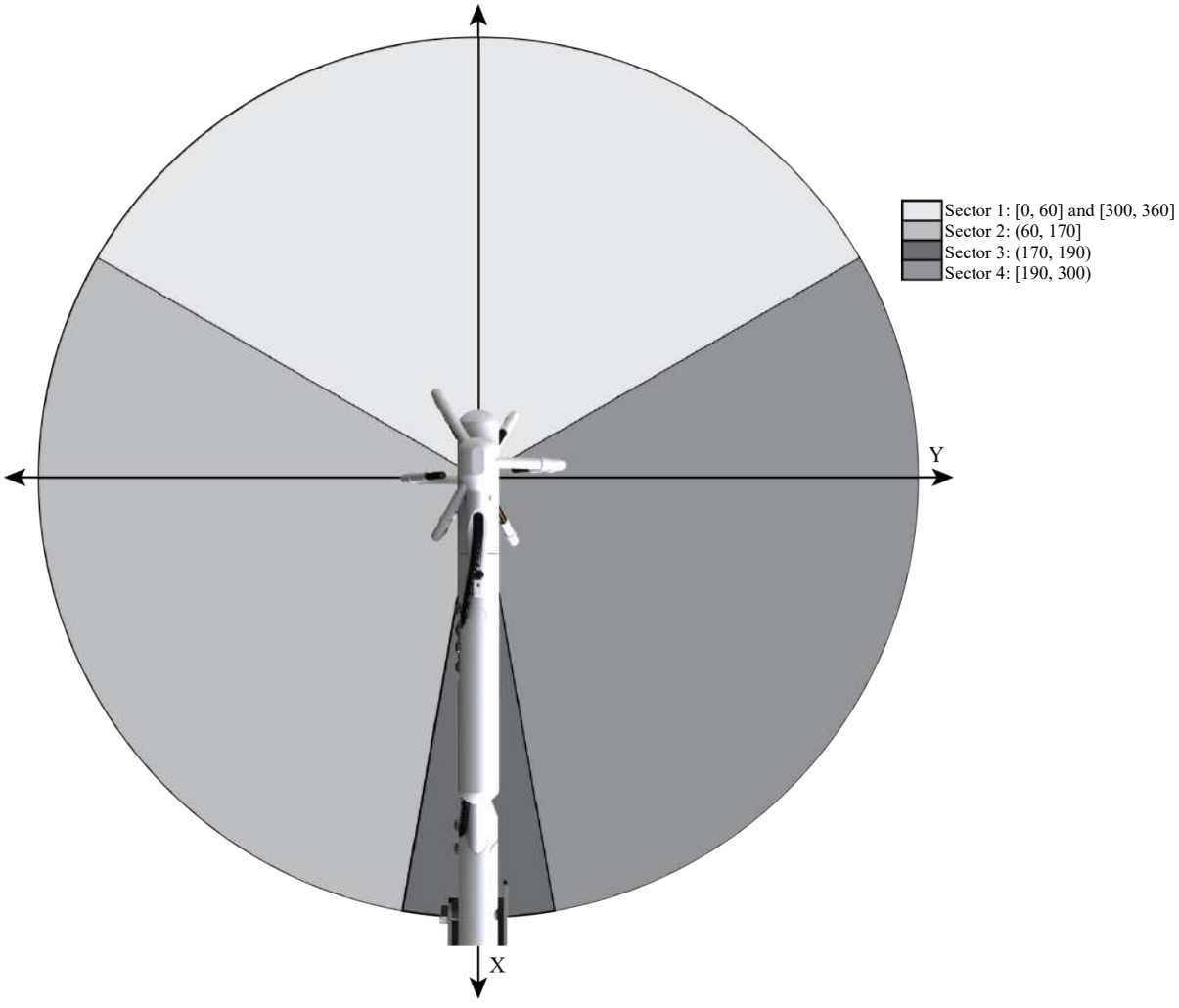

FIGURE C-1. Wind direction sectors for which planar fit angles are found by the user and entered into the program.

C.2 Algorithm

C.2.1 Variables and Model

To use the planar fit method, the user must independently (using post-processing software and time-series data for an appropriate length of time) determine the angles for each wind sector and enter these values with the datalogger keypad (see Section 4.2, *Enter Site-Specific Variables with Datalogger Keypad* (p. 10)). The online flux program will then select the appropriate angles based on the mean wind direction during the averaging interval. The CRBasic code that corresponds to this is as follows:

If (wind direction ≤ 60) OR (wind direction ≥ 300) then:
$\alpha = \alpha\_60\_300$
$\beta = \beta\_60\_300$

If (60 < wind direction ≤ 170) then:
$\alpha = \alpha\_60\_170$
$\beta = \beta\_60\_170$

If (170 < wind direction < 190) then:
$\alpha = \alpha\_170\_190$
$\beta = \beta\_170\_190$

If (190 < wind direction < 300) then:
$\alpha = \alpha\_190\_300$
$\beta = \beta\_190\_300$

Given a pitch angle of α and a roll angle of β, the three orthogonal wind velocities (u, v, w) after the two rotations can be expressed in terms of the two angles (α, β) and three directly measured wind velocities (u_m, v_m, w_m) as:

$$\begin{bmatrix} u \\ v \\ w \end{bmatrix} = \begin{bmatrix} \cos\alpha & 0 & -\sin\alpha \\ 0 & 1 & 0 \\ \sin\alpha & 0 & \cos\alpha \end{bmatrix} \begin{bmatrix} 1 & 0 & 0 \\ 0 & \cos\beta & \sin\beta \\ 0 & -\sin\beta & \cos\beta \end{bmatrix} \begin{bmatrix} u_m \\ v_m \\ w_m \end{bmatrix} \quad \text{(C-1)}$$

Further:

$$\begin{bmatrix} u \\ v \\ w \end{bmatrix} = \begin{bmatrix} \cos\alpha & \sin\alpha\sin\beta & -\sin\alpha\cos\beta \\ 0 & \cos\beta & \sin\beta \\ \sin\alpha & -\cos\alpha\sin\beta & \cos\alpha\cos\beta \end{bmatrix} \begin{bmatrix} u_m \\ v_m \\ w_m \end{bmatrix} = \mathbf{R}_p \begin{bmatrix} u_m \\ v_m \\ w_m \end{bmatrix} \quad \text{(C-2)}$$

Where $\mathbf{R_p}$ is the 3 x 3 matrix in (C-2), and subscript p indicates the planar fit approach for the rotations.

C.2.2 Covariance of Momentum Variables After Two Coordinate Rotations

Using matrix operations, the covariance of the momentum variables can be reasonably found as follows.

Using equation (C-2), we can express the mean terms as:

$$\begin{bmatrix} \overline{u} \\ \overline{v} \\ \overline{w} \end{bmatrix} = \mathbf{R}_P \begin{bmatrix} \overline{u}_m \\ \overline{v}_m \\ \overline{w}_m \end{bmatrix} = \begin{bmatrix} \overline{u}_m \cos\alpha + \sin\alpha\left(\overline{v}_m \sin\beta - \overline{w}_m \cos\beta\right) \\ \overline{v}_m \cos\beta + \overline{w}_m \sin\beta \\ \overline{u}_m \sin\alpha - \cos\alpha\left(\overline{v}_m \sin\beta - \overline{w}_m \cos\beta\right) \end{bmatrix} \tag{C-3}$$

and fluctuation terms as:

$$\begin{bmatrix} u' \\ v' \\ w' \end{bmatrix} = \mathbf{R}_p \begin{bmatrix} u'_m \\ v'_m \\ w'_m \end{bmatrix} \tag{C-4}$$

Self-multiplication generates:

$$\begin{bmatrix} u' \\ v' \\ w' \end{bmatrix} \begin{bmatrix} u' & v' & w' \end{bmatrix} = \mathbf{R}_p \begin{bmatrix} u'_m \\ v'_m \\ w'_m \end{bmatrix} \begin{bmatrix} u'_m & v'_m & w'_m \end{bmatrix} \mathbf{R}_p^T \tag{C-5}$$

Applying Reynolds averaging yields:

$$\begin{bmatrix} \overline{u'^2} & \overline{u'v'} & \overline{u'w'} \\ \overline{u'v'} & \overline{v'^2} & \overline{v'w'} \\ \overline{u'w'} & \overline{v'w'} & \overline{w'^2} \end{bmatrix} = \mathbf{R}_p \begin{bmatrix} \overline{u'^2_m} & \overline{u'_m v'_m} & \overline{u'_m w'_m} \\ \overline{u'_m v'_m} & \overline{v'^2_m} & \overline{v'_m w'_m} \\ \overline{u'_m w'_m} & \overline{v'_m w'_m} & \overline{w'^2_m} \end{bmatrix} \mathbf{R}_p^T \tag{C-6}$$

These matrix operations can then be expanded to be used in the online flux program. See Appendix C.3, *Extended Equations* *(p. C-6)*, for the coding.

C.2.3 Covariance of a Scalar Variable with Momentum Variable After Planar Fit Coordinate Rotation

The covariance of a scalar variable, *Q,* and each rotated wind variable is found by multiplying the fluctuation of the scalar, *Q'*, to equation (C-4):

$$Q' \begin{bmatrix} u' \\ v' \\ w' \end{bmatrix} = \mathbf{R}_p Q' \begin{bmatrix} u'_m \\ v'_m \\ w'_m \end{bmatrix} \tag{C-7}$$

Applying Reynolds averaging yields:

$$\begin{bmatrix} \overline{Q'u'} \\ \overline{Q'v'} \\ \overline{Q'w'} \end{bmatrix} = \mathbf{R}_P \begin{bmatrix} \overline{Q'u'_m} \\ \overline{Q'v'_m} \\ \overline{Q'w'_m} \end{bmatrix} = \begin{bmatrix} \overline{Q'u'_m}\cos\alpha + \sin\alpha\left(\overline{Q'v'_m}\sin\beta - \overline{Q'w'_m}\cos\beta\right) \\ \overline{Q'v'_m}\cos\beta + \overline{Q'w'_m}\sin\beta \\ \overline{Q'u'_m}\sin\alpha - \cos\alpha\left(\overline{Q'v'_m}\sin\beta - \overline{Q'w'_m}\cos\beta\right) \end{bmatrix} \quad \text{(C-8)}$$

C.3 Extended Equations

The extended form of Equation (C-6) is given by:

$$\begin{bmatrix} \overline{u'^2} & \overline{u'v'} & \overline{u'w'} \\ \overline{u'v'} & \overline{v'^2} & \overline{v'w'} \\ \overline{u'w'} & \overline{v'w'} & \overline{w'^2} \end{bmatrix} = \begin{bmatrix} \cos\alpha & \sin\alpha\sin\beta & -\sin\alpha\cos\beta \\ 0 & \cos\beta & \sin\beta \\ \sin\alpha & -\cos\alpha\sin\beta & \cos\alpha\cos\beta \end{bmatrix} \begin{bmatrix} \overline{u_m'^2} & \overline{u_m'v_m'} & \overline{u_m'w_m'} \\ \overline{u_m'v_m'} & \overline{v_m'^2} & \overline{v_m'w_m'} \\ \overline{u_m'w_m'} & \overline{v_m'w_m'} & \overline{w_m'^2} \end{bmatrix} \begin{bmatrix} \cos\alpha & 0 & \sin\alpha \\ \sin\alpha\sin\beta & \cos\beta & -\cos\alpha\sin\beta \\ -\sin\alpha\cos\beta & \sin\beta & \cos\alpha\cos\beta \end{bmatrix} \quad \text{(C-9)}$$

In equation (C-9), the extended forms of variance terms in the matrix on the left hand side are expressed in terms of the matrices on the right hand side:

$$\begin{cases} \overline{u'^2} = \overline{u_m'^2}\cos^2\alpha + \sin^2\alpha\left(\overline{v_m'^2}\sin^2\beta - \overline{v_m'w_m'}\sin 2\beta + \overline{w_m'^2}\cos^2\beta\right) + \sin 2\alpha\left(\overline{u_m'v_m'}\sin\beta - \overline{u_m'w_m'}\cos\beta\right) \\ \overline{v'^2} = \overline{v_m'^2}\cos^2\beta + \overline{v_m'w_m'}\sin 2\beta + \overline{w_m'^2}\sin^2\beta \\ \overline{w'^2} = \overline{u_m'^2}\sin^2\alpha + \cos^2\alpha\left(\overline{v_m'^2}\sin^2\beta - \overline{v_m'w_m'}\sin 2\beta + \overline{w_m'^2}\cos^2\beta\right) - \sin 2\alpha\left(\overline{u_m'v_m'}\sin\beta - \overline{u_m'w_m'}\cos\beta\right) \end{cases} \quad \text{(C-10)}$$

In equation (C-9), the extended forms of covariance terms in the matrix of the left hand side are expressed in terms of the matrices on the right hand side:

$$\begin{cases} \overline{u'v'} = \sin\alpha\left[\frac{1}{2}\left(\overline{v_m'^2} - \overline{w_m'^2}\right)\sin 2\beta - \overline{v_m'w_m'}\cos 2\beta\right] + \cos\alpha\left(\overline{u_m'v_m'}\cos\beta + \overline{u_m'w_m'}\sin\beta\right) \\ \overline{u'w'} = \frac{1}{2}\sin 2\alpha\left(\overline{u_m'^2} - \overline{v_m'^2}\sin^2\beta - \overline{w_m'^2}\cos^2\beta + \overline{v_m'w_m'}\sin 2\beta\right) - \cos 2\alpha\left(\overline{u_m'v_m'}\sin\beta - \overline{u_m'w_m'}\cos\beta\right) \\ \overline{v'w'} = -\cos\alpha\left[\frac{1}{2}\left(\overline{v_m'^2} - \overline{w_m'^2}\right)\sin 2\beta - \overline{v_m'w_m'}\cos 2\beta\right] + \sin\alpha\left(\overline{u_m'v_m'}\cos\beta + \overline{u_m'w_m'}\sin\beta\right) \end{cases} \quad \text{(C-11)}$$

C.4 References

Tanner, C. B. and Thurtell, G. W.: 1969, "Anemoclinometer measurements of Reynolds stress and heat transport in the atmospheric surface layer", *Research and Development Tech. Report ECOM 66-G22-F*.

Wilczak, J.M., S. P. Oncley, S. A. Stage.: 2001, "Sonic Anemometer tilt correction algorithm", *Boundary-Layer Meteorol*. **99**: 127-150.

Foken et al. (2012) ″Eddy Covariance: A Practical Guide to Measurement and Data Analysis" by Aubinet, Vesala, and Papale from Springer. This book consists of chapters that are written by specialists in the field. Chapter 4 titled "Corrections and Data Quality Control" is written by Foken et al.

Appendix D. Frequency Corrections

D.1 Introduction

The flux of any scalar (e.g., heat, CO_2, or H_2O) or momentum is a summed amount of the scalar or momentum through a unit area per unit time (e.g., g m^{-2} s^{-1} for H_2O) that is transported by eddies of various frequencies (i.e., various sizes and velocities). The relative contribution of flux as a function of eddy frequency results in a cospectrum for covariance. The total or net flux is found by integrating over this cospectrum. In order to generate an accurate cospectrum, a measurement system must be able to measure and process fluctuations at all frequencies that contribute to the flux. In practice, however, sensor measurements and digital processing methods cannot fully capture the instantaneous changes at all frequencies. The uncaptured changes related to larger eddies results in low frequency losses, and the uncaptured changes related to smaller eddies results in high frequency losses. Accounting for these frequency losses requires the corrections described herein.

D.2 Frequency Loss

D.2.1 High Frequency Loss

High frequency loss is caused by sensor response delay, signal averaging over the measurement path or volume (line/volume averaging), sensor separation, and low-pass filtering. A brief description of each of these causes is provided below.

Response delay: A sensor requires a finite amount of time to measure a stimulus. When fluctuations of a scalar or wind occur faster than this time, high frequency losses occur. The response delay is described using a time constant defined as the time the sensor requires to respond to 63.2% of a change in the input stimulus.

Line/volume averaging: Most sensors measure the change in a variable of interest over a linear measurement path (CSAT3) or measurement volume (KH20) and report its spatially averaged value over that path or volume at the measurement time. Such a sensor cannot accurately report a change in the variable at a scale of eddies smaller than the dimension of the path or volume, which attenuates the signal at high frequencies.

Separation: A covariance of wind velocity with CO_2 or H_2O concentration is measured using two sensors: a sonic anemometer and an infrared gas analyzer (IRGA). In most two-sensor combinations, except for the IRGASON which integrates both sensors into a single head, the wind velocities and gas concentrations are measured separately in different measurement volumes. This means that a single eddy may be measured at different times by the two sensors when the eddy dimension is smaller than the separation, or when a large eddy boundary moves between the two sensors during measurement. This results in signal attenuation at high frequencies because the cross correlation of wind velocities to scalar variable decreases with increases in separation (Kaimal and Finnigan 1994). Another example of two separated sensors is to use a sonic anemometer and a fine-wire thermocouple (for example, FW05, FW1, and FW3) for sensible heat flux to measure covariance of wind velocity with air temperature.

Low-pass filtering: A low-pass filter of Finite Impulse Response (FIR) improves the data quality for spectral analysis by removing the aliasing effect on the pass-frequency band due to signals at higher frequencies (i.e., frequency stop-band), but sharply attenuates the signal beyond the user-selected bandwidth (i.e., frequency pass-band; Campbell Scientific, 2014). This attenuation helps reduce unwanted aliasing effect on the frequency pass-band, but it may also result in the loss of high frequency fluxes depending on the sampling rate and frequency pass-band.

NOTE The EC100 electronics used with the IRGASON and the EC150/CSAT3A has five options for bandwidth (i.e., pass-band): 5, 10, 12.5, 20, or 25 Hz. For each option, the filter attenuates the signals at frequencies beyond the bandwidth.

D.2.2 Low Frequency Loss

Fluxes are typically calculated by taking a block average of the covariance and other related variables over a 30-minute or longer interval. The bock averaging is a high-pass filter, which causes low-frequency loss (Kaimal et al., 1989).

D.3 Model for Frequency Loss Corrections

The frequency loss of covariance is determined by the frequency losses of each variable from which the covariance is calculated. The correction for this loss is described using a general correction model for covariance of any two variables.

Suppose the measured covariance is given by:

$$\overline{\left(\alpha' w'\right)}_r$$

Where α can represent T for temperature (°C), ρ_{co2} for partial CO_2 density (mg·m^{-3}), ρ_{h2o} for partial H_2O density (g·m^{-3}), or u (or v) for horizontal wind speed (m·s^{-1}); w is vertical wind speed (m·s^{-1}); prime is the departure of variable from its mean; over-bar denotes the block time average; and subscript r represents a variable after coordinate rotation correction. Then, the frequency-corrected covariance is given by:

$$\overline{\left(\alpha' w'\right)}_{rf}$$

where subscript f indicates a variable after frequency correction and is defined as [eq. 1 in Moore (1986)]:

$$\overline{\left(\alpha' w'\right)}_{rf} = \overline{\left(\alpha' w'\right)}_r \left\{ \frac{\int_0^\infty C_{\alpha w}(f)df}{\int_0^\infty T_{\alpha w}(f) C_{\alpha w}(f)df} \right\} \qquad \text{(D-1)}$$

where other variables are defined as follows:

f – cyclic frequency

$C_{\alpha w}(f)$ – cospectrum of α with w, which is the distribution of covariance of α and w as a function of frequency.

$T_{\alpha w}(f)$ – transfer function, defined as the relative response to a measured signal of wind or scalar at f, ranging from 0 for no response to 1 for full response. The transfer function here is the total transfer function that is the combined system response of all sensors and digital processors to report the signals of covariance of α with w. It is a product of all sub-transfer functions (see Appendix D.8, *Sub-Transfer Functions* *(p. D-12)*).

The term in the curly brackets is defined as a frequency correction factor. Evaluating this factor requires determination of the total transfer function and the cospectrum within the integration. The total transfer function is a multiplication of sub-transfer functions (see Appendix D.8, *Sub-Transfer Functions* *(p. D-12)*). A sub-transfer function is covariance-specific, depending on flow aerodynamics, sensor configuration, and data processing method. The cospectrum is also covariance-specific, depending on aerodynamic height, wind speed, and atmospheric stability in the surface layer (see Appendix D.6, *Surface Layer Atmospheric Stability* *(p. D-8)*).

D.4 Covariance Variables Requiring Frequency Corrections

This section lists the covariances of variables that require frequency corrections.

D.4.1 Momentum Covariance

Rotated wind components including *u, v,* and *w* are derived from the sonic anemometer. The covariance of these variables shown below require frequency correction:

$$\overline{\left(v'w'\right)_r} \quad \text{and} \quad \overline{\left(u'w'\right)_r}$$

Note that both of these covariances are used for calculating friction velocity (a scaling parameter in the surface layer).

D.4.2 Sonic Temperature Related Covariance

The following covariances are from measurements from the sonic anemometer and IRGA and require frequency correction:

$$\overline{\left(T_s'w'\right)_r} \quad \text{and} \quad \overline{\left(T_c'w'\right)_r}$$

Where T_s is sonic temperature and T_c is air temperature calculated from sonic temperature, water vapor density, and pressure. The datalogger program calculates sonic buoyancy flux, $\overline{\left(T_s'w'\right)_r}$, each half hour and then applies the sonic sensible heat flux (SND) correction to convert the result to buoyancy flux. The SND correction requires inputs such as the mean water vapor as measured by the IRGA and air density, which requires mean air temperature. The mean air temperature may come from the EC100's temperature probe in the case of the EC150/CSAT3A, or from T_c in the case of the IRGASON since the colocated measurements allow for time series calculation of T_c from T_s and water vapor density.

NOTE T_c is considered the most accurate since it does not suffer from solar heating or radiative cooling. However, T_c can only be calculated using an IRGASON since the sonic temperature and water vapor density measurements must be made in the exact same volume. Pressure in the sample volume is also required, but it is assumed that there is negligible difference between the pressure in the sample volume and the pressure measured by the EC100's barometer.

D.4.3 Air Temperature Related Covariance

Similar to sonic temperature, covariances from measurements of air temperature from a fine-wire thermocouple such as the FW05, FW1, and FW3 (hereafter referred as FW), also should be corrected.

$$\left(\overline{T'_{FW}w'}\right)_r$$

where T_{FW} is air temperature and subscript FW indicates a fine-wire thermocouple measurement.

D.4.4 CO_2 and H_2O Related Covariance

Covariances of CO_2 or H_2O (measured by the IRGA) with vertical wind (measured by the sonic anemometer) must be corrected.

$$\left(\overline{\rho'_{CO2}w'}\right)_r \ , \ \left(\overline{\rho'_{H2O}w'}\right)_r$$

where ρ_{CO2} is the mass density of CO_2, and ρ_{H2O} is mass density of H_2O.

D.5 Sensor Configuration and Separation Variables

Sensor configuration variables, which are required for determining frequency corrections used in sub-transfer functions that lead to the overall transfer function in Equation D-1, are described in this section and include descriptors such as the measurement path dimensions of the sonic anemometer and gas analyzer, sensor separation between the sonic anemometer and gas analyzer, and the diameter of the fine-wire thermocouple.

All of these configuration variables are set inside the program. Some of the variables, such as those dealing with sensor separation, depend on how the sensors are installed at a site; following installation, the variables should be measured, recorded, and entered into the program through the datalogger keypad (see Section 4.2, *Enter Site-Specific Variables with Datalogger Keypad (p. 10)*).

D.5.1 Path Length Variables

For the CSAT3A or IRGASON sonic anemometer, the path length, $l_{pt\_CSAT,}$ is equal to 0.11547 m. The subscript *pt* indicates path.

For the EC150 or IRGASON gas analyzer, the path length, $l_{pt\_IRGA,}$ is equal to 0.1531 m.

D.5.2 Separation Variables

In order to find the separation variables, which are entered into the program through the datalogger keypad (see Section 4.2, *Enter Site-Specific Variables with Datalogger Keypad (p. 10)*), the center of the gas analyzer measurement path relative to the sonic coordinate system (see FIGURES D-1 and D-2) must be known. Determination of each of these variables is described below.

*IRGA Coord x (*reported as the datafield *separation_x_irga* in the Flux_Notes output table) is the abscissa (x-coordinate) of the center of the gas analyzer optical path in the sonic coordinate system. It should be set to 0 m for the IRGASON and ranges from 0.041 to 0.091 m for the EC150 and CSAT3A, depending on the EC150's position in its standard mounting bracket. When an EC150 and CSAT3A are used, the program assumes a default value of 0.041 m, which corresponds to the furthest forward position of the EC150 in its standard mounting bracket.

IRGA Coord y (reported as the datafield *separation_y_irga* in the Flux_Notes output table) is the ordinate (y-coordinate) of the center of the gas analyzer optical path in the sonic coordinate system. It should be set to 0 m for the IRGASON and ranges from 0.029 to 0.033 for the configuration of EC150 and CSAT3A, depending on the EC150's position in its standard mounting bracket. When an EC150 and CSAT3A are used, the program assumes a default value of 0.029 m, which corresponds to the furthest forward position of the EC150 in its standard mounting bracket.

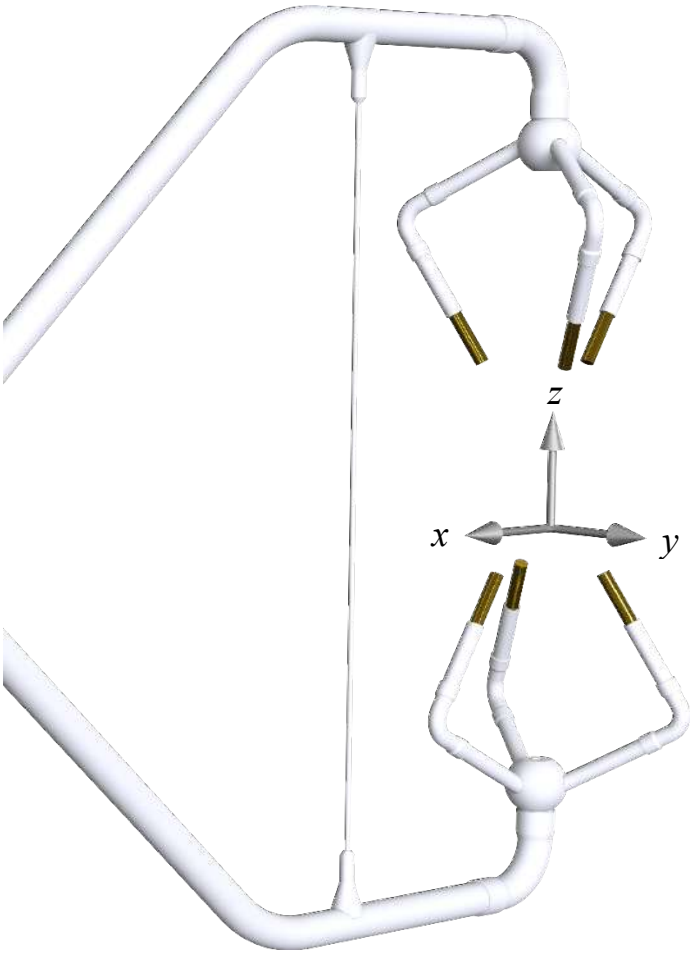

FIGURE D-1. The sonic coordinate system is shown with positive x, y, and z axes. Note that the origin of the coordinate system should be exactly in the center of the sonic volume; as shown, the origin has been moved slightly downwards for convenience in displaying the positive z-axis.

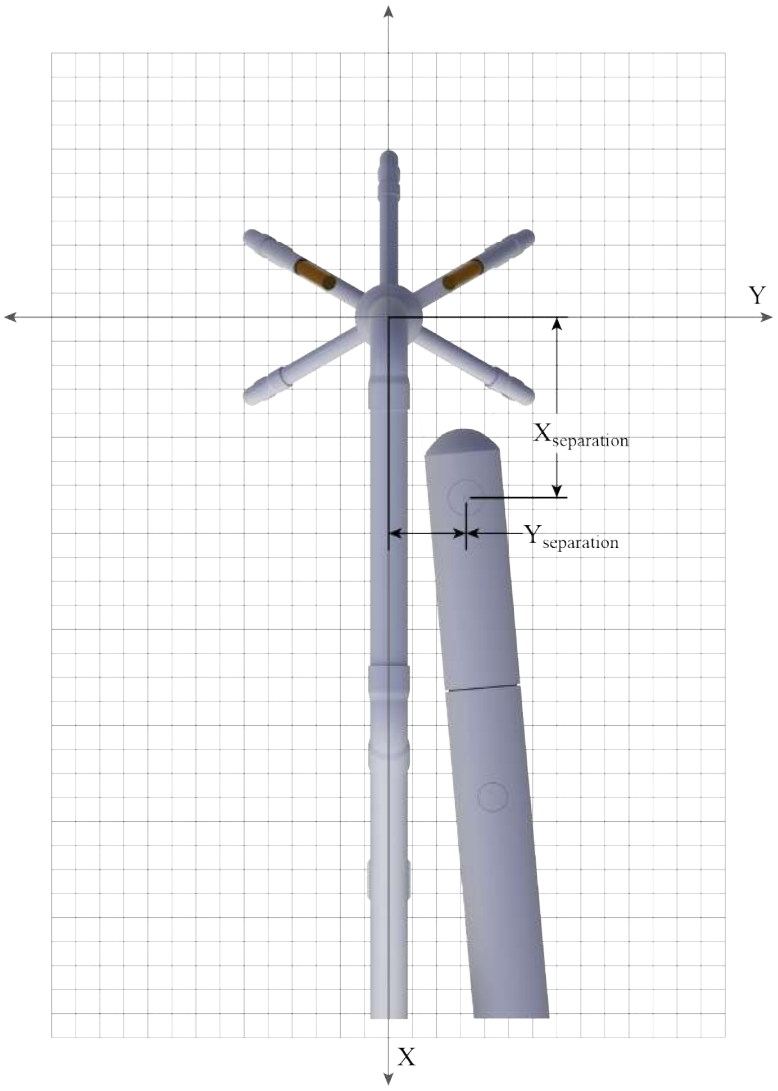

FIGURE D-2. The x and y spatial separations between a CSAT3A and EC150.

D.5.3 Fine-Wire Thermocouple

If a fine wire thermocouple is used, additional configuration and separation variables must be entered into the program using the datalogger keypad (see Section 4.2, *Enter Site-Specific Variables with Datalogger Keypad* (p. 10)). These variables are described below.

Configuration Variable *FW Dim*
Depending on the fine wire thermocouple model being used, one of the following constants should be selected as the value for *FW Dim,* the configuration variable for dimension or diameter of the fine wire*:*

FW05_DIA = 1.27×10^{-5} m for the diameter of the FW05

FW1_DIA = 2.54×10^{-5} m for the diameter of the FW1

FW3_DIA = 7.62×10^{-5} m fir the diameter of the FW3

Separation variables
FW Coord x (reported as the datafield *separation_x_FW* in the *Flux_Notes* output table) is the abscissa (x-coordinate) of fine-wire thermocouple junction in the sonic coordinate system (see FIGURES D-1 and D-2).

FW Coord y (reported as the datafield *separation_y_FW* in the *Flux_Notes* output table) is the ordinate (y-coordinate) of fine-wire thermocouple junction in the sonic coordinate system.

The values for *FW Coord x* and *FW Coord y* are defaulted to 0.006m and 0.03259 m, respectively, for the IRGASON and CSAT3A. These correspond to the standard mounting and lengths of the FW05, FW1, and FW3. These values may be easily edited at the site using the datalogger keypad (see Section 4.2, *Enter Site-Specific Variables with Datalogger Keypad* (p. 10)).

D.6 Surface Layer Atmospheric Stability

The cospectrum in model (D-1) depends on surface layer stability. The stability is defined as the ratio of aerodynamic height (z) to Obukhov length (L). This ratio is greater than 0 if surface layer is stable, 0 if neutral, and less than 0 if unstable. The cospectrum has different model forms for neutral/unstable and stable conditions (Kaimal et al., 1972). The stability is used as a variable in the cospectrum model for stable conditions, but not in the models for neutral or unstable conditions. The sub-sections below describe how the program calculates values for aerodynamic height and Obukhov length in order to determine stability. Stability during each averaging interval is reported in the *Flux_Notes* output table as *stability_zL*.

D.6.1 Aerodynamic Height

Aerodynamic height is the measurement height (z_m) minus zero displacement height, given by:

$$z = z_m - d \tag{D-2}$$

where d is the zero displacement height.

1. *Measurement height* is the height of the center of the measurement volume of the eddy-covariance sensors above the surface of the ground. It is entered into the program as the variable *Meas Height* through the datalogger keypad (see Section 4.2, *Enter Site-Specific Variables with Datalogger Keypad* (p. 10)) following installation and whenever the sensor height is adjusted. In the *Flux_Notes* output table, the last value to be entered is reported as *height_measurement.*

2. *Displacement height* is the mean height at which the momentum flux is balanced by the momentum absorption into rough surface elements such as plants or the ground surface. In the case of flat, bare land, the height of aerodynamic ground surface is effectively zero. Inside a canopy, the aerodynamic surface is elevated to some height above the ground surface. This elevated height is defined as the displacement height.

The displacement height can be provided through three options:

a. Provided by user and input through the datalogger keypad (see Section 4.2, *Enter Site-Specific Variables with Datalogger Keypad (p. 10)*) as the variable *d*. The last value to be entered is recorded as *displacement_user* in the *Flux_Notes* output table.

b. If the user leaves the displacement height variable, *d*, as zero and the surface type is a crop or grass canopy, the displacement height is estimated in the program using equation 4.5 on page 138 in Rosenberg, et al. (1983):

$$d = 10^{0.979 \log_{10} h_c - 0.154} \quad \text{(D-2a)}$$

where h_c is canopy height that is measured periodically by the user throughout the growing season and entered into the program with the datalogger keypad (see Section 4.2, *Enter Site-Specific Variables with Datalogger Keypad (p. 10)*). It should be set to a constant in the non-growing season.

For surface stypes other than crop, grass, or forest, the ¾ rule, or $d = 3h_c/4$, is an alternative [p. 71 in Kaimal and Finnigan (1994)].

c. If eddy-covariance variables are measured above a forest canopy, the 2/3 rule (page 116, Oke, 1987) will be used in the program as:

$$d = 2h_c / 3 \quad \text{(D-2b)}$$

In the program, whenever the canopy height and surface type are re-entered (see Section 4.2, *Enter Site-Specific Variables with Datalogger Keypad (p. 10)*), the zero displacement height is recalculated [Equations (D-2a) and (D-2b)] unless the user entered a specific value. Aerodynamic height (Equation D-2) is also recalculated. In the *Flux_Notes* output table, the value for displacement height used during each averaging period is reported as *d.*

D.6.2 Obukhov Length (L)

Obukhov length, as given by Rebmann et al. (2012) is an indication of surface layer depth, in which both shear and buoyancy drive the turbulent flows, generating turbulence kinetic energy. It is given by:

$$L = -\frac{u_*^3}{k \cdot (g_0 / \overline{T}_s) \cdot \left(\overline{w' T_s'}\right)_{rf}} \quad \text{(D-3)}$$

where: k = von Karman constant (0.41)

g_0 = acceleration due to gravity at the sea level (9.81 m·s^{-2})

$\overline{T}_s$ = sonic temperature (K)

u_* – friction velocity (m s^{-1}), given by [p. 67 in Stull (1988) and p. 384 in Wallace and Hobbs (2006)]:

$$u_* = \left(\left(\overline{u'w'} \right)_{rf}^2 + \left(\overline{v'w'} \right)_{rf}^2 \right)^{\frac{1}{4}} \quad \text{(D-4)}$$

NOTE Recalculation of the Obukhov length improves accuracy of the frequency correction factor.

The Obukhov length is used to determine the form of a cospectrum for a given covariance and as an independent variable in the cospectrum for stable conditions (see Appendix D.7, *Cospectra* *(p. D-10)*, also see Kaimal 1972). During initial operation of the program and in each calculation interval (for example, 30 min), the Obukhov length must be preliminarily estimated using uncorrected friction velocity and buoyancy flux. Based on this preliminary Obukhov length, the appropriate cospectra function, $C_{\alpha w}(f)$, [see Equation (D-1)] can be identified and used for the calculation of correction factors to preliminarily correct these three covariance variables :

$$\left(\overline{u'w'} \right)_r, \left(\overline{v'w'} \right)_r, \text{ and } \left(\overline{w'T'} \right)_r$$

Thereafter, the Obukhov length can be recalculated using these corrected covariance variables, which then requires the frequency correction factors to be recalculated, which can then be used to further correct the covariance values. This iterative calculation of Obukhov length, frequency correction factors, and covariance values is accomplished in the program using the While()… Wend() instructions and continues until the change in frequency correction factors is smaller than 0.0001 (Foken et al., 2012) or until 10 iterations have completed. The final Obukhov value is reported in the *Flux_Notes* output table as *L*, and the number of iterations performed is reported as *iteration_FreqFactor*.

NOTE For stable conditions, only the initial calculation of Obukhov length is required; recalculation is not needed because Obukhov length is not used in the equations for cospectra under stable conditions and the sign of Obukhov does not change after recalculations of correction for covariance values used to calculate Obukhov length (see Appendix D.7, *Cospectra* *(p. D-10)*).

D.7 Cospectra

This section contains mathematical descriptions of the cospectra functions used in Equation (D-1) for various covariance variables in different stabilities.

D.7.1 Cospectra for z/L > 0 (stable surface layer)

For covariances $\left(\overline{u'w'} \right)_r$ or $\left(\overline{v'w'} \right)_r$:

[from equation 21 in Moore (1986) and eq. 2.80 and Table 2.1 in van Dijk (2002b)]

$$fS_{uw}(f) = \frac{\frac{z}{\overline{u}} f}{A_{uw} + B_{uw}\left(\frac{z}{\overline{u}} f\right)^{2.1}}$$

$$A_{uw} = 0.124\left(1 + 7.9\frac{z}{L}\right)^{0.75} \qquad \text{(D-5)}$$

$$B_{uw} = 23.252\left(1 + 7.9\frac{z}{L}\right)^{-0.825}$$

where $\overline{u}$ is the total mean velocity, or the mean horizontal velocity after rotation about *w*-axis.

For covariances $\overline{(T_s' w')}_r$, $\overline{(T_c' w')}_r$, $\overline{(T_{FW}' w')}_r$, $\overline{(\rho_{CO2}' w')}_r$, and $\overline{(\rho_{H2O}' w')}_r$:

[from equation 21 in Moore (1986), equations 12 and 13 in Moncrieff et al. (1997), and equation 2.80 and Table 2.1 in van Dijk (2002b)]

$$fS_{sw}(f) = \frac{\frac{z}{\overline{u}} f}{A_{sw} + B_{sw}\left(\frac{z}{\overline{u}} f\right)^{2.1}}$$

$$A_{sw} = 0.284\left(1 + 6.4\frac{z}{L}\right)^{0.75} \qquad \text{(D-6)}$$

$$B_{sw} = 9.3447\left(1 + 6.4\frac{z}{L}\right)^{-0.825}$$

where subscript *s* is used to represent a scalar variable such as T_s, T_c, T_{fw}, ρ_{co2}, ρ_{co2_LI}, ρ_{h2o}, ρ_{h2o_kh}, or ρ_{h2o_LI}.

D.7.2 Cospectra for z/L ≤ 0 (neutral to unstable)

For covariances $\overline{\left(u'w'\right)}_r$ or $\overline{\left(v'w'\right)}_r$:

[from equation 21 in Moore (1986) and eq. 2.80 and Table 2.1 in van Dijk (2002b)]

$$fS_{uw}(f)=\begin{cases}\dfrac{20.78\dfrac{z}{\overline{u}}f}{\left(1+31\dfrac{z}{\overline{u}}f\right)^{1.575}} & \dfrac{z}{\overline{u}}f<0.24\\[2ex] \dfrac{12.66\dfrac{z}{\overline{u}}f}{\left(1+9.6\dfrac{z}{\overline{u}}f\right)^{2.4}} & \dfrac{z}{\overline{u}}f\geq 0.24\end{cases} \quad \text{(D-7)}$$

For covariances $\overline{(T_s'w')}_r$, $\overline{(T_c'w')}_r$, $\overline{(T_{FW}'w')}_r$, $\overline{(\rho_{CO2}'w')}_r$, and $\overline{(\rho_{H2O}'w')}_r$:

[from equation 25 in Moore (1986), equations 15 and 16 in Moncrieff. et al. (1997) and eq. 2.84 and Table 2.1 in van Dijk (2002b)]

Similar to stable conditions, the cospectrum of temperature with vertical velocity in neutral or unstable conditions presented below may be used as the cospectrum of other individual scalars with vertical velocity.

$$fS_{sw}(f)=\begin{cases}\dfrac{12.92\dfrac{z}{\overline{u}}f}{\left(1+26.7\dfrac{z}{\overline{u}}f\right)^{1.375}} & \dfrac{z}{\overline{u}}f<0.54\\[2ex] \dfrac{4.378\dfrac{z}{\overline{u}}f}{\left(1+3.78\dfrac{z}{\overline{u}}f\right)^{2.4}} & \dfrac{z}{\overline{u}}f\geq 0.54\end{cases} \quad \text{(D-8)}$$

D.8 Sub-Transfer Functions

The total transfer function found in Equation (D-1) consists of the products of all sub-transfer functions of each variable used to calculate a covariance. Sub-transfer functions account for block averaging, line averaging, sensor volume averaging (negligible in the cases of the IRGASON and EC150), electronic data filtering, sensor time response (for example, air temperature measured using FW sensors), and sensor separation (for example, the *x* and *y* separations of CSAT3A and EC150). These sub-transfer functions are described in the following sections.

D.8.1 Finite Time Block Averaging

The sub-transfer function for finite time block averaging is derived from equation 4 in Kaimal et al. (1989) and equation 3 in Massman (2000).

Every covariance is an average covariance over a finite block of time as defined by the user (e.g., 30 or 60 minutes). Having a finite time block leads to

attenuation of low frequencies, and therefore, all covariance variables require a sub-transfer function to account for this. The sub-transfer function [$T_{sw\_BA}(f, T_{ba})$] due to a finite block averaging period (T_{ba}) is given by:

$$T_{sw\_BA}(f, T_{ba}) = 1 - \frac{\sin^2(\pi T_{ba} f)}{(\pi T_{ba} f)^2} \tag{D-9}$$

where subscript *BA* or *ba* indicates ***b***lock ***a***veraging and T_{ba} =1800 seconds if a period of 30 minutes is used.

D.8.2 Line Averaging

Sub-transfer functions for variances of individual variables
The attenuation of variance of vertical velocity (*w*) from line average is described using equation 9 in Moore (1986), page 610 in Moncrieff (1997), and equation 4.10 in Foken et al (2012).

The resulting sub-transfer function applied to vertical wind variance [$T_{ww\_LA}(f, l_{pt\_csat}, u)$] is as follows:

$$T_{ww\_LA}(f, l_{pt\_csat}, \overline{u}) = \frac{4}{\left(2\pi l_{pt\_csat} / \overline{u}\right) f} \left(1 + \frac{\exp(-\frac{2\pi l_{pt\_csat}}{\overline{u}} f)}{2} - \frac{1.5\left[1 - \exp(-\frac{2\pi l_{pt\_csat}}{\overline{u}} f)\right]}{\left(2\pi l_{pt\_csat} / \overline{u}\right) f} \right) \tag{D-10}$$

The sub-transfer function for horizontal velocity variance [$T_{uu\_LA}(f, l_{pt\_csat}, u)$] has not been well defined for sonic anemometry [page 22 in Moore (1986) and page 46 in van Dijk (2002b)]. Therefore, the sub-transfer function used by van Dijk (2002b) for horizontal wind is adopted as an approximation [eq. 2.70 in van Dijk (2002b)]:

$$T_{uu\_LA}(f, l_{pt\_csat}, \overline{u}) = \left[\frac{\sin\left(\frac{\pi l_{pt\_csat}}{\overline{u}} f\right)}{\frac{\pi l_{pt\_csat}}{\overline{u}} f} \right]^2 \tag{D-11}$$

For the variance of a scalar, *s,* measured by a gas analyzer, the sub-transfer function , $T_{ss\_LA}(f, l_{pt\_irga}, \overline{u})$, is given as follows [eq. 7 in Moore (1986) and eq. 2.68 in van Dijk (2002b), eq. 4.12 in Foken et al (2012)]:

$$T_{ss\_LA}(f, l_{pt\_irga}, \overline{u}) = \frac{1}{\frac{2\pi l_{pt\_irga}}{\overline{u}} f} \left(3 + \exp(-\frac{2\pi l_{pt\_irga}}{\overline{u}} f) - \frac{4\left[1 - \exp(-\frac{2\pi l_{pt\_irga}}{\overline{u}} f)\right]}{\frac{2\pi l_{pt\_irga}}{\overline{u}} f} \right) \tag{D-12}$$

Sub-transfer functions for covariance due to line averaging
Sub-transfer functions for covariance of certain scalars with vertical wind are given below:

$\overline{u'w'}$ or $\overline{v'w'}$

$$T_{uw\_LA}(f, l_{pt\_csat}, \overline{u}) = \sqrt{T_{uu\_LA}(f, l_{pt\_csat}, \overline{u}) T_{ww\_LA}(f, l_{pt\_csat}, \overline{u})} \quad \text{(D-13)}$$

$\overline{s'w'}$ (where s is a variable from the IRGA)

$$T_{sw\_LA}(f, l_{pt\_IRGA}, l_{pt\_csat}, \overline{u}) = \sqrt{T_{ss\_LA}(f, l_{pt\_IRGA}, \overline{u}) T_{ww\_LA}(f, l_{pt\_csat}, \overline{u})} \quad \text{(D-14)}$$

$\overline{T_s'w'}$ (from equations 5 to 8 in van Dijk, 2002a)

In cylindrical coordinates, the sub-transfer function for line averaging of buoyancy flux measured using Campbell sonic anemometer is as follows:

$$T_{T_s w\_LA}(f, l_{pt\_csat}, \overline{u}) = \frac{91}{180\pi k^2} \int_0^{\infty} \int_0^{2\pi} K\sqrt{k^2 + K^2} \frac{k^2 + K^2 \sin^2\theta}{k^2 + K^2} \sum_{i=1}^{3} \text{sinc}\frac{\mathbf{k} \cdot \mathbf{l}_i}{2} d\theta dK \quad \text{(D-15)}$$

where k is the wave number in the streamwise direction given by

$$k = \frac{2\pi f}{\overline{u}} \quad \text{(D-16)}$$

and where k is the wave number vector in cylindrical coordinates given by:

$$k = \begin{bmatrix} k & K\sin\theta & K\cos\theta \end{bmatrix} \quad \text{(D-17)}$$

and where $\mathbf{l}_i$ (i = 1, 2, or 3) is a path vector that expresses a path length as three components in three dimensions, given by:

$$\mathbf{l}_1 = l_{pt\_csat} \begin{bmatrix} -\sin 30^o \\ 0 \\ \cos 30^o \end{bmatrix}, \mathbf{l}_2 = \frac{l_{pt\_csat}}{2} \begin{bmatrix} \sin 30^o \\ \sqrt{3}\sin 30^o \\ 2\cos 30^0 \end{bmatrix}, \text{ and } \mathbf{l}_3 = \frac{l_{pt\_csat}}{2} \begin{bmatrix} \sin 30^0 \\ -\sqrt{3}\sin 30^0 \\ 2\cos 30^0 \end{bmatrix} \quad \text{(D-18)}$$

The integration of equation (D-15) requires much computation, so its numerical form in Table 1 of van Dijk (2002a) is used (see TABLE D-1).

TABLE D-1. Numerical form (transfer function values versus normalize frequencies) of sub-transfer function of buoyancy flux measured by a CSAT3

Normalized Frequency [a]	< 0.01	0.1	0.2	0.5	1.0	1.2	1.4	1.6
Sub-transfer function values	1.0000	0.9992	0.9976	0.9900	0.9670	0.9550	0.9417	0.9274
Normalized frequency	1.8	2.0	2.2	2.4	2.6	2.8	3.0	4.0
Sub-transfer function values	0.9122	0.8962	0.8797	0.8626	0.8452	0.8274	0.8096	0.7201
Normalized frequency	5.0	6.0	7.0	8.0	9.0	10.0	14.0	20.0
Sub-transfer function values	0.6353	0.5588	0.4922	0.4355	0.3879	0.3481	0.2445	0.1700
Normalized frequency	30.0	40.0	50.0	60.0	70.0	80.0	90.0	100.0
Sub-transfer function values	0.1134	0.08503	0.06802	0.05668	0.04859	0.04251	0.03779	0.03401

For normalized frequencies between the values listed in the table, the sub-transfer function is linearly interpolated between two neighboring independent normalized frequencies. For normalized frequencies less than or equal to 0.01 Hz, the transfer function value is set to 1. For normalized frequencies greater than 100 Hz, trends from the first and second order numerical derivatives show that this sub-transfer function becomes nearly constant beyond 300 Hz at a value of 1.155511×10^{-4}. Therefore, for normalized frequencies from 300 Hz to 10,000 Hz, the sub-transfer function is set to this value, and for frequencies falling between 100 Hz and 300 Hz, the sub-transfer function is estimated by linear interpolation.

D.8.3 Volume Averaging

Volume averaging is considered negligible in the cases of an IRGASON and EC150 due to the very small diameter to path length ratio, however the sub-transfer function for volume averaging is briefly described here for completeness. A sensor such as a krypton hygrometer (KH20) has a much higher diameter-path length ratio, so the volume averaging must be taken into account. Its optical beam diameter is 8 mm, and its path length is 12 to 15 mm (see the calibration document for the unique path length for a particular KH20). Andreas (1981) derived an exact transfer function for volume averaging [equation (18) in Andreas (1981)]. This transfer function includes a first-order Bessel function of the first kind, which makes the integration of the sub-transfer function over the frequency domain in need of significant computation time.

Later, Moene (2003) used a simpler function to approximate equation (18) of Andreas (1981) for Krypton hygrometers. His approximation was developed using the transfer function of Andreas (1981) for a diameter-length ratio between 0.5 and 1.0 when the ratio of the Kolmogorov microscale (1 mm in atmosphere) to the path length is 0.1 [Fig. 2 in Andreas (1981)]. The approximation equation [see page 650 in Moene (2003)] is given by:

$$T_{h2o\_KH\_VA}(f, p_{KH}, \overline{u}) = \exp\left[-2\left(\frac{p_{KH}}{\overline{u}} f\right)^2\right] \quad \text{(D-19)}$$

where p_{KH} is the path length of KH20.

D.8.4 FIR Filtering

The sub-transfer function for the various data filters available on the EC100 electronics (the EC100 is the electronics module used with the EC150, CSAT3A, and IRGASON) has not been developed yet. However, it is assumed to be negligible compared to other sub-transfer functions, assuming the bandwidth has been appropriately selected for flux measurements.

D.8.5 Time Constant

If a fine wire thermocouple is used, a sub-transfer function describing the frequency response of the thermocouple should be used and is described by a simple first order gain function [Square of equation 2 in Moore (1986)]:

$$T_{TT\_TC}(f, \tau_{FW}) = \frac{1}{1 + \left(2\pi\tau_{FW} f\right)^2} \quad \text{(D-20)}$$

where τ_{FW} is the time constant of the FW.

The value of τ_{FW} depends on the physical properties of air, physical properties of the thermocouple, the diameter of the thermocouple wire (*D,* entered by a user), and the Nusselt number (Nu). It is given by [equation 3 in Moore (1986) and equation 4 in Shapland et al. (2014)]:

$$\tau_{FW} = \gamma \frac{\rho_{FW} C_{FW}}{k_a \mathbf{Nu}} D^2 \quad \text{(D-21)}$$

where:

γ is the shape coefficient. It is 0.25 for cylindrical and 0.167 for spherical sensors. For a FW, a cylindrical shape is assumed since heat can be conducted through two paths around the junction, each having a cylindrical shape.

ρ_{FW} is the material density of the thermocouple {[8920(constantan) + 8730(chromel)]/2 = 8825 kg /m^3, Omega product literature (undated)}

C_{FW} is the specific heat of the thermocouple materials {[0.094(constantan) + 0.107 (chromel)]/2 = 0.1005 cal / (g °C) =420.7734 J / (kg °C), Omega product literature (undated)}

k_a is the thermal conductivity of air [$7.038086\times10^{-5}T + 2.42507\times10^{-2}$ in W/ (m °C), where T is air temperature in °C, Table 1 in Montgomery (1947)]

Nu is the Nusselt number. The Nusselt number for a sphere is used because the aerodynamics around the junction are

influenced by its 3D dimensions [equation 4 in Moore (1986)]. It is calculated as follows:

$$\mathbf{Nu} = 2.00 + 0.18\mathbf{Re}^{0.67} \quad \text{(D-22)}$$

where Re is Reynolds' number [equation 3.1-2 in Geankoplis (1993)]

$$\mathrm{Re} = \frac{2\rho_a D\overline{u}}{\mu} \quad \text{(D-23)}$$

Where: ρ_a is air density (calculated online by the datalogger),

$\overline{u}$ is horizontal wind speed (use sonic data),

μ is viscosity of air [$4.9821\times10^{-8}T + 1.7168\times10^{-5}$ in kg/(m·s), see Table 1 in Montgomery (1947)]

D.8.6 Spatial Separation

For eddy covariance measurements that use two spatially-separated sensors for measurements of wind velocity and a scalar, a passing eddy may be measured by the two sensors at different times if the sensors are mounted along the mean wind direction, creating a time lag in the measurements of the downstream sensor relative to the upstream one. Alternatively, it is possible that the eddy will be measured by only one of the two sensors if the sensors are mounted with a separation perpendicular to the mean wind direction (for example, a lateral separation with sensors mounted in a cross-wind orientation) and the eddy is smaller than the separation distance, or if the boundary of the eddy passing through one sensor's measurement volume does not reach the measurement volume of the other sensor. Accordingly, we define the separation along the wind direction as lag distance and the separation in cross-wind direction as lateral distance.

The magnitude of covariance is decreased due to both the lag distance and the lateral distance (Horst and Lenschow 2009). In data processing, the loss of covariance due to the lag distance may be significantly or largely recovered by realigning the data with various time lags in order to maximize the covariance (such as, lag maximization), and the loss of covariance due to lateral distance may be recovered using a frequency correction (Foken et al. 2012). For both of these corrections, the physical lag and lateral distances are needed.

In the installation of sensors, the horizontal coordinates of the center of the measurement volume of the scalar sensor relative to the sonic coordinate system (see FIGURE D-1) should be recorded. The coordinates can be expressed as a separation vector [x , y].

When wind comes from a direction of zero degrees (i.e., against the direction in which the sonic anemometer points), the x component of the vector is the lag distance and the y component of the vector is lateral distance. When the wind direction is not zero degrees, the separation vector may be projected onto the wind and cross-wind axes by knowing the wind direction (θ_w) relative to the sonic coordinate system and using a coordinate rotation. The resulting projection along the wind direction is lag distance (d_{lag}) and the projection in cross-wind direction is lateral distance (d_{lat}).

These are given by:

$$\begin{bmatrix} d_{lag} \\ d_{lat} \end{bmatrix} = \begin{bmatrix} \cos\theta_w & \sin\theta_w \\ -\sin\theta_w & \cos\theta_w \end{bmatrix} \begin{bmatrix} x \\ y \end{bmatrix} \tag{D-24}$$

The lag distance (d_{lag}) along with wind speed will be used by the datalogger for lag maximization by applying an appropriate lag of measurement scans to align the sensors (see lag maximization) and the lateral distance is used in a sub-transfer function of frequency response due to sensor separation, $T_{sw\_SP}(f, d_{lat}, \overline{u})$, which is given as follows [equation 4.8 in Foken, et. al. (2012)]:

$$T_{sw\_SP}(f, d_{lat}, \overline{u}) = \exp\left[-9.9 \left(\frac{f d_{lat}}{\overline{u}} \right)^{1.5} \right] \tag{D-25}$$

D.8.7 Total Transfer Function

A composite or total transfer function is given by the product of the appropriate sub-transfer functions for a particular covariance. The total transfer functions used by the datalogger are given in this section (FIR correction currently not included).

For $\overline{u'w'}$ or $\overline{v'w'}$:

$$T_{uw}(f, l_{pt\_csat}, T_{ba}, \overline{u}) = T_{uw\_BA}(f, T_{ba}) T_{uw\_LA}(f, l_{pt\_csat}, \overline{u}) \tag{D-26}$$

For $\overline{T_s'w'}$:

$$T_{T_sw}(f, l_{pt\_csat}, T_b, \overline{u}) = T_{T_sw\_BA}(f, T_{ba}) T_{T_sw\_LA}(f, l_{pt\_csat}, \overline{u}) \tag{D-27}$$

For $\overline{s'w'}$ (where s is a variable measured by the IRGA) :

$$T_{sw}(f, l_{pt\_csat}, l_{pt\_IRGA}, d_{lat}, T_{ba}, \overline{u}) = T_{sw\_BA}(f, T_{ba}) T_{sw\_LA}(f, l_{pt\_csat}, l_{pt\_IRGA}, \overline{u}) T_{sw\_SP}(f, d_{lat}, \overline{u}) \tag{D-28}$$

For $\overline{T_{FW}'w'}$:

$$T_{T_{Fw}w}(f, l_{pt\_csat}, d_{lat}, \tau_{FW}, T_{ba}, \overline{u}) = T_{T_{Fw}w\_BA}(f, T_{ba}) \sqrt{T_{ww\_LA}(f, l_{pt\_csat}, \overline{u}) T_{TT\_TC}(f, \tau_{FW})} T_{sw\_SP}(f, d_{lat}, \overline{u}) \tag{D-29}$$

D.9 Working Model

Evaluating the correction factor in Equation (D-1) in the datalogger program requires numerical integration. Because the cospectrum changes exponentially faster at low frequencies than at high frequencies, the interval of integration can be exponentially increased throughout the integration in order to save computation time without significantly reducing accuracy. Accordingly, $\ln f$ is used as an integration variable that increases at equal logarithmic intervals of

frequency (f), which effectively increments the frequency interval exponentially for fast integration over the integration domain. This results in a working formula that is used to find the covariance:

$$\overline{\left(\alpha' w'\right)}_{rf} = \left(\overline{\alpha' w'}\right)_r \left\{ \frac{\int_0^\infty \left[f S_{\alpha w}(f) \right] d\left(\ln f\right)}{\int_0^\infty T_{\alpha w}(f) \left[f S_{\alpha w}(f) \right] d\left(\ln f\right)} \right\} \tag{D-30}$$

Recall that even though simple notation for $T_{\alpha w}(f)$ has been used, this is an overall transfer function that is comprised of the sub-transfer functions presented in the sections above and includes independent variables such as wind speed ($\overline{u}$), block average period, measurement path length, and/or sensor time constant and/or lateral separation distance. Accordingly, the components of the combined transfer function for different variables of vectors and scalars are unique due to sensor specifications and measurement installations.

D.10 Programmatic Approach to Computations for Correction Factors

The correction factor in model (D-30) has a numerator and denominator. Its numerator is found from a normalized spectrum, and its denominator is determined by numerical integration. For both normalized and non-normalized cospectra, we numerically integrate both the numerator and denominator. Moore (1986) used the Composite Simpson's rule to estimate this denominator. In his estimation, 19 equal integration intervals at a scale of natural logarithm from 10^{-5} to 5 Hz were used, which resulted in an integration error smaller than 1%. Currently, this can be further improved due to faster computational speeds in Campbell dataloggers compared to micro-computers at that time. By increasing the integration range and decreasing the integration intervals, the datalogger can more accurately account for frequency attenuation, particularly in the lower frequencies of the block averaging sub-transfer function. Specifically, we extend the integration range from 10^{-6} to 10^4 Hz and divide the range into 100 frequency bins. It is believed that the integration error should be significantly smaller than Moore (1986) and the accuracy sufficient.

Because the cospectrum may change exponentially and dramatically in lower frequencies, the logarithm scale of cyclic frequency may be used for a numerical integration interval (bin width). For 100 bins from 10^{-6} to 10^4 Hz, the base frequency interval (Δf) is 1.258925 since $10^{-6} \times 1.258925^{100} = 10000$. The lower frequency boundary of the jth interval is indexed as the $(j\text{-}1)^{th}$ frequency and the right boundary frequency is indexed as the j^{th} frequency. The interval of integration (bin width) at natural logarithm scale [$\Delta \ln(f)$] is given by:

$$\begin{aligned} \Delta \ln\left(f\right) &= \ln\left(10^{-6} \Delta f^{\,j}\right) - \ln\left(10^{-6} \times \Delta f^{\,j-1}\right) \\ &= \ln \frac{10^{-6} \Delta f^{\,j}}{10^{-6} \Delta f^{\,j-1}} = \ln \Delta f \end{aligned} \tag{D-31}$$

The Composite Simpson's rule writes the integration for the numerator in model (8.1) as (Page 186 in Burden and Faires (1993):

$$\begin{aligned}\int_0^{\infty}\left[fS_{\alpha w}(f)\right]d\left(\ln f\right) &\approx \int_{10^{-6}}^{10000}\left[fS_{\alpha w}(f)\right]d\left(\ln f\right)\\ &= \frac{\ln\left(\Delta f\right)}{3}\left\{\left[10^{-6}S_{\alpha w}(10^{-6})\right]+4\sum_{k=1}^{50}\left[10^{-6}\Delta f^{2k-1}S_{\alpha w}(10^{-6}\Delta f^{2k-1})\right]\right.\\ &\left.+2\sum_{k=1}^{49}\left[10^{-6}\Delta f^{2k}S_{\alpha w}(10^{-6}\Delta f^{2k})\right]+\left[10^{4}S_{\alpha w}(10^{4})\right]\right\}\end{aligned} \quad \text{(D-32)}$$

With an error term as describe on page 186 (Burden and Faires (1993):

$$\begin{aligned}Error &= \frac{10^{4}-10^{-6}}{180}\times\left(\ln\Delta f\right)^{4}\frac{2}{100}\sum_{j=1}^{50}\left[\xi_j S_{\alpha w}(\xi_j)\right]^{(4)}\\ &\approx \frac{20}{18}\times\left(\ln\Delta f\right)^{4}\sum_{j=1}^{50}\left[\xi_j S_{\alpha w}(\xi_j)\right]^{(4)}\end{aligned} \quad \text{(D-33)}$$

where ζ is a value of frequency that can maximize the value in the square bracket. The evaluation of this term requires more complicated calculations because the 4th order derivative of the integrated function is needed. We do not evaluate this term now, but equation (D-33) can show how the error can be reduced by adding the number of integration intervals and narrowing the width of the interval.

Similarly, the denominator with Simpson's rule applied becomes:

$$\begin{aligned}\int_0^{\infty}T_{\alpha w}(f)\left[fS_{\alpha w}(f)\right]d\left(\ln f\right) &\approx \int_{10^{-6}}^{10000}T_{\alpha w}(f)\left[fS_{\alpha w}(f)\right]d\left(\ln f\right)\\ &= \frac{\ln\left(\Delta f\right)}{3}\left\{\left[T_{\alpha w}(10^{-6})10^{-6}S_{\alpha w}(10^{-6})\right]+4\sum_{k=1}^{50}T_{\alpha w}(10^{-6}\Delta f^{2k-1})\left[10^{-6}\Delta f^{2k-1}S_{\alpha w}(10^{-6}\Delta f^{2k-1})\right]\right.\\ &\left.+2\sum_{k=1}^{49}T_{\alpha w}(10^{-6}\Delta f^{2k})\left[10^{-6}\Delta f^{2k}S_{\alpha w}(10^{-6}\Delta f^{2k})\right]+T_{\alpha w}(10^{4})\left[10^{4}S_{\alpha w}(10^{4})\right]\right\}\end{aligned} \quad \text{(D-34)}$$

The error term of this numerical integration can be calculated using equation (D-33) if the term $\xi_j S_{\alpha w}(\xi_j)$ is replaced with $T_{\alpha w}\left[\xi_j\right]\xi_j S_{\alpha w}(\xi_j)$.

The code in the program used to calculate the correction factor of one covariance (*Cor_factor*) is outlined below:

Cor_factor = 0

for *j* = 0 to 100 (100 steps)

$f = 10^{-6} \times 1.258925^{J}$ (Calculation of frequency)

$m = 2+4 \times (j \text{ MOD } 2) - \text{ABS}(j = 0) - \text{ABS}(j = 100)$

NOTE M = 1 for $j = 0$ and $j = 100$. For all other j, $m = 4$ if j is odd and $m = 2$ if j is even).

$$\text{Numerator} = \text{Numerator} + m \times \left[fS_{\alpha\beta}(f) \right]$$

$$\text{Denominator} = \text{Denominator} + m \times T_{\alpha\beta}(f) \left[fS_{\alpha\beta}(f) \right]$$

Next j

Cor_factor = Numerator/Denominator

D.11 References

Andreas, E. L.: 1981, "The effects of volume averaging on spectra measured with Lyman-Alpha hygrometer", *J. Applied Meteorol*. **20**: 467-475.

Burden, R. L. and Faires, J. D.: 1993, Numerical Analysis. PWS Publishing Company, Boston. pp. 184-189.

Campbell Scientific, Inc. 1998. CSAT3 Three Dimensional Sonic Anemometer. pp. 25.

Campbell Scientific, Inc. 2006. Type E, Fine Wire Thermocouples: Models FW05, FW1, and FW3. pp: 2.

Campbell Scientific Inc. 2014. IRGSON Integrated CO2/H2O Open-Path Gas Analyzer and 3D Sonic Anemometer. Campbell Scientific, Inc. Logan UT. p. 43.

Geankoplis, C.J. 1993. Transportation Processes and Unit Operation. 3rd Edition. PTR Prentice Hall, New Jersey. pp 114-131 and Appendix.

Foken, T, R. Leuning, S.R. Onley, M. Mauder, M. Aubinet. 2012. Corrections and data quality control. In M, Aubient, T. Vesala, D. Papale. (eds). Eddy Covariance: A Practice Guide to Measurement and Data Analysis. Springer, New York. p. 85-131.

Horst, T.W., 1997. A simple formula for attenuation of eddy fluxes measured with first-order response scalar sensors. Boundary-Layer Meteorology 94: 517-520.

Horst, T.W., and D.H. Lenschow, 2009: Attenuation of scalar fluxes measured with spatially-displaced sensors. *Boundary-Layer Meteorology*, **130**, 275-300, DOI: *10.1007/s10546-008-9348-0*.

Kaimal, J.C., S.F. Clifford, R.J. Lataitis. 1989. Effect of finite sampling on atmospheric spectra. Boundary-Layer Meteorology 7: 827-837.

Kaimal, J. C. and J. J. Finnigan, 1994. Atmospheric Boundary Layer Flows: Their Structure and Measurement. Oxford University Press, Oxford, 289 p.

Kaimal, J.C., J.C., Wyngaard, Y. Izumi, O.R. Cote. 1972. Deriving power spectra from a three-component sonic anemometer. J. Appl. Meteorol. 7: 827-837.

Leuning, R., K.M. King. 1992. Comparison of eddy-covariance measurements of CO2 flux by open- and close-path CO2 Analyzers. Boundary-Layer Meteorology 59: 297-311.

Laubach, J., K.G. McNaughton. 1998. A spectrum-independent procedure for correcting eddy flux measured with separated sensors. Boundary-Layer Meteorol. 89: 445-467.

LI-COR Bioscience. 2001. CO2/H2O Gas Analyzers. Pp:19.

Massman, W.J. 2000. A simple method for estimating frequency response corrections for eddy covariance systems. Agricultural and Forest Meteorology 104: 185-198.

Moncrieff, J.B., J.M. Massheder, H.de Bruin, J.A. Elbers, T. Friborg, B. Heusinkveld, P. Kabat, S. Scott, H. Soegaard, A. Verhoef. 1997. A system to measure surface fluxes of momentum, sensible heat, water vapour and carbon dioxide. Journal of Hydrology 188-189: 589-611.

Moene, A.F. 2003. Effects of water vapor on the structure parameter of the refractive index for near-infrared radiation. Boundary-Layer Meteorology 107: 635-653.

Moore C.J. 1986. Frequency response corrections for eddy correlation systems. Boundary-Layer Meteorology 37: 17-35.

Omega. Undated. Physical Properties of Thermoelement Materials. Omega.com website.

Rosenberg, N.J., B.L. Blad, S.B. Verma. 1983. Microclimate: The Biology Environment, 2nd Edition. John Wiley & Sons. Pp. 495.

Shapland, T.M., R.L. Snyder, K.T. Paw U, A.J. McElrone. 2014. Thermocouple frequency response compensation leads to convergence of the surface renewal alpha calibration. Agricultural and Forest Meteorology 189-190: 36-47.

Stull, R.B. 1988. An introduction to Boundary Layer Meteorology. Kluwer Academic Publisher, Boston, 666p.

van Dijk, A. 2002a. Extension of 3D of “the effect of linear averaging on scalar flux measurements with a sonic anemometer near the surface” by Kristensen and Fitzjarrald. Journal of Atmospheric and Ocean Technology. 19: 80-19.

van Dijk, A. 2002b. The Principle of Surface Flux Physics. Research Group of the Royal Netherlands Meteorological Institute and Department of Meteorology and Air Quality with Agricultural University Wageningen. 65p.

Wallace, J. M. and P. V. Hobbs, 2006: Atmospheric Science: An Introductory Survey. Academic Press, 350 pp.

Appendix E. WPL Corrections

Due to the vertical gradient of air temperature in the atmospheric surface layer, rising air parcels have different temperatures and densities than descending air parcels. For example, in the case of upward (positive) heat flux when the air closest to the ground is warmest, rising air parcels on average will be warmer and less dense than descending ones. If we suppose in this same case that the CO_2 or H_2O fluxes are zero (rising and descending parcels carry the same amount of CO_2 and H_2O), the measurements from an open-path eddy-covariance system will still report negative (downward) fluxes simply because of the correlation between rising air parcels and lower air density. This is explained by mass conservation or air continuity; the decrease in air density due to the increase in air temperature while the total pressure in surface layer changes very little, forces air to expand upwards in the atmospheric surface layer. This expansion generates an upward (positive) flux of air at the measurement point and leads to a slightly positive mean vertical velocity. Thus the downward CO_2 or H_2O flux measured by open-path eddy covariance system may be explained by the upward flux of air from a net upward vertical velocity.

Depending on whether the temperature profile increases or decreases with height, the mean vertical velocity may be negative or positive. Typically it ranges from –0.75 to 1.5 mm/s when sensible heat flux is between –200 and 600 W/m^2 [Fig.1 in Webb et al. (1980)]. This change in vertical velocity due to change in air density is too small to be measured by a 3D sonic anemometer with sufficient accuracy.

Since typical applications of the open-path eddy-covariance method do not account for fluxes associated with non-zero mean flows ($\overline{w} \neq 0$), an appropriate correction for the vertical velocity due to heat and water vapor transfer is needed.

E.1 Basic Considerations

Air density (ρ_a) is a sum of partial densities: dry air density (ρ_d), water vapor density (ρ_v), and CO_2 density (ρ_{co2}), given by:

$$\rho_a = \rho_d + \rho_v + \rho_{co2} \tag{E-1}$$

The contribution of ρ_{CO2} relative to ρ_d and ρ_v vapor is very small, and thus can be considered negligible to the total air density. The equation therefore becomes:

$$\rho_a = \rho_d + \rho_v \tag{E-2}$$

The individual gas laws give the partial pressures of dry air (p_d), water vapor (p_v), and (p_{co2}) as follows:

$$p_d = \frac{R^*}{m_d}\rho_d T$$

$$p_v = \frac{R^*}{m_v}\rho_v T \qquad \text{(E-3)}$$

$$p_{CO2} = \frac{R^*}{m_{CO2}}\rho_{CO2} T$$

where subscripts *d*, *v*, and *CO2* denote dry air, water vapor, and carbon dioxide, respectively, and are used throughout; *m* is molecular mass; R^* is the universal gas constant [8.3143 J K^{-1} mol^{-1}, page 467 of Wallace and Hobbs (2006)], and T is absolute temperature.

The total air pressure (p_a) is given by:

$$p_a = p_d + p_v + p_{CO2} \qquad \text{(E-4)}$$

The air pressure, dry-air density, water-vapor density, and CO_2 density are measured and calculated in an eddy covariance system. Although the partial pressures of the different gas components are normally not measured, the other measured variables may be used to derive the partial pressures. Submitting equation (E-3) into equation (E-4) yields:

$$\frac{p_a}{R^* T} = \frac{\rho_d}{m_d} + \frac{\rho_v}{m_v} + \frac{\rho_{CO2}}{m_{CO2}} \approx \frac{\rho_d}{m_d} + \frac{\rho_v}{m_v} \qquad \text{(E-5)}$$

Equation (E-5) describes the basic relationship of air and water-vapor densities to temperature and atmospheric pressure. If the term

$$\frac{1}{T} = \frac{1}{(\overline{T} + T')} = \frac{1}{\overline{T}\left(1 + \frac{T'}{\overline{T}}\right)} \qquad \text{(E-6)}$$

is expended in a power series of $T' / \overline{T}$, the partial densities in equation (E-5) can be written in forms of instantaneous, mean, and fluctuation variables as follows:

$$\begin{cases} \dfrac{\rho_d}{m_d} + \dfrac{\rho_v}{m_v} = \dfrac{p_a}{R^* \overline{T}}\left\{1 - \dfrac{T'}{\overline{T}} + \left(\dfrac{T'}{\overline{T}}\right)^2 - \left(\dfrac{T'}{\overline{T}}\right)^3 + ...\right\} & \text{(E7}a\text{)} \\ \dfrac{\overline{\rho}_d}{m_d} + \dfrac{\overline{\rho}_v}{m_v} = \dfrac{p_a}{R^* \overline{T}}\left\{1 + \dfrac{\overline{T'^2}}{\overline{T}^2} - \dfrac{\overline{T'^3}}{\overline{T}^3} + ...\right\} & \text{(E7}b\text{)} \\ \dfrac{\rho_d'}{m_d} + \dfrac{\rho_v'}{m_v} = \dfrac{p_a}{R^* \overline{T}}\left\{-\dfrac{T'}{\overline{T}} + \dfrac{T'^2 - \overline{T'^2}}{\overline{T}^2} - \dfrac{T'^3 - \overline{T'^3}}{\overline{T}^3} + ...\right\} & \text{(E7}c\text{)} \end{cases} \qquad \text{(E-7)}$$

Equation (E7b) can further be expressed as:

$$\frac{p_a}{R^*\overline{T}} = \left(\frac{\overline{\rho}_d}{m_d} + \frac{\overline{\rho}_v}{m_v}\right)\left\{1 + \frac{\overline{T'^2}}{\overline{T}^2} - \frac{\overline{T'^3}}{\overline{T}^3} + \ldots\right\}^{-1} \tag{E-8}$$

Substituting equation (E-8) into equation (E7c) yields:

$$\frac{\rho_d'}{m_d} + \frac{\rho_v'}{m_v} = \left(\frac{\overline{\rho}_d}{m_d} + \frac{\overline{\rho}_v}{m_v}\right)\left\{-\frac{T'}{\overline{T}} + \frac{T'^2 - \overline{T'^2}}{\overline{T}^2} - \frac{T'^3 - \overline{T'^3}}{\overline{T}^3} + \ldots.\right\}\left\{1 + \frac{\overline{T'^2}}{\overline{T}^2} - \frac{\overline{T'^3}}{\overline{T}^3} + \ldots\right\}^{-1} \tag{E-9}$$

By dropping the second order term (< 10^{-4}) of absolute temperature, the fluctuation of dry air density can be expressed as:

$$\begin{aligned}\rho_d' &= -\frac{m_d}{m_v}\rho_v' - \overline{\rho}_d\left(1 + \frac{m_d}{m_v}\frac{\overline{\rho}_v}{\overline{\rho}_d}\right)\frac{T'}{\overline{T}} \\ &= -\mu\rho_v' - \overline{\rho}_d\left(1 + \mu\sigma\right)\frac{T'}{\overline{T}}\end{aligned} \tag{E-10}$$

where μ is the molecular weight ratio of dry air to water vapor, and σ is the mean water vapor mixing ratio.

E.2 Governing Constraint and Mean Vertical Velocity

The governing constraint that the mean vertical flux of dry air constituent should be zero is given by:

$$\overline{w\rho_d} = 0 \tag{E-11}$$

Equation (E-11) is equivalent to:

$$\overline{w\rho_d} = \overline{\left(\overline{w} + w'\right)\left(\overline{\rho}_d + \rho_d'\right)} = \overline{\overline{w}\overline{\rho}_d + \overline{w}\rho_d' + w'\overline{\rho}_d + w'\rho_d'} = \overline{w}\overline{\rho}_d + \overline{w'\rho_d'} \tag{E-12}$$

Equations (E-11) and (E-12) give:

$$\overline{w} = -\frac{\overline{w'\rho_d'}}{\overline{\rho}_d} \tag{E-13}$$

Submitting equation (E-10) into this equation yields:

$$\overline{w} = \mu\frac{\overline{w'\rho_v'}}{\overline{\rho}_d} + \left(1 + \mu\sigma\right)\frac{\overline{w'T'}}{\overline{T}} \tag{E-14}$$

E.3 Eddy Covariance Measurements

E.3.1 CO_2

The flux of CO_2 can be written as:

$$F_{CO2} = \overline{w\rho_{CO2}} = \overline{w'\rho'_{CO2}} + \overline{w}\,\overline{\rho}_{CO2} \tag{E-15}$$

Replacing the mean vertical velocity ($\overline{w}$) in the equation with equation (E-14) yields:

$$F_{CO2} = \overline{w'\rho'_{CO2}} + \left[\mu \frac{\overline{\rho_{CO2}}}{\overline{\rho}_d} \overline{w'\rho'_v} + (1+\mu\sigma) \frac{\overline{\rho_{CO2}}}{\overline{T}} \overline{w'T'} \right] \tag{E-16}$$

The term in the rectangle bracket is the WPL correction. The first term is due to water flux and the second is due to heat flux.

$\overline{\rho}_{CO2}$ is the mean CO_2 density measured by an IRGA

$\overline{\rho}_d$ is the mean dry air density calculated from air temperature, pressure, and water vapor density

$\overline{T}$ is the mean air temperature in Kelvin

μ is 1.60802 [the ratio of dry air molecular weight (md = 28.97 kg·kmol^{-1}) to water molecular weight (mv = 18.016 kg·kmol^{-1}), page 466 in Wallace and Hobbs (2006)]

σ is the mean water vapor mixing ratio [ratio of mean water vapor density ($\overline{\rho}_v$) to mean dry air density ($\overline{\rho}_d$).

$\overline{w'\rho'_v}$ is the water vapor flux measured using a sonic anemometer and IRGA.

$\overline{w'T'}$ is the heat flux (after rotations, frequency, and SND corrections) calculated from a sonic anemometer and optionally with a fine-wire thermocouple.

E.3.2 H_2O

The flux of water vapor can be written as:

$$E = \overline{w\rho_v} = \overline{w'\rho'_v} + \overline{w}\,\overline{\rho}_v \tag{E-17}$$

Replacing the mean vertical velocity ($\overline{w}$) in the equation with eq. (2.4) yields:

$$E = \overline{w'\rho'_v} + \left[\mu\sigma \overline{w'\rho'_v} + (1+\mu\sigma) \frac{\overline{\rho_v}}{\overline{T}} \overline{w'T'} \right] \tag{E-18}$$

The term in the rectangle bracket is the WPL correction term. The first term is due to water flux itself and the second is due to heat flux.

$\overline{\rho_v}$ is the mean water vapor density measured by IRGA

$\overline{w'\rho_v'}$ is the water vapor flux (after rotation and frequency corrections) measured using sonic anemometer and IRGA.

E.4 References

Campbell Scientific, Inc. 2015. CSAT3 Three Dimensional Sonic Anemometer. Logan, pp: 25.

Schotanus, P.S., F.T.M. Nieuwstadt, H.A.R. Debruin. 1983. Temperature measurement with a sonic anemometer and its application to heat and moisture flux. Boundary-Layer Meteorology 26: 81-93.

Wallace, J.M., P.V. Hobbs. 2006. Atmospheric Science: An Introductory Survey, 2nd edition. Elsvier, Amesterdam. pp: 483.

Webb, E.K., G.I. Pearman, R. Leuning. 1980. Correction of flux measurements for density effects due to heat and water transfer. Quart. J. Met. Soc. 106: 85-100.

Appendix F. Data Quality Grading

Data quality assurance (QA) and quality control (QC) are recommended for EC measurements because of complex calculation procedures (Foken et al., 2012). A number of publications on QA and QC for EC measurements are available (for example, Foken and Wichura 1996; Vickers and Mahurt 1997; Shearman 1992; Moncrieff et al. 1997; Aubinet et al. 2000; Foken et al 2004; 2012).

In the case of this datalogger program, QA is accomplished using diagnostic outputs from the measurement system's sonic anemometer and infrared gas analyzer. Specifically, the datalogger only uses raw data for flux calculations when the diagnostic values from both sensors are zero (i.e., sensors work normally and measurements are in their reasonable ranges), when the measurements are within the calibrated range of the sensors, and when the signal strengths are adequate (i.e. nothing is blocking the optical path). Even when raw data are not used for flux calculations, they are still stored in the time series data table. More details on diagnostics may be found in the manual of the respective sensor. Regarding QC, the datalogger program follows the method presented in Foken at al. (2012) to grade the relative quality of CO_2, latent heat, sensible heat, and momentum fluxes. Specifically, the following three variables are calculated and used to grade the quality of the data:

- ***R***elative ***N***on-stationarity (RN_{cov}) to describe the steady state,
- relative ***I***ntegral ***T***urbulence ***C***haracteristics (*ITC*) to define the developed turbulence condition, and
- horizontal wind angle in the sonic anemometer coordinate system.

Sections F.1 through F.3 give more information on each of these variables and how a quality grade for each is assigned. Section F.4 then describes how an overall quality grade is found. Finally, Section F.5 describes how this is implemented into the datalogger program.

F.1 Relative Non-stationarity (RNcov) for Steady State

Turbulence flux measurement theory is valid under the steady state conditions of turbulent flows. In such conditions, the surface layer turbulent flow structure is independent of time within an averaging interval (e.g., 30 min). The extent to which conditions conform to a steady state may be described using a variable called relative non-stationarity, RN_{cov}, which is defined as the relative difference between the averaged 5-minute and 30-minute covariance values, given by [equations (4.36) to (4.38) in Foken, et al. (2012)]:

$$RN_{cov} = 100 \times \left| \frac{\frac{1}{6}\sum_{i=1}^{6}\left(\overline{s'w'}\right)_{ri} - \left(\overline{s'w'}\right)_{r}}{\left(\overline{s'w'}\right)_{r}} \right| \qquad \text{(F-1)}$$

where s can be T_s for sonic temperature, T_c for corrected temperature, ρ_{co2} for CO_2 density, ρ_{h2o} for H_2O density, or u or v for horizontal wind speed; w represents vertical wind velocity; subscript r indicates the variable after coordinate rotation; subscript i (for example, 1, 2,…, or 6 if a 30 min averaging period is used) indicates the covariance of the i^{th} 5 min interval within an averaging period; and the numerical number of 100 converts the relative non-stationarity into percent. Based on the calculated value of RN_{cov}, the steady state is classified into nine grades. Grade 1 is most steady and indicates highest data quality, whereas grade 9 is least steady and indicates relatively lower data quality (see TABLE F-1).

TABLE F-1. Grades of relative non-stationarity, relative integral turbulence characteristics, and wind direction in the sonic instrument coordinate system.

RN_{cov} Relative non-stationarity [model (2.3) in Foken et al. (2012)]		ITC_{sw} and ITC_{tau} Relative integral turbulence characteristics [model (2.5) in Foken et al. (2012)]		wnd_dir_sonic Wind direction	
Grade	**Range (%)**	**Grade**	**Range (%)**	**Grade**	**Range**
1 (highest)	[0 , 15)	1 (highest)	[0 , 15)	1 (highest)	[0 – 150°], [210 – 360°]
2	[15 , 30)	2	[15 , 30)	2	[150 – 170°], [190 – 210°]
3	[30 , 50)	3	[30 , 50)	3 (lowest)	[170 – 190°]
4	[50 , 75)	4	[50 , 75)		
5	[75 , 100)	5	[75 , 100)		
6	[100 , 250)	6	[100 , 250)		
7	[250 , 500)	7	[250 , 500)		
8	[500 , 1000)	8	[500 , 1000)		
9 (lowest)	≥1,000%	9 (lowest)	> 1,000%		

F.2 Turbulent Conditions

Turbulence conditions are characterized using a term called integral turbulence characteristics (*ITC*), which is defined as a standard deviation of a fluctuating variable (e.g., momentum variance or temperature variance) normalized by a scaling factor, for example, friction velocity or scaling temperature (Tilmann 1972). In a surface layer with fully developed turbulence, a given *ITC* term is a constant or at least follows a universal function of the scaling factor.

The most commonly used scaling factor is stability, defined as the ratio of aerodynamic height (z, sensor sensing height minus zero displacement height) to the Obukhov length (L, Stull 1988; Kaimal and Finnigan 1994), or z/L. The other scaling factor used is (Thomas and Foken 2002):

$$\frac{z_{+} f}{u_{*}} \tag{F-2}$$

where f is the Coriolis parameter in s^{-1}, u_* is friction velocity in m s^{-1}, and z_+ is a constant in m that was introduced and set to "1" to make the scaling factor dimensionless. For a given site, the Coriolis parameter can be calculated using:

$$f = 2\Omega \sin\phi$$

where Ω is angular velocity (7.292 x 10-5·s^{-1}) and ϕ is latitude (positive in the north hemisphere and negative in the south hemisphere).

ITC values have been accurately simulated using a well-known model (i.e., a function of the scaling factor) in conditions of fully developed turbulence. *ITC* may also be measured and then compared to the modeled *ITC* to show the degree to which turbulence has developed at that moment in time. The relative difference in percentage between the modeled and measured values are noted by ITC_α, where the subscript α indicates the variable of interest. When α is vertical velocity, w, or horizontal wind speed, u, ITC_α is defined as follows:

$$ITC_\alpha = 100 \times \frac{\left| ITC_{\alpha\_model} - \left(\frac{\sqrt{\left(\overline{\alpha'^2}\right)_r}}{u_*} \right)_{measured} \right|}{ITC_{\alpha\_model}} \tag{F-2}$$

where the ITC_{α_model} term is evaluated using:

$$ITC_{\alpha\_model} = \begin{cases} c_{\alpha 1} \ln \frac{z_+ f}{u_*} + c_{\alpha 2} & \frac{z}{L} > 0 \\ c_{\alpha 1} \left(\frac{z}{|L|} \right)^{c_{\alpha 2}} & \frac{z}{L} \le 0 \end{cases} \tag{F-3}$$

where $c_{\alpha 1}$ and $c_{\alpha 2}$ are parameters that depend on surface-layer stability (see TABLE F-2).

The relative difference in measured and theoretical *ITC* for temperature (T) is noted by ITC_T and is given by [equation (4.41) in Foken et al. (2012)]:

$$ITC_T = 100 \times \frac{\left| ITC_{T\_model} - \left(\frac{\sqrt{\left(\overline{T'^2}\right)_r}}{|T^*|} \right)_{measured} \right|}{ITC_{T\_model}} \tag{F-4}$$

where T^* is scaling temperature, given by [equation (1.25b) in Kaimal and Finnigan (1994)]:

$$T^* = -\frac{\overline{T'w'}}{u_*} \tag{F-5}$$

and the ITC_{T_model} term is evaluated using:

$$ITC_{T\_model} = c_{T1}\left(\frac{z}{|L|}\right)^{c_{T2}} \tag{F-6}$$

where c_{T1} and c_{T2} are parameters also depending on surface layer stability (see TABLE F-2).

TABLE F-2. Parameters in the model of integral turbulence characteristics (ITC).[1]

Variable in variance	c_{a1}	c_{a2}	z/L
Vertical velocity $a = W$	0.21	3.1	$0 < z/L < 0.4$
	1.3	0	$-0.032 < z/L \leq 0$
	2.0	1/8	$z/L \leq -0.032$
Horizontal wind speed $a = U$	0.44	6.3	$0 < z/L < 0.4$
	2.7	0	$-0.032 < z/L \leq 0$
	4.15	1/8	$z/L \leq -0.032$
Air temperature $a = T$	1.4	−1/4	$0.02 < z/L < 1$
	0.5	−1/2	$0.02 > z/L > -0.062$
	1.0	−1/4	$-0.062 > z/L > -1$
	1.0	−1/3	$-1 > z/L$

[1]Summarized from Tables 4.2 and 4.3 in Foken et al. (2012)

Similarly, ITC_{sw} is used to describe the turbulent conditions when measuring the covariance of a scalar, s, and vertical wind, w. However, instead of an explicit equation for ITC_{sw}, its value is conservatively estimated by setting it equal to ITC_T or $ITCw$, whichever is greater; that is:

$$ITC_{sw} = \max\left(ITC_T, ITC_w\right) \tag{F-7}$$

ITC_{sw} for fully developed turbulence conditions should be close to zero. The greater the value of ITC_{sw} becomes, the less developed the turbulence. Foken et al. (2012) suggested classifying the resulting value into nine grades, where grade 1 indicates conditions of fully developed turbulence, and grade 9 indicates conditions of undeveloped turbulence (see TABLE F-1).

Similarly, for momentum flux, a conservative approach is used:

$$ITC_{tau} = \begin{cases} \max\left(ITC_u, ITC_w\right) & \text{double rotations used} \\ ITC_w & \text{planar fit rotations used} \end{cases} \tag{F-8}$$

It should be noted that the variable u used in calculating ITC_u and ITC_{tau}, in the case of Table 4.2 of Foken et al., (2012), is stream-wise wind speed, although

the authors did not explicitly specify this. Accordingly, the raw variable U_x from a sonic anemometer, which is rarely a stream-wise wind speed, must undergo coordinate rotations. It becomes the stream-wise wind speed only after the first rotation of Tanner and Thurtell (1969) or the third rotation of Wilczak et al. (2001).

The datalogger program uses either method of coordinate rotations, depending on the selection of the user; however, only the first two rotations of each method are done in order to reduce unnecessary computation time on the third rotation. Accordingly, u and subsequently ITC_u, are only available to find ITC_{tau} if the method of Tanner and Thurtell (1969) is selected. If the planar fit method [Wilczak et al (2001)] is used, ITC_{tau} is simply found from ITC_w as an approximation (see equation F-8).

Similar to the other relative turbulence characteristics, the greater the value of ITC_{tau}, the less developed the turbulence. The resulting value is classified into nine grades, where grade 1 indicates fully developed conditions of turbulence, and grade 9 indicates least developed conditions of turbulence (see TABLE F-1).

Further, for stable surface-layer conditions beyond the ranges where parameters are defined in TABLE F-2, the quality grades for ITC_α, ITC_T, and ITC_{tau} are conservatively assigned as 9.

F.3 Wind Direction in the Sonic Instrument Coordinate System (wnd_dir_sonic)

The sonic anemometer has a boom-mount design that may affect the wind flow when the wind is blowing from behind the boom towards the sonic transducers. Accordingly, Foken et al. (2012) assigned a poorer data quality grade of 3 to wind coming from angles 180 ± 10° relative to the sonic coordinate system, a medium grade of 2 to winds outside of this range but within 29° of 180°, and a good grade of 1 for all other angles (see TABLE F-1).

F.4 Overall Quality Grade System

Each covariance variable over the averaging period is assigned an overall quality grade from 1 to 9 based on the individual grades of RN_{cov}, ITC_{sw}, and *wnd_dir_sonic* (see TABLE F-3). Grade 1 is the highest overall quality, and grade 9 is the poorest.

TABLE F-3. Overall grades for each flux variable by the grades of relative non-stationary, relative integral turbulence characteristic, and wind direction in sonic instrument coordinate system.[1]

Overall quality grade	RN_{cov} Relative non-stationarity	ITC_{sw} Relative integral turbulence characteristic	wnd_dir_sonic Wind direction
1 (best)	1	1 – 2	1
2	2	1 – 2	1
3	1 – 2	3 – 4	1
4	3 – 4	1 – 2	1

TABLE F-3. Overall grades for each flux variable by the grades of relative non-stationary, relative integral turbulence characteristic, and wind direction in sonic instrument coordinate system.[1]			
Overall quality grade	***RN*$_{cov}$ Relative non-stationarity**	***ITC*$_{sw}$ Relative integral turbulence characteristic**	**wnd_dir_sonic Wind direction**
5	1 – 4	3 – 5	1
6	5	5	2
7	6	6	2
8	7 – 8	7 – 8	2
9 (worst)	9	9	3

[1]Simplified Table 4.5 in Foken et al. (2012)

F.5 Programmatic Approach

The datalogger program determines an overall quality grade using these steps:

1. Calculate quality variables:

   RN_{cov} for $\overline{u'w'}$, $\overline{v'w'}$, $\overline{T_s'w'}$, $\overline{\rho_{co2}'w'}$, and $\overline{\rho_{h2o}'w'}$

   ITC_{tau} for momentum flux

   ITC_{Tsw} for sensible heat, CO_2, and H_2O fluxes

2. Use RN_{cov} to grade stationarity, ITC_{tau} and ITC_{Tsw} to grade the integral turbulence characteristics, and wind angle in the sonic coordinate system to grade wind direction (see TABLE F-2).

3. Define an array with three elements:

   The first element records the best possible quality grade in the overall grade system for a given grade of relative non-stationarity. For example, a grade 2 for RN_{cov} can be assigned as grade 2 or 3 in the overall grade system. In this case the datalogger will store the value of "2" as the first element in the array.

   Similarly, the second element in the array is the best possible quality grade in the overall grade system for a given grade of the integral turbulence characteristics.

   The third element in the array is the best possible quality grade in the overall grade system for a given grade of wind direction.

4. The maximum value of the three elements is the overall quality grade for the variable being evaluated (such as, flux of CO2, H2O, sensible heat, or momentum).

F.6 References

Aubinet M, B. Chermanne, M. Vandenhaute, B. Longdoz, M. Yernaux, E. Laitat. 2001. Long term carbon dioxide exchange above a mixed forest in the Belgian Ardennes. Agricultural and Forest Meteorology. 108:293-315.

Foken, T, R. M. Göckede, M. Mauder, L. Mahrt, B.D. Amiro, J.W. Munger. 2004. Post-field data quality control. In Lee, X., W. Massman, B. Law (eds). Handbook of Micrometeorology: A guide for surface flux measurement and analysis. Kluwer, Dordrecht, pp181-208.

Foken, T, R. Leuning, S.R. Onley, M. Mauder, M. Aubinet. 2012. Corrections and data quality control. In M, Aubient, T. Vesala, D. Papale. (eds). Eddy Covariance: A Practice Guide to Measurement and Data Analysis. Springer, New York. p.85-131.

Foken, T., B. Wichura. 1996. Tools for quality assessment of surface-based flux measurements. Agricultural and Forest Meteorology 78: 83-105

Kaimal, J. C. and J. J. Finnigan, 1994. Atmospheric Boundary Layer Flows: Their Structure and Measurement. Oxford University Press, Oxford, 289 p.

Moncrieff, J.B., J.M. Massheder, H.de Bruin, J.A. Elbers, T. Friborg, B. Heusinkveld, P. Kabat, S. Scott, H. Soegaard, A. Verhoef. 1997. A system to measure surface fluxes of momentum, sensible heat, water vapour and carbon dioxide. Journal of Hydrology 188-189: 589-611.

Shearman, R.J. 1992. Quality assurance in the observation area of the Meteorological Office. Meteorological Magazine 121: 212-216.

Stull, R.B. 1988. An introduction to Boundary Layer Meteorology. Kluwer Academic Publisher, Boston, 666p.

Thomas, C., T. Foken. 2002. Re-evaluation of integral turbulence characteristics and their parameterizations. In 15th Conference on turbulence and boundary layer, Wageningen, NL, 15-19 July 2002, American Meteorological Society. Pp129-132.

Tillmann, H. 1972. The direct determination of stability, heat and momentum fluxes in the atmospheric boundary layer from simple scalar variables during dry unstable conditions. Journal of Applied Meteorology 11: 783-792.

Vickers, D., L. Mahrt. 1997. Quality control and flux sampling problems for tower and aircraft data. Journal of Atmospheric Ocean Technology 14: 512-526.

Appendix G. Footprint

The percentage of measured scalar flux from an area of interest is a major indicator of appropriate site selection and station design. The upwind range within which the sources/sinks contribute a given percent of total fluxes (for example, 40, 55, and 90%) is typically desired by an investigator. Additionally, the location of sources/sinks that contributes most to the measured fluxes is often of interest (Kljun et al. 2004). These footprint characteristics can be calculated using a footprint function of the measured scalar flux.

A footprint function of measured scalar flux, given by $f(x, y, z_m)$ where x and y are horizontal spatial variables with positive x-axis pointing into the streamwise direction and z_m is measurement height, is a probability spatial distribution of the relative contribution to the fluxes measured at the point (0, 0, z_m), assuming that surface sources/sinks in the x-y domain as described by $F(x, y, 0)$ are horizontally homogenous, or in other words $F(x,y,0)$ is a constant. The footprint, $f(x, y, z_m)$, can be implicitly defined using the measured flux, $F(0,0,z_m)$, and the flux spatial function at the surface, $F(x,y,0)$, given by:

$$F(0,0,z_m) = \int_{-\infty}^{\infty}\int_{0}^{\infty} F\left(x,y,0\right) f\left(x,y,z_m\right) dxdy \qquad \text{(G-1)}$$

The two functions inside the double integration describe the amount of contribution to the measured flux from sources/sinks across the integrated area. Given the two functions, the proportion of the measured flux from a smaller defined area can also be calculated. For a general case, this equation may be simplified by the assumption that $F(x,y,0)$ is a constant (in example, sources/sinks of flux are horizontally homogenous). The CRBasic online calculations are designed for this general case. Therefore, $F(x,y,0)$ is treated as a constant and only the footprint [$f(x, y, z_m)$] requires greater characterization.

To calculate the footprint in the CRBasic online flux program, an analytical equation, $f(x, y, z_m)$, is needed. Several studies (Gash, 1986; Schuepp, et al., 1990; Schmid, 1994; Hsieh, et al., 2000; Kormann and Meixner, 2001; Kljun, et al, 2004) provide analytical footprint equations. The equations of Kljun, et al (2004) were developed more recently than the others, and accordingly are used in the CRBasic program. Their application, however, is limited to the following ranges of atmospheric stability, friction velocity, and measurement height:

1. $-200 \le (z_m - d)/L \le 1$
2. $u_* \ge 0.2$ (G-2)
3. $z_m - d \ge 1$ m

where d is zero displacement height and L is Obukhov length. For cases outside of the ranges above, the analytical footprint equation of Kormann and Meixner (2001) is used.

G.1 Kljun, et. al. (2004) Analytical Footprint Equations

G.1.1 Models and Parameters

By applying dimensional analysis (Buckingham Π method, see Stull 1988) and analyzing numerical simulations, Kljun et al (2004) summarized footprints in field scale for a given roughness length (z_0) and ratio of aerodynamic height to planetary boundary-layer (PBL) height as a dimensionless footprint (F_*) in terms of dimensionless length (X_*) for the range of conditions presented in (G-2). The summarized footprint is represented by the model:

$$F_*(X_*) = k_1 \left(\frac{X_* + k_4}{k_3} \right)^{k_2} \exp\left[k_2 \left(1 - \frac{X_* + k_4}{k_3} \right) \right] \qquad \text{(G-3)}$$

where k_i (subscript i = 1, 2, 3, and 4) is a parameter. If the parameters in the model are given, the dimensionless footprint can be calculated for different dimensionless lengths. These parameters can be statistically estimated using the sampled values of X_* and F_*. The dimensionless length is a combination of vertical wind standard deviation (σ_w), friction velocity (u_*), measurement aerodynamic height (z), and stream-wise distance to measurement location (x), given by:

$$X_* = \left(\frac{\sigma_w}{u_*} \right)^{a_1} \frac{x}{z} \qquad \text{(G-4a)}$$

where a_1 is a parameter that was found to be 0.8 by numerical simulations using the software *LPDM-B*. To consider the zero displacement height (d) over different surface types, the variable z should be interpreted as the measurement aerodynamic height ($z = z_m - d$), which was confirmed by Dr. Kljun per email on November 14, 2014. The dimensionless footprint of F_* is a combination of vertical wind standard deviation, friction velocity, planetary boundary-layer height (h), measurement aerodynamic height, and streamwise footprint integrated over cross-wind (i.e., marginal streamwise footprint) at a field scale [$f_y(x,z)$ in m^{-1}], given by:

$$F_* = \left(\frac{\sigma_w}{u_*} \right)^{a_2} \left(1 - \frac{z}{h} \right)^{-1} z f_y(x,z) \qquad \text{(G-4b)}$$

where a_2 is a parameter that was found to be -0.8 by simulation using the software *LPDM-B*.

For a given case, the values of σ_w, u_*, h, and z are known and the value of $f_y(x,z)$ can be numerically simulated (Horst and Weil 1992). Given these values, X_* and F_* can be calculated using (G-4a) and (G-4b). Kljun, et al (2004) then used calculated values of dimensionless footprint and

dimensionless length as samples to statistically estimate the parameters of k_1 to k_4 in model (G3) for four roughness lengths and four ratios of aerodynamic height to PBL height as shown in TABLE G-1.

TABLE G-1. Estimated parameters in dimensionless footprint model (F3)

z/h	k_1	k_2	k_3	k_4	k_1	k_2	k_3	k_4
	$z_0 = 0.01$ m				$z_0 = 0.1$ m			
0.005	0.024	3.84	31.0	18.0	0.028	2.47	22.0	12.0
0.075	0.024	4.11	33.0	15.0	0.027	2.87	24.0	10.0
0.250	0.021	3.61	35.0	12.0	0.026	3.40	27.0	10.0
0.500	0.025	4.23	33.0	9.0	0.028	5.06	32.0	12.0
	$z_0 = 0.30$ m				$z_0 = 1.0$ m			
0.075	0.042	4.06	19.0	7.00	0.052	2.40	11.0	5.00
0.250	0.038	4.24	21.0	7.00	0.050	3.19	14.0	4.00
0.500	0.042	6.02	23.0	6.00	0.051	3.93	15.0	3.00

Even without the PBL height, it is possible to use these parameters. From figure 7 in Kljun et al (2004) it is evident that k_1 can be well described using a function of the natural logarithm of z_0, which is independent of z/h. This function is given by [left-top panel in figure 7, equation 13 in Kljun et al (2004), and email from Dr. Kljun in Feb 10, 2015].

$$k_1 \approx \frac{0.175}{3.418 - \ln z_0} \tag{G-5a}$$

Parameters k_3 and k_4 are both linear functions of ln z_0. Parameter k_3 is given by [left-bottom panel in figure 7 and equation 15 in Kljun et al (2004)].

$$k_3 \approx 4.277 \times \left(3.418 - \ln z_0\right) \tag{G-5b}$$

and parameter k_4 is given by [right-bottom panel in figure 7 and equation 16 in Kljun et al (2004)].

$$k_4 \approx 1.685 \times \left(3.418 - \ln z_0\right) \tag{G-5c}$$

Note: Although the parameters published in Kljun et al. (2004) had fewer significant digits, email correspondence with Dr. Kljun dated Feb 10, 2015, led to the adoption of three digits after the decimal for parameters in Equation G-5a through G-4c.

Parameter k_2 is independent of z_0 and is a constant. Determining its value requires taking the integral of $\hat{F}_*(\hat{X}_*)$ (the over-hat indicates they are equations with statistically-estimated parameters) over the entire domain of $\hat{X}_*$ and setting it equal to one, as shown here [see appendix in Kljun et al. (2004)]:

$$\int_{k_4}^{\infty} \hat{F}_*(\hat{X}_*)d\hat{X}_* = k_1 k_3 \exp(k_2) k_2^{-k_2} \Gamma\left(k_2\right) = 1 \quad \text{(G-5d)}$$

Substituting (G-5a) and (G-5b) into (G-5d) leads to:

$$\exp(k_2) k_2^{-k_2} \Gamma\left(k_2\right) = 1.336050 \quad \text{(G-5e)}$$

A numerical solution then generates k_2:

$$k_2 = 3.682540 \quad \text{(G-5f)}$$

G.1.2 Application of Analytical Footprint

The marginal stream-wise footprint [$f_y(x,z)$] in (G-4b) is required to calculate the needed footprint characteristics. However, for many years its analytical form and the resulting cumulative footprint were unavailable for a wide range of stabilities and wind velocity profiles. This motivated several studies to conduct numerical simulations (Hsieh et al. 2000, Kljun et al 2004), which could then be used to develop analytical footprint equations [for example model (G3) and TABLE G-1].

Given an analytical form of $f_y(x,z)$, the calculation of footprint characteristics is straight forward. The sections below present equations for footprint characteristics such as the percentage of flux from a defined upwind range of interest and the point of maximum source/sink contribution to the measured flux. These equations relate $f_y(x,z)$, $F_*(X_*)$, and footprint characteristics.

Percentage of measured scalar flux from the upwind range of interest
Given the marginal stream-wise footprint $f_y(x,y)$, the percentage of contribution from the sources/sinks within the upwind range of R, [$P_F(R)$], can be calculated using:

$$p_F\left(R\right) = 100 \int_{-R_{k4}}^{R} f_y(x,z)dx \quad \text{(G-6)}$$

where $-R_{k4}$ is the downwind location of starting contribution of sources/sinks to measured fluxes.

Since:

$$\int_{-R_{k4}}^{R} f_y(x,z)dx = \frac{\left(\frac{\sigma_w}{u_*}\right)^{a_2}\left(1-\frac{z}{h}\right)^{-1} z \int_{-R_{k4}}^{R} f_y(x,z)dx}{\left(\frac{\sigma_w}{u_*}\right)^{a_2}\left(1-\frac{z}{h}\right)^{-1} z} \quad \text{(G-7)}$$

$$= \left(\frac{\sigma_w}{u_*}\right)^{-a_2} \frac{1}{z}\left(1-\frac{z}{h}\right) \int_{-R_{k4}}^{R} \hat{F}_*(\hat{X}_*)dx$$

and because $F_*(X_*)$ is defined in the domain of $X_* > -k_4$, this low limit of integration is the value of x at $X_*(x) = -k_4$. Thus, R_{k4} is given by:

$$R_{k4} = k_4 z \left(\frac{u_*}{\sigma_w} \right)^{a_1} \tag{G-8}$$

Submitting (G-7) into (G-6) generates:

$$p_F(R) = 100 \left(\frac{\sigma_w}{u_*} \right)^{-a_2} \frac{1}{z} \left(1 - \frac{z}{h} \right) \int_{-R_{k4}}^{R} F_* \left[X_*(x) \right] dx \tag{G-9}$$

Calculation for this is possible using numerical integration of the dimensionless footprint $F_*\left[X_*(x) \right]$ at discrete, incremental values of x, starting at a low value given by $-R_{k4}$ and increasing until the value for R is reached. Specifically, the value for dimensionless footprint at each value of x is found by using equations (G-3) and (G-4a) with measured variables (σ_w and u_*), known variables (z), and estimated parameters [k_i, given by (G-5a), (G-5b), (G-5c), and (G-5f)], as shown here:

$$F_*[X_*(x)] = k_1 \left[\frac{\left(\frac{\sigma_w}{u_*} \right)^{0.8} \frac{x}{z} + k_4}{k_3} \right]^{k_2} \exp\left\{ k_2 \left[1 - \frac{\left(\frac{\sigma_w}{u_*} \right)^{0.8} \frac{x}{z} + k_4}{k_3} \right] \right\} \tag{G-10}$$

The values for dimensionless footprint at every interval of x may then be summed to estimate the value of the integral term in equation (G-9) for calculation of $p_F(R)$.

Upwind location of source/sink that contributes most to the measured flux

Differentiating both sides of (G-4b) with respect to x generates:

$$\frac{df_y(x,z)}{dx} = \left(\frac{\sigma_w}{u_*} \right)^{-a_2} \left(1 - \frac{z}{h} \right) z^{-1} \frac{dF_*}{dX_*} \frac{dX_*}{dx} \tag{G-11}$$

The marginal stream-wise footprint [$f_y(x,z)$] is a bell-shape function with respect to x, with a maximum occurring at x_{max}, which follows that:

$$\left. \frac{df_y(x,z)}{dx} \right|_{x=x_{\max}} = 0 \tag{G-12}$$

For real-world cases in the field, the terms of measured variables in the right-hand-side of (G-11) will never equal zero, therefore, equation (G-12) can only be true when the last two derivative terms are evaluated as zero at x_{max}, that is:

$$\left.\frac{dF_*}{dX_*}\frac{dX_*}{dx}\right|_{x=x_{\max}} = 0 \qquad \text{(G-13)}$$

This can be expanded to the following equation:

$$\left.\frac{dF_*}{dX_*}\frac{dX_*}{dx}\right|_{x=x_{\max}} = \frac{k_1 k_2}{k_3 z}\left(\frac{\sigma_w}{u_*}\right)^{a_1}\left[\frac{X_*(x_{\max})+k_4}{k_3}\right]^{k_2-1}\exp\left[k_2\left(1-\frac{X_*(x_{\max})+k_4}{k_3}\right)\right]\left[1-\frac{X_*(x_{\max})+k_4}{k_3}\right] = 0$$

This equation is then solved for $X_*(x_{\max}) > -k_4$, resulting in the upwind distance from the measurement station to the location that contributes most to the measured flux being expressed as:

$$x_{\max} = (k_3 - k_4) z \left(\frac{u_*}{\sigma_w}\right)^{0.8} \qquad \text{(G-14)}$$

According to (G-6) and (G-9), the percentage of contribution to the measured flux within an upwind range of x_p, where subscript p indicates percent and can have a value of 0 to 100 [e.g., $P_F(x_{10}) = 10$ and $P_F(x_{90}) = 90$], can be expressed as:

$$p_F(x_p) = 100\left(\frac{\sigma_w}{u_*}\right)^{0.8}\frac{1}{z}\left(1-\frac{z}{h}\right)\int_{-R_{k4}}^{x_p} F_*\left[X_*(x)\right]dx \qquad \text{(G-15)}$$

This is an increasing monotonic function of x_p. Given this, for a value of $p_F(x_p)$, only one value of x_p can be found. The value of x_p may be estimated by performing a numerical integration of $p_F(R)$ as described in the section above. Using a subscript i for x indicates the sequential number of numerical integration steps, the two neighbor values of $p_F(x_i)$ less than the target value of p (for example, p = 10) and $p_F(x_{i+1})$ greater than the target value can then be used to interpolate a more precise value of x_p where $P_F(x_p) = p$.

G.1.3 Programmatic Approach

Roughness length

Applying model (G3) requires knowing the roughness length in order to calculate the parameters (G-5a) to (G-5c). The roughness length depends on surface type (for example, bare land, water surface, crops, grasses, trees, and shrubs) and is approximately $0.13h_c$ for crops and grasses, where h_c represents canopy height (Tanner and Pelton, 1960; Stanhill, 1969), $0.06h_c$ for forests (Jarvis, et al., 1976; Raupach, et al., 1991), and $0.033h_r$, where h_r represents roughness element height for bare land (for example, sands) (Raupach, et al., 1991). A more accurate value of roughness length depends not only on the surface type but also on surface roughness texture (for a canopy, this texture can be described using vegetative surface area per unit volume). However, this texture, the canopy height, and the resulting roughness length may change quickly during certain periods of the growing season. This makes it impractical to input a single roughness length that will be valid for a long time periods.

Accordingly, the roughness length should be updated periodically, which is possible using the well-known equation of a wind profile under neutral conditions [equation (4.2) in Rosenberg et al. (1983)]:

$$z_0 = (z_m - d)\exp\left(-\frac{k\sqrt{\bar{u}^2 + \bar{v}^2}}{u_*}\right) \quad \text{(G-16)}$$

where k is von Karman constant (0.41) and $\bar{u}$ and $\bar{v}$ are the two orthogonal components of mean horizontal wind speeds, respectively. The roughness length is automatically updated by the datalogger at the end of each averaging interval as long as the surface layer stability is under neutral conditions, as defined by the strict criterion of $|z / L| < 0.02$ (Hsieh et al. 2000). The updated roughness length will then be used for the calculation of parameters k_1, k_3, and k_4 using (G-5a) to (G-5c).

Until an averaging period occurs with neutral stability, an initial value for roughness length must be estimated and used. Accordingly, our programmatic approach is to require that the user select, among the options in a menu, the land type that most closely matches the area around their eddy covariance station. The program then uses this input to calculate an initial roughness length as follows:

$$z_0 = 10^{0.997\log_{10} h_c - 0.883} \quad \text{(G-17)}$$

for crops and grasses (Szeicz et al 1969), $0.06h_c$ for forests and shrubs, and 0.01 m for bare land and water surfaces (i.e., corresponds to the parameters for lowest roughness length in TABLE G-1). As soon as measured half-hourly data are available and the stability is under neutral conditions, this initial roughness length will be updated using (G-16).

Calculation for parameters of k_1 to k_4

$$k_1 \approx \frac{0.175}{3.418 - \ln z_0}$$

$$k_2 \approx 3.682540$$

$$k_3 \approx 4.277(3.418 - \ln z_0)$$

$$k_4 \approx 1.685(3.418 - \ln z_0)$$

Calculation of planetary boundary-layer height

TABLE G-2. Relationship of Obukhov length (L) to planetary boundary-layer height (h)

***L* (m)**	–5	–30	–650	∞	1000	130	84
***h* (m)**	2000	1500	1200	1000	800	250	200

The Obukhov length is calculated in eddy covariance flux measurements, and then it is used to find the PBL height using the data points in TABLE G-2 and linear interpolation.

Upwind location of source/sink that contributes most to the measured flux (maximum location)
The following equation is used in the datalogger:

$$x_{\max} = \left(k_3 - k_4\right) z \left(\frac{u_*}{\sigma_w}\right)^{0.8}$$

Upwind inflection points of footprint
The footprint is a bell-shaped function with one maximum point (turning point) and two inflection points. Because the footprint changes most in the segments from the left inflection point (x_{IL}) to x_{max} and from x_{max} to the right inflection point (x_{IR}), these inflection points may be used as boundaries for special numerical integration segments where the integration intervals are smaller to provide greater accuracy. Outside of these special segments, the integration intervals may be larger and thereby decrease the computation required. Specifically, the inflection point located at the left side of x_{max} (x_{IL}) is given as:

$$x_{IL} = \frac{x_{\max}}{k_3 - k_4}\left[k_3\left(\frac{\sqrt{k_2} - 1}{\sqrt{k_2}}\right) - k_4\right]$$

and the other is at the right side of x_{max} (x_{IR}):

$$x_{IR} = \frac{x_{\max}}{k_3 - k_4}\left[k_3\left(\frac{\sqrt{k_2} + 1}{\sqrt{k_2}}\right) - k_4\right]$$

See the derivation of the inflection points in Appendix G.2, *Derivation of Equations for Upwind Locations at Inflection Points of Footprint in Kljun et al (2004)* **(p. G-10)**.

Percentage of measured scalar flux from the upwind rand of interest to measurements
As explained previously, the percentage of measured flux coming from an area of interest may be calculated with the datalogger using the following equation:

$$p_F\left(R\right) = 100 k_1 \left(\frac{\sigma_w}{u_*}\right)^{0.8} \frac{1}{z}\left(1 - \frac{z}{h}\right) \int_{-R_{k4}}^{R} \left[\frac{\left(\frac{\sigma_w}{u_*}\right)^{0.8} \frac{x}{z} + k_4}{k_3}\right]^{k_2} \exp\left\{k_2\left[1 - \frac{\left(\frac{\sigma_w}{u_*}\right)^{0.8} \frac{x}{z} + k_4}{k_3}\right]\right\} dx$$

where the integral is evaluated using numerical integration.

Within the first integration segment (from R_{k4} to x_{IL}), the trapezoidal rule for numerical integration is used with the segment divided into q intervals, where q is an integer selected such that the resolution of the numerical integration

yields reasonable accuracy without a large burden in computation (for example, q = 20*)*.

Within the second segment (x_{IL} to x_{max}), the trapezoidal rule is still used with an integration interval of (x_{max} - x_{IL})/q.

The third segment also uses the trapezoidal rule and extends from x_{max} to x_{IR} + (x_{IR} - x_{max}) with an integration interval of (x_{IR}- x_{max})/q. The fourth and final segment begins at the end of the 3rd segment. The fourth segment uses integration intervals with a size of 4z. Although these intervals may be significantly larger than the intervals used in the other segments, the integration accuracy should still be acceptable since Boole's rule, rather than the trapezoidal rule, is used within this segment and the slope of the footprint should be changing very slowly throughout the segment. The fourth segment initially extends to 200z beyond the segment starting point or until the the cumulative flux reaches 90%. If the distance of interest is not reached at the end of the fourth segment but is within another 100z, an additional 25 integration intervals are added to the segment, with the end point being the distance of interest. If the distance of interest is beyond another 100z, it is assumed that the cumulative footprint would be wholly contained within the distance of interest, thus 99% is reported as the cumulative flux within the distance of interest. If the cumulative flux never reaches 90%, which is possible under certain conditions where the numerical integration is inadequate or the model doesn't truly reflect the real footprint distribution, the distance for 90% flux will be reported as *NAN* (not a number).

Scaling the integration intervals within each segment provides a way to have higher integration resolution when the slope of footprint changes more dramatically while still limiting the size of the integration interval when the slope is not changing as much. This approach is successful in converging the percentage flux to a value of one if numerically integrated over the entire domain. An additional advantage of this approach is that because x_{max} must be used as a segment boundary, the peak value of the function is never missed, which contributes to greater accuracy of the overall numerical integration.

Upwind range within which the sources/sinks contributes a given percent to measured flux

If this upwind range is denoted using x_p where subscript p indicates the given percent, it can be implicitly expressed in an equation as:

$$p = 100k_1\left(\frac{\sigma_w}{u_*}\right)^{0.8}\frac{1}{z}\left(1-\frac{z}{h}\right)\int_{-R_{k4}}^{x_p}\left[\frac{\left(\frac{\sigma_w}{u_*}\right)^{0.8}\frac{x}{z}+k_4}{k_3}\right]^{k_2}\exp\left\{k_2\left[1-\frac{\left(\frac{\sigma_w}{u_*}\right)^{0.8}\frac{x}{z}+k_4}{k_3}\right]\right\}dx$$

Among the values of $p_F(x_p)$ that were found in the process of numerical integration described above, if the value in current iteration is just greater than the target percentage (for example, p = 40), a more precise value of x_{40} [for example, $p_F(x_{40}) = 40$] can be interpolated using this value along with the value in previous iteration. In this way, x_{40}, x_{55}, and x_{90} are found.

G.2 Derivation of Equations for Upwind Locations at Inflection Points of Footprint in Kljun et al. (2004)

As described above, integration segment boundaries should be determined by the upwind inflection points of the footprint. Since the footprint is known to be a bell-shaped function, there is one maximum point (x_{max}) and two inflection points (x_{IL} and x_{IR}) on both sides of the maximum, respectively. Accordingly, x_{max} may be found by setting the first order derivative of the footprint function to zero. Similarly, x_{IL} and x_{IR} may be found by setting the second order derivative to zero. The following section shows this derivation for these points.

G.2.1 Footprint Model

The footprint in Kljun et al. (2004) is given in the form of a dimensionless footprint [$F_*(X_*)$]:

$$F_*(X_*) = k_1 \left(\frac{X_* + k_4}{k_3} \right)^{k_2} \exp\left[k_2 \left(1 - \frac{X_* + k_4}{k_3} \right) \right] \tag{G-18}$$

where k_i (subscript i = 1, 2, 3, and 4) is a parameter, and X_* is the dimensionless length. It is a combination of vertical wind standard deviation (σ_w), friction velocity (u_*), measurement aerodynamic height ($z = z_m - d$), and the upwind distance (x) from the measurement location given by:

$$X_* = \left(\frac{\sigma_w}{u_*} \right)^{a_1} \frac{x}{z} \tag{G-19}$$

where a_1 is a parameter. The dimensionless footprint of F_* is a combination of vertical wind standard deviation, friction velocity, planetary boundary-layer height (h), measurement aerodynamic height, and stream-wise footprint integrated over cross-wind (i.e., marginal stream-wise footprint) at a field scale [$f_y(x,z)$ in m^{-1}], given by:

$$F_* = \left(\frac{\sigma_w}{u_*} \right)^{a_2} \left(1 - \frac{z}{h} \right)^{-1} z f_y(x,z) \tag{G-20}$$

where a_2 is a parameter.

G.2.2 Upwind location of maximum footprint

Differentiating both sides of (G-20) with respect to x generates:

$$\frac{df_y(x,z)}{dx} = \left(\frac{\sigma_w}{u_*} \right)^{-a_2} \left(1 - \frac{z}{h} \right) z^{-1} \frac{dF_*}{dX_*} \frac{dX_*}{dx} \tag{G-21}$$

The derivative of dimensionless length with respective to x is greater than zero and is independent of x; therefore:

$$\frac{df_y(x,z)}{dx} = 0 \text{ at } \frac{dF_*}{dX_*} = 0 \tag{G-22}$$

which indicates $f_y(x,z)$ and F_* reaches the maximum at the same upwind location (x_{max}). Therefore, the location of maximum footprint satisfies the following equation:

$$\left.\frac{dF_*}{dX_*}\right|_{x=x_{max}} = \frac{k_1 k_2}{k_3}\left[\frac{X_*(x_{max})+k_4}{k_3}\right]^{k_2-1}\exp\left[k_2\left(1-\frac{X_*(x_{max})+k_4}{k_3}\right)\right]\left[1-\frac{X_*(x_{max})+k_4}{k_3}\right] = 0 \tag{G-23}$$

Solving this equation for $X_*(x_{max}) > -k_4$ generates:

$$x_{max} = (k_3 - k_4)\, z\left(\frac{u_*}{\sigma_w}\right)^{0.8} \tag{G-24}$$

G.2.3 Upwind locations of inflection points

Differentiating both sides of (G-21) with respect to x generates:

$$\frac{d^2 f_y(x,z)}{dx^2} = \left(\frac{\sigma_w}{u_*}\right)^{-a_2}\left(1-\frac{z}{h}\right)z^{-1}\frac{d^2F_*}{dX_*^2}\left(\frac{dX_*}{dx}\right)^2 \tag{G-25}$$

The derivative of dimensionless length with respective to x is greater than zero and is independent of x; therefore:

$$\frac{d^2 f_y(x,z)}{dx^2} = 0 \text{ at } \frac{d^2F_*}{dX_*^2} = 0 \tag{G-26}$$

which indicates $f_y(x,z)$ and F_* have inflection points at the same upwind locations, and therefore:

$$\frac{d^2F_*}{dX_*^2} = 0 \tag{G-27}$$

This can be used to find the upwind locations of the inflection points in the footprint curve.

Referencing (G-23), the first order derivative of dimensionless footprint can be written as:

$$\frac{dF_*}{dX_*} = \frac{k_2}{k_3}\left[\left(\frac{X_*+k_4}{k_3}\right)^{-1}-1\right]F_* \tag{G-28}$$

Using this equation, the derivative at the second order can be derived as:

$$\frac{d^2F_*}{dX_*^2} = \frac{k_2}{k_3}\left[-\frac{1}{k_3}\left(\frac{X_* + k_4}{k_3}\right)^{-2} F_* + \left(\frac{X_* + k_4}{k_3}\right)^{-1}\frac{dF_*}{dX_*} - \frac{dF_*}{dX_*}\right]$$

$$= -\frac{k_2}{k_3^2}\left(\frac{X_* + k_4}{k_3}\right)^{-2} F_* + \frac{k_2^2}{k_3^2}\left[\left(\frac{X_* + k_4}{k_3}\right)^{-1} - 1\right]^2 F_* \qquad \text{(G-29)}$$

$$= -\frac{k_2}{k_3^2} F_*\left\{\left(\frac{X_* + k_4}{k_3}\right)^{-2} + k_2\left[\left(\frac{X_* + k_4}{k_3}\right)^{-1} - 1\right]^2\right\}$$

In this equation, the term ahead of the curly bracket is not zero. Therefore, in order to satisfy (G-27), the term inside the curly bracket must be zero. If assuming:

$$X = \left(\frac{X_* + k_4}{k_3}\right)^{-1} \qquad \text{(G-30)}$$

The term inside the curly bracket satisfies (G-27) in the following form:

$$X^2 + k_2\left[X - 1\right]^2 = 0 \qquad \text{(G-31)}$$

Solving this equation, substituting (G-19) into X, and referencing (G-24) leads to an equation for the left inflection point:

$$x_{IL} = \frac{x_{\max}}{k_3 - k_4}\left[k_3\left(\frac{\sqrt{k_2} - 1}{\sqrt{k_2}}\right) - k_4\right] \qquad \text{(G-32)}$$

Similarly, the equation for the right inflection point is obtained by:

$$x_{IR} = \frac{x_{\max}}{k_3 - k_4}\left[k_3\left(\frac{\sqrt{k_2} + 1}{\sqrt{k_2}}\right) - k_4\right] \qquad \text{(G-33)}$$

G.3 Kormann and Meixner (2001) Analytical Footprint Equations

G.3.1 Footprint

As an alternative to the analytical approach used by Kljun, et al., (2004), which is limited by the conditions presented in (G-2), the footprint was derived by Kormann and Meixner (2001) based on Van Ulden (1978) as [(see the detailed

derivations in Appendix G.4, *Derivation of Analytical Footprint in Kormann and Meixner (2001)* (p. G-19)]:

1. Two dimensional (2D) marginal stream-wise footprint

$$f_y(x,z) = \frac{1}{\Gamma(\mu)} \xi^{\mu} \left(\frac{z^{m+1}}{x^{\mu+1}} \right) \exp\left(-\xi \frac{z^r}{x} \right) \tag{G-34}$$

where r, μ, and ξ are composites of other variables which have been combined for succinctness in the expression. Each of these variables is defined below.

r (shape factor):

$$r = 2 + m - n \tag{G-35}$$

where m is the exponent in a vertical profile of horizontal wind [see (G-74) in Appendix G.4, *Derivation of Analytical Footprint in Kormann and Meixner (2001)* (p. G-19)], and n is the exponent in a vertical profile of eddy diffusivity [see (G-63) in Appendix G.4, *Derivation of Analytical Footprint in Kormann and Meixner (2001)* (p. G-19).

μ:

$$\mu = \frac{m+1}{r} \tag{G-36}$$

ξ :

$$\xi = \frac{U}{\kappa r^2} \tag{G-37}$$

where U is the wind constant in a vertical profile of horizontal wind [see (G) in74 Appendix G.4, *Derivation of Analytical Footprint in Kormann and Meixner (2001)* (p. G-19)], and κ is the constant in power-law profile of the eddy diffusivity.

$$\kappa = \frac{k u_* z^{1-n}}{\varphi_c(z/L)} \tag{G-38}$$

The calculations for the variables: m, n, U, and κ will be given in the following sections.

G.3.2 Programmatic Approach

The 3D footprint [$f(x,y,z)$] can be expressed in terms of a marginal stream-wise footprint and a *down-wind* probability distribution of scalar concentrations from *upwin*d sources in a domain of x and y [$c(x, y)$] [see model (9) in Horst and Weil, (1992) and model (8) in Kormann and Meixner, (2001)], given by:

$$f\left(x,y,z\right)=c(x,y)f_{y}\left(x,z\right) \tag{G-39}$$

where:

$$c(x,y)=\frac{\overline{u}\left(x\right)}{\sqrt{2\pi}x\sigma_{y}}\exp\left[-\frac{1}{2}\left(\frac{y\overline{u}\left(x\right)}{x\sigma_{y}}\right)^{2}\right] \tag{G-40}$$

where the constant σ_y is the standard deviation of crosswind scalar concentration and $\bar{u}(x)$ is the effective velocity of the scalar plume. This equation is derived from model (10) in Horst and Weil (1992) and model (9) in Kormann and Meixner (2001) after the simple scalar dispersion (σ) in the model is replaced with a detailed descriptive dispersion [$\sigma_y x / \overline{u}(x)$], which depends on distance from the station (x) and effective velocity of the scalar plume [$\bar{u}(x)$]. Substituting (G-34) and (G-40) into (G-39) leads to the three-dimensional footprint:

$$f\left(x,y,z\right)=\frac{\overline{u}\left(x\right)}{\sqrt{2\pi}\sigma_{y}\Gamma\left(\mu\right)}\xi^{\mu}\left(\frac{z^{m+1}}{x^{\mu+2}}\right)\exp\left[-\frac{1}{x^{2}}\left(\xi xz^{r}+\frac{1}{2}\left(\frac{y\overline{u}\left(x\right)}{\sigma_{y}}\right)^{2}\right)\right] \tag{G-41a}$$

where:

$$\overline{u}\left(x\right)=U\frac{\Gamma\left(\mu\right)}{\Gamma\left(\frac{1}{r}\right)}\left(\frac{\kappa r^{2}}{U}x\right)^{\frac{m}{r}} \tag{G-41b}$$

See (G-82) to (G-92) in Appendix G.4, *Derivation of Analytical Footprint in Kormann and Meixner (2001)* *(p. G-19)*, for associated derivations.

G.3.3 Application of analytical footprint

Unlike the dimensionless footprint in Kljun et al., (2004), the footprint developed by Kormann and Meixner, (2001) explicitly gives the analytical marginal (cross-wind integrated) stream-wise footprint (G-34) and three-dimensional footprint (G-41a and G-41b). Both can be directly used to calculate the footprint characteristics.

Percentage of measured scalar flux from the upwind range of interest
The percentage of contribution from these sources/sinks, within the upwind range of interest, to the measured flux [$p_F(R)$] is given by:

$$\begin{aligned}p_{F}\left(R\right)&=100\int_{0}^{R}f_{y}\left(x,z\right)dx\\&=100\frac{\xi^{\mu}z^{m+1}}{\Gamma\left(\mu\right)}\lim_{\Delta x\to 0}\int_{0+\Delta x}^{R}\frac{1}{x^{\mu+1}}\exp\left(-\xi\frac{z^{r}}{x}\right)dx\end{aligned} \tag{G-42}$$

where the Gamma function of μ can be accurately approximated using Memes (2010):

$$\Gamma(\mu) \approx \sqrt{\frac{2\pi}{\mu}}\left[\frac{1}{e}\left(\mu + \frac{1}{12\mu - \frac{1}{10\mu}}\right)\right]^{\mu} \tag{G-43}$$

Location of source/sink that contributes most to the measured flux

1. Approach using 2D marginal stream-wise footprint [$f_y(x,z)$]

   Differentiating (G-34) with respect to x generates:

$$\frac{df_y(x,z)}{dx} = \frac{\xi^{\mu} z^{m+1}}{\Gamma(\mu)} \frac{d}{dx}\left[\frac{1}{x^{\mu+1}} \exp\left(-\xi \frac{z^r}{x}\right)\right]$$

$$= \frac{\xi^{\mu} z^{m+1}}{\Gamma(\xi)} \exp\left(-\xi \frac{z^r}{x}\right)\left\{\frac{-(\mu+1)}{x^{\mu+2}} + \frac{\xi z^r}{x^{\mu+3}}\right\} \tag{G-44}$$

$$= \frac{\xi^{\mu} z^{m+1}}{\Gamma(\mu)} \exp\left(-\xi \frac{z^r}{x}\right)\left[\frac{\xi z^r - x(\mu+1)}{x^{\mu+3}}\right]$$

   The marginal stream-wise footprint [$f_y(x,z)$] is a bell-shape function with respect to x, with the maximum found at x_{max}, which follows that:

$$\left.\frac{df_y(x,z)}{dx}\right|_{x=x_{\max}} = 0 \tag{G-45}$$

   All terms except for the term in the square bracket in (G-44) are greater than zero for any real-world case in the field, and therefore setting that term equal to zero results in the solution for x_{max}:

$$x_{\max} = \frac{\xi z^r}{\mu + 1} \tag{G-46}$$

2. Approach using 3D footprint [$f(x,y,z)$]

   Differentiating (G-41a) with respect to x at y = 0

$$\frac{df(x,0,z)}{dx} = \frac{\xi^{\mu} z^{m+1}}{\sqrt{2\pi}\sigma_y \Gamma(\mu)} \frac{d}{dx}\left[\frac{\overline{u}(x)}{x^{\mu+2}} \exp\left(-\xi \frac{z^r}{x}\right)\right]$$

$$= \frac{\xi^{\mu} z^{m+1}}{\sqrt{2\pi}\sigma_y \Gamma(\mu)} \exp\left(-\xi \frac{z^r}{x}\right)\left\{\frac{1}{x^{\mu+2}} \frac{d\overline{u}(x)}{dx} - \frac{(\mu+2)\overline{u}(x)}{x^{\mu+3}} + \frac{\xi z^r \overline{u}(x)}{x^{\mu+4}}\right\} \quad \text{(G-47a)}$$

The footprint [$f(x,0,z)$] is a bell-shape function along *x,* with the maximum found at x_{max}, which follows that:

$$\left.\frac{df(x,0,z)}{dx}\right|_{x=x_{\max}} = 0 \quad \text{(G-47b)}$$

To satisfy this equation, the term inside curly bracket in (G-47a) must be zero, or:

$$\left[\frac{1}{x^{\mu+2}} \frac{d\overline{u}(x)}{dx} - \frac{(\mu+2)\overline{u}(x)}{x^{\mu+3}} + \frac{\xi z^r \overline{u}(x)}{x^{\mu+4}}\right]_{x=x_{\max}} = 0 \quad \text{(G-47c)}$$

Using (G-41b), the derivative term is expressed as:

$$\frac{d\overline{u}(x)}{dx} = U \frac{m\Gamma(\mu)}{r\Gamma\left(\frac{1}{r}\right)} \left(\frac{\kappa r^2}{U}\right)^{\frac{m}{r}} x^{\frac{m}{r}-1} \quad \text{(G-47d)}$$

Substituting this equation along with (G-41b) into (G-47c) leads to:

$$\left[\frac{m x^{\frac{m}{r}-1}}{r x^{\mu+2}} - \frac{(\mu+2)x^{\frac{m}{r}}}{x^{\mu+3}} + \frac{\xi z^r x^{\frac{m}{r}}}{x^{\mu+4}}\right]_{x=x_{\max}} = 0 \quad \text{(G-47e)}$$

Because $x \neq 0$, it can be simplified as:

$$\left[mx - r(\mu+2)x + r\xi z^r\right]_{x=x_{\max}} = 0 \quad \text{(G-47f)}$$

The solution of this equation is the location of source/sink that contributes most to the measured flux and is given as:

$$x_{\max} = \frac{r\xi z^r}{2r+1} \quad \text{(G-48)}$$

For practical purposes of handling the computation required for the numerical integration, we use x_{max} from the 2D footprint approach, although, admittedly, in some cases the solution from the 3D footprint may be preferable since the

3D footprint uses the detailed descriptive dispersion [see page 215 in Kormann and Meixner (2001)].

Upwind range within which the sources/sinks contribute 10 or 90 percent to measured flux. According to (G-42), the percentage of contribution to the measured flux from the upwind range of x_p, where subscript p indicates percent of 0 to 100, and can be expressed as:

$$p_F\left(x_p\right) = 100\frac{\xi^{\mu} z^{m+1}}{\Gamma\left(\mu\right)} \lim_{\Delta x \to 0} \int_{0+\Delta x}^{x_p} \frac{1}{x^{\mu+1}} \exp\left(-\xi \frac{z^r}{x}\right) dx \qquad \text{(G-49)}$$

This is an increasing monotonic function of x_p; therefore, for a given value of $p_F\left(x_p\right)$, there is a unique value of x_p that can be found. Similar to the method described for applying the Kljun et al (2004) model, the value of x_p may be estimated by performing a numerical integration for intervals of x and then interpolating values of $P_F(x_p)$ to find the corresponding value of x_p for $p_F\left(x_p\right) = p$ where p = 40, 55, or 90.

G.3.4 Programmatic Approach

Calculate the individual variables

Find the exponent of vertical profile of eddy diffusivity [see (G-65) Appendix G.4, *Derivation of Analytical Footprint in Kormann and Meixner (2001)* **(p. G-19)**]:

$$n = \begin{cases} \dfrac{1}{1+5z/L} & z/L > 0 \\ \dfrac{1-24z/L}{1-16z/L} & z/L \le 0 \end{cases} \qquad \text{(G-50)}$$

Find the exponent of vertical profile of horizontal wind [see (G-76) Appendix G.4, *Derivation of Analytical Footprint in Kormann and Meixner (2001)* **(p. G-19)**]:

$$m = \frac{u_*}{k\sqrt{\overline{u}^2\left(z\right)+\overline{v}^2\left(z\right)}} \phi_m\left(\frac{z}{L}\right) \qquad \text{(G-51)}$$

where $\phi_m\left(z/L\right)$ is wind shear, given by:

$$\phi_m\left(\frac{z}{L}\right) = \begin{cases} 1+5z/L & z/L > 0 \\ \left(1-16z/L\right)^{-\frac{1}{4}} & z/L \le 0 \end{cases} \qquad \text{(G-52)}$$

Find the wind constant [see (G-74) in Appendix G.4, *Derivation of Analytical Footprint in Kormann and Meixner (2001)* **(p. G-19)**]

$$U = \frac{\sqrt{\overline{u}^2\left(z\right)+\overline{v}^2\left(z\right)}}{z^m} \qquad \text{(G-53)}$$

Composite variables
Calculate the shape factor and other composite variables:

$$r = 2 + m - n \tag{G-54}$$

μ:

$$\mu = \frac{m+1}{r} \tag{G-55}$$

ξ:

$$\xi = \frac{U}{\kappa r^2} \tag{G-56}$$

Calculate the gamma function of μ [see Nemes (2010), verified as accurate]

$$\Gamma(\mu) \approx \sqrt{\frac{2\pi}{\mu}} \left[\frac{1}{e} \left(\mu + \frac{1}{12\mu - \frac{1}{10\mu}} \right) \right]^{\mu} \tag{G-57}$$

Footprint characteristics
Percent of measured scalar flux from upwind range of interest to measurements:

$$p_F(R) = 100 \frac{\xi^{\mu} z^{m+1}}{\Gamma(\mu)} \lim_{\Delta x \to 0} \int_{0+\Delta x}^{R} \frac{1}{x^{\mu+1}} \exp\left(-\xi \frac{z^r}{x} \right) dx \tag{G-58}$$

Similar to the description of applying the Kljun et al (2004) model, the integral is evaluated by the datalogger using four integration segments, each containing scaled integration intervals so as to increase resolution when the slope of the function is changing more and decrease computation when the slope is changing less. The segment boundaries and interval sizes are the same as described previously, except that when applying the Kormann and Mexiner (2001) model, zero instead of R_{k4} is used as the first segment's lower boundary.

Location of source/sink that contributes most to the measured flux:

$$x_{\max} = \frac{\xi z^r}{\mu + 1} \tag{G-59}$$

Upwind inflection location of footprint, where the Kormann and Meixner (2001) model is a bell-shaped function, there is one maximum point (turning point) and two inflection points. As described previously, these points should be used as boundaries for the numerical integration segments. One of the

inflection points (x_{IL}) is located at the left side of the maximum point and given by:

$$x_{IL} = x_{\max}\left(1 - \frac{1}{\sqrt{\mu+2}}\right)$$

and the other is at the right side (x_{IR}) and given by:

$$x_{IL} = x_{\max}\left(1 + \frac{1}{\sqrt{\mu+2}}\right)$$

See the derivation of these inflection points in Appendix G.5, *Upwind Locations at Inflection Points of Footprint in Kormann and Meixner (2001)* **(p. G-28)**.

Upwind range within which the sources/sinks contributes a given percent to measured flux:

$$p = 100\frac{\xi^{\mu} z^{m+1}}{\Gamma(\mu)} \lim_{\Delta x \to 0} \int_{0+\Delta x}^{x_p} \frac{1}{x^{\mu+1}} \exp\left(-\xi \frac{z^r}{x}\right) dx \qquad \text{(G-60)}$$

Because an analytical solution for x_p is not available, the value of x_p can be interpolated in the process of numerical integration of (G-58) when p is between two consecutive integrated values. In this way, x_{40}, x_{55}, and x_{90} are found.

G.4 Derivation of Analytical Footprint in Kormann and Meixner (2001)

G.4.1 Model Derivation

Following Horst and Weil (1992), the probability distribution of a scalar concentration downwind of a sink/source in three dimensions may be described using a function $c(x, y, z)$, where x and y are horizontal spatial variables with x-axis following mean wind direction, and z is a vertical spatial variable. The function is approximated using two independent probability distributions of downwind scalar concentration in two dimensions and the vertical profile of horizontal wind speed [$u(z)$], given by:

$$c(x,y,z) = \frac{c(x,y)c(x,z)}{\int_0^{\infty} u(z)c(x,z)\,dz} = \frac{c(x,y)c(x,z)}{\overline{u}(x)} \qquad \text{(G-61)}$$

where $\overline{u}(x)$ is termed as a plume effective velocity. In probability theory, integration of $c(x, y, z)$ over the entire domain of y is the marginal (cross-wind integrated) probability distribution of the downwind scalar concentration in x and z [$c_y(x, z)$]. Applying this integration to both sides of (G-61) generates:

$$c_y(x,z) = \frac{c(x,z)}{\overline{u}(x)} \tag{G-62}$$

According to K-theory, the product of the vertical profile of eddy diffusivity [$K(z)$] and the vertical scalar concentration gradient is the scalar flux. Therefore, the cross-wind integrated footprint [$f_y(x,z)$, i.e. the cross-wind integrated probability distribution of flux] is given as:

$$f_y(x,z) = -K(z)\frac{dc_y(x,z)}{dz} \tag{G-63}$$

To analytically express $f_y(x,z)$ for real-world applications, $K(z)$ and $c_y(x,z)$ must be analytically expressed in terms of measured variables.

G.4.2 Analytical expression: Vertical profile of eddy diffusivity

The vertical profile of eddy diffusivity can be described as:

$$K(z) = kz^n \tag{G-64}$$

where *k* is the von Karman constant (0.41), and *n* is the power exponent depending on the surface layer stability, given by (Huang 1979):

$$n = \frac{z}{K(z)}\frac{dK(z)}{dz} = \begin{cases} \dfrac{1}{1+5z/L} & z/L > 0 \\ \dfrac{1-24z/L}{1-16z/L} & z/L \le 0 \end{cases} \tag{G-65}$$

Equations (G-64) and (G-65) express the vertical profile of eddy diffusivity in terms of measured variables.

G.4.3 Analytical expression: Crosswind integrated scalar concentration distribution

The most common analytic expression for the cross-wind integrated scalar concentration distribution [$c_y(x,z)$] is a Gaussian plume model (van Ulden 1978, Horst and Weil 1992), given by:

$$c_y(x,z) = \frac{A}{\overline{u}(x)\overline{z}(x)}\exp\left[-\left(\frac{Bz}{\overline{z}(x)}\right)^r\right] \tag{G-66}$$

where *A, B,* and *r* are parameters. $\overline{u}(x)$ is the effective speed of plume advection along the streamwise wind vector, implicitly defined in (G-61), given explicitly by:

$$\overline{u}(x)=\frac{\int_0^\infty u(z)c_y(x,z)\,dz}{\int_0^\infty c_y(x,z)\,dz} \tag{G-67}$$

and $\overline{z}(x)$ is the effective height of plume advection along the wind stream, defined by:

$$\overline{z}(x)=\frac{\int_0^\infty zc_y(x,z)\,dz}{\int_0^\infty c_y(x,z)\,dz} \tag{G-68}$$

The remaining work is to find parameters of *A, B,* and *r,* and analytically express $\overline{u}(x)$ and $\overline{z}(x)$ in terms of measured variables.

Parameter estimation: *A* and *B*

Examination of equation (G-62) reveals that because $c(x,z)$ is the probability distribution of scalar concentration in two dimensions, we effectively have:

$$\int_0^\infty c_y(x,z)dz=\frac{1}{\overline{u}(x)} \tag{G-69}$$

which means:

$$A=\frac{\overline{z}(x)}{\int_0^\infty \exp\left[-\left(\frac{Bz}{\overline{z}(x)}\right)^r\right]dz}=\frac{B}{\int_0^\infty \exp\left[-\left(\frac{Bz}{\overline{z}(x)}\right)^r\right]d\left(\frac{Bz}{\overline{z}(x)}\right)}=\frac{B}{\frac{1}{r}\Gamma\left(\frac{1}{r}\right)} \tag{G-70}$$

The solution to parameter *B* is needed. Submitting (G-66) into (G-68) generates:

$$\overline{z}(x)=\frac{\int_0^\infty z\exp\left[-\left(\frac{Bz}{\overline{z}(x)}\right)^r\right]d\left(\frac{Bz}{\overline{z}(x)}\right)}{\int_0^\infty \exp\left[-\left(\frac{Bz}{\overline{z}(x)}\right)^r\right]d\left(\frac{Bz}{\overline{z}(x)}\right)} \tag{G-71}$$

Multiplying $B/\overline{z}(x)$ to both sides of this equation leads to:

$$B=\frac{\int_0^\infty \frac{Bz}{\overline{z}(x)}\exp\left[-\left(\frac{Bz}{\overline{z}(x)}\right)^r\right]d\left(\frac{Bz}{\overline{z}(x)}\right)}{\int_0^\infty \exp\left[-\left(\frac{Bz}{\overline{z}(x)}\right)^r\right]d\left(\frac{Bz}{\overline{z}(x)}\right)}=\frac{\Gamma\left(\frac{2}{r}\right)}{\Gamma\left(\frac{1}{r}\right)} \tag{G-72}$$

Equations (G-70) and (G-72) give:

$$A = \frac{r\Gamma\left(2/r\right)}{\left[\Gamma\left(1/r\right)\right]^2}$$

$$B = \frac{\Gamma\left(2/r\right)}{\Gamma\left(1/r\right)} \tag{G-73}$$

Parameter estimation: *r*
This parameter is a shape factor of the plume, given by van Ulden (1978):

$$r = 2 + m - n \tag{G-74}$$

where n is the power exponent of the vertical profile of eddy diffusivity [see (G-64) and (G-65)], and m is the exponent of the vertical profile of horizontal wind, given by:

$$u\left(z\right) = Uz^m \tag{G-75}$$

which depends on the surface layer stability, given by [page 16, Kaimal and Finnigan (1994)]:

$$m = \frac{z}{u\left(z\right)}\frac{du\left(z\right)}{dz} = \frac{u_*}{ku(z)}\phi_m\left(\frac{z}{L}\right) \tag{G-76}$$

where $\phi_m\left(z/L\right)$ is wind shear and given by:

$$\phi_m\left(\frac{z}{L}\right) = \begin{cases} 1 + 5z/L & z/L > 0 \\ \left(1 - 16z/L\right)^{-\frac{1}{4}} & z/L \le 0 \end{cases} \tag{G-77}$$

The other parameter U in (G-75) is a wind constant and can be calculated using measured $\overline{u}\left(z\right)$ and calculated m:

$$U = \frac{u\left(z\right)}{z^m} = \frac{\sqrt{\overline{u}_x(z) + \overline{u}_y(z)}}{z^m} \tag{G-78}$$

Analytical expression: Effective height of plume advection [$\overline{z}(x)$]
Examining (G-71) reveals that the numerator can be analytically evaluated only if the term $B/\overline{z}(x)$ is multiplied to both sides of the equation. As a result, it becomes a Gamma function; therefore, the effective speed of plume advection cannot be analytically expressed in terms of measured variables using its definition in (G-68). Alternatively, differentiating both sides of (G-68) with respect to x generates:

$$\frac{d\bar{z}(x)}{dx} = \frac{\int_0^\infty z\frac{\partial c_y(x,z)}{\partial x}dz}{\int_0^\infty c_y(x,z)dz} - \frac{\int_0^\infty z c_y(x,z)dz}{\int_0^\infty c_y(x,z)dz}\frac{\int_0^\infty \frac{\partial c_y(x,z)}{\partial x}dz}{\int_0^\infty c_y(x,z)dz}$$

$$= \frac{\int_0^\infty [z-\bar{z}(x)]\frac{\partial c_y(x,z)}{\partial x}dz}{\int_0^\infty c_y(x,z)dz} \qquad \text{(G-79)}$$

Neglecting the stream-wise eddy diffusion, the change in concentration along the wind direction (derivative term) must cause a change in flux due to the continuity in air mass (van Ulden 1978, Horst and Weil 1992), given by:

$$u(z)\frac{\partial c_y(x,z)}{\partial x} = -\frac{\partial}{\partial z}\left[-K(z)\frac{\partial c_y(x,z)}{\partial z}\right] \qquad \text{(G-80)}$$

Submitting (G-64) and (G-75) into this equation generates:

$$\frac{\partial c_y(x,z)}{\partial x} = \frac{k}{U}z^{-m}\frac{\partial}{\partial z}\left[z^n\frac{\partial c_y(x,z)}{\partial z}\right] \qquad \text{(G-81)}$$

Submitting this equation into (G-79) generates:

$$\frac{d\bar{z}(x)}{dx} = \frac{k}{U}\frac{1}{\int_0^\infty c_y(x,z)dz}\left[\int_0^\infty z^{1-m}\frac{\partial}{\partial z}z^n\frac{\partial c_y(x,z)}{\partial z}dz - \bar{z}(x)\int_0^\infty z^{-m}\frac{\partial}{\partial z}z^n\frac{\partial c_y(x,z)}{\partial z}dz\right] \qquad \text{(G-82)}$$

The equation can then be evaluated by substituting (G-66) into the three integration terms on the right-hand side. Performing these three substitutions at once becomes overly complex, so substitution and simplication of each integral term is presented separately here:

Integration term in the denominator

$$\int_0^\infty c_y(x,z)dz = \frac{A}{\bar{z}(x)\bar{u}(x)}\int_0^\infty \exp\left[-\left(\frac{Bz}{\bar{z}(x)}\right)^r\right]dz = \frac{A}{Br\bar{u}(x)}\Gamma\left(\frac{1}{r}\right) \qquad \text{(G-83)}$$

The first integration term in the numerator

Assuming that the gradient of scalar concentration at the surface ($z = 0$) and beyond the top of boundary-layer ($z \to \infty$) is zero and the concentration beyond the top of boundary-layer is zero, this integration can be evaluated as follows:

$$\int_0^\infty z^{1-m}\frac{\partial}{\partial z}z^n\frac{\partial c_y(x,z)}{\partial z}dz = z^{1-m+n}\frac{\partial c_y(x,z)}{\partial z}\bigg|_0^\infty - \int_0^\infty z^n\frac{\partial c_y(x,z)}{\partial z}d\,z^{1-m}$$

$$= -(1-m)\left[z^{n-m}c_y(x,z)\big|_0^\infty - \int_0^\infty c_y(x,z)\,dz^{n-m}\right]$$

$$= (1-m)(n-m)\int_0^\infty z^{n-m-1}\frac{A}{\overline{z}(x)\overline{u}(x)}\exp\left[-\left(\frac{Bz}{\overline{z}(x)}\right)^r\right]dz$$

$$= \frac{A(1-m)(n-m)\overline{z}^{n-m-1}(x)}{B^{n-m}\overline{u}(x)}\int_0^\infty\left(\frac{Bz}{\overline{z}(x)}\right)^{n-m-1}\exp\left[-\left(\frac{Bz}{\overline{z}(x)}\right)^r\right]d\left(\frac{Bz}{\overline{z}(x)}\right)$$

$$= \frac{A(1-m)(n-m)\overline{z}^{n-m-1}(x)}{rB^{n-m}\overline{u}(x)}\Gamma\left(\frac{n-m}{r}\right)$$

$$= \frac{A(1-m)\overline{z}^{n-m-1}(x)}{B^{n-m}\overline{u}(x)}\Gamma\left(\frac{2}{r}\right) \qquad \text{(G-84)}$$

The second integration term in the numerator

Using the same derivation approach, the second integration terms in the numerator can be evaluated as:

$$\int_0^\infty z^{-m}\frac{\partial}{\partial z}z^n\frac{\partial c_y(x,z)}{\partial z}dz = z^{-m+n}\left.\frac{\partial c_y(x,z)}{\partial z}\right|_0^\infty - \int_0^\infty z^n\frac{\partial c_y(x,z)}{\partial z}d\,z^{-m}$$

$$= m\left[z^{n-m-1}c_y(x,z)\Big|_0^\infty - \int_0^\infty c_y(x,z)\,dz^{n-m-1}\right]$$

$$= -m(n-m-1)\int_0^\infty z^{n-m-2}\frac{A}{\overline{z}(x)\overline{u}(x)}\exp\left[-\left(\frac{Bz}{\overline{z}(x)}\right)^r\right]dz$$

$$= -\frac{Am(n-m-1)\overline{z}^{n-m-2}(x)}{B^{n-m-1}\overline{u}(x)}\int_0^\infty\left(\frac{Bz}{\overline{z}(x)}\right)^{n-m-2}\exp\left[-\left(\frac{Bz}{\overline{z}(x)}\right)^r\right]d\left(\frac{Bz}{\overline{z}(x)}\right)$$

$$= -\frac{Am(n-m-1)\overline{z}^{n-m-2}(x)}{rB^{n-m-1}\overline{u}(x)}\Gamma\left(\frac{n-m-1}{r}\right)$$

$$= -\frac{Am\overline{z}^{n-m-2}(x)}{B^{n-m}\overline{u}(x)}B\Gamma\left(\frac{1}{r}\right) \qquad \text{(G-85)}$$

$$= -\frac{Am\overline{z}^{n-m-2}(x)}{B^{n-m}\overline{u}(x)}\Gamma\left(\frac{2}{r}\right)$$

Substituting the evaluated terms in (G-83), (G-84), and (G-85) into (G-82) expresses the derivative of the effective height with respective to x as a fundamental differential equation:

$$\frac{d\overline{z}(x)}{dx} = \frac{\kappa}{U}\frac{1}{\frac{A}{Br\overline{u}(x)}\Gamma\left(\frac{1}{r}\right)}\left\{\frac{A(1-m)\overline{z}^{n-m-1}(x)}{B^{n-m}\overline{u}(x)}\Gamma\left(\frac{2}{r}\right) - \overline{z}(x)\left[-\frac{Am\overline{z}^{n-m-2}(x)}{B^{n-m}\overline{u}(x)}\Gamma\left(\frac{2}{r}\right)\right]\right\}$$

$$= \frac{\kappa}{U}rB\frac{\Gamma\left(\frac{2}{r}\right)}{\Gamma\left(\frac{1}{r}\right)}\frac{\overline{z}^{n-m-1}(x)}{B^{n-m}}$$

$$= \frac{\kappa}{U}rB^2\frac{\overline{z}^{n-m-1}(x)}{B^{n-m}} \qquad \text{(G-86)}$$

$$= \frac{\kappa}{U}rB^{2+m-n}\overline{z}^{1-(2+m-n)}(x)$$

$$= \frac{\kappa}{U}rB^{r}\overline{z}^{1-r}(x)$$

This fundamental equation can be written as:

$$\int r\overline{z}^{r-1}(x)\,d\overline{z}(x) = \frac{\kappa}{U}r^2B^r\int dx \qquad \text{(G-87)}$$

therefore:

$$\overline{z}(x) = B\left(\frac{\kappa r^2}{U}x\right)^{\frac{1}{r}} \qquad \text{(G-88)}$$

Analytical expression: Effective speed of plume advection [$\overline{u}(x)$]

Substituting (G-75) into (G-67) gives:

$$\overline{u}(x) = \frac{U\int_0^\infty z^m c_y(x,z)\,dz}{\int_0^\infty c_y(x,z)\,dz} \qquad \text{(G-89)}$$

The denominator was evaluated in (G-83) and the integration term in the numerator can be evaluated as:

$$\int_0^\infty z^m c_y(x,z)dz = \int_0^\infty z^m \frac{A}{\overline{z}(x)\overline{u}(x)} \exp\left[-\left(\frac{Bz}{\overline{z}(x)}\right)^r\right] dz$$

$$= \frac{A\overline{z}^m(x)}{B^{m+1}\overline{u}(x)} \int_0^\infty \left(\frac{Bz}{\overline{z}(x)}\right)^m \exp\left[-\left(\frac{Bz}{\overline{z}(x)}\right)^r\right] d\left(\frac{Bz}{\overline{z}(x)}\right) \quad \text{(G-90)}$$

$$= \frac{A\overline{z}^m(x)}{rB^{n-m}\overline{u}(x)} \Gamma\left(\frac{m+1}{r}\right)$$

Substituting this equation along with (G-83) into (G-89) generates:

$$\overline{u}(x) = \frac{U\dfrac{A\overline{z}^m(x)}{rB^{m+1}\overline{u}(x)}\Gamma\left(\dfrac{m+1}{r}\right)}{\dfrac{A}{rB\overline{u}(x)}\Gamma\left(\dfrac{1}{r}\right)} = U\frac{\overline{z}^m(x)}{B^m}\frac{\Gamma\left(\dfrac{m+1}{r}\right)}{\Gamma\left(\dfrac{1}{r}\right)} \quad \text{(G-91)}$$

Substituting the analytical expression of effective height of plume advection [$\overline{z}(x)$] into this equation generates:

$$\overline{u}(x) = U\frac{\Gamma\left(\dfrac{m+1}{r}\right)}{\Gamma\left(\dfrac{1}{r}\right)}\left(\frac{\kappa r^2}{U}x\right)^{\frac{m}{r}} \quad \text{(G-92)}$$

By substituting the solved parameters of A and B (G-73), analytically expressed effective height of plume advection [$\overline{u}(x)$, see (G-88)], and analytical expressed effective speed of plume advection [$\overline{z}(x)$, see (G-92)] into (G-66), finally, the cross-wind integrated scalar concentration distribution can be analytically expressed in terms of spatial variables (x and z), the constant in the power-law profile of the eddy diffusivity (κ), and calculated variables from measurements (m, n, and U). That is:

$$c_y(x,z) = \frac{r\dfrac{\Gamma(2/r)}{\Gamma^2(1/r)}}{U\dfrac{\Gamma[(m+1)/r]}{\Gamma(1/r)}\left(\dfrac{\kappa r^2}{U}x\right)^{\frac{m}{r}} B\left(\dfrac{\kappa r^2}{U}x\right)^{\frac{1}{r}}} \exp\left[-\left(\frac{Bz}{B\left(\dfrac{\kappa r^2}{U}x\right)^{\frac{1}{r}}}\right)^r\right]$$

$$= \frac{r}{U\Gamma[(m+1)/r]}\left(\frac{U}{\kappa r^2 x}\right)^{\frac{m+1}{r}} \exp\left[-\frac{Uz^r}{\kappa r^2 x}\right] \quad \text{(G-93)}$$

More succinctly, given that:

$$\xi = \frac{U}{\kappa r^2}$$

$$\mu = \frac{m+1}{r} \quad \text{(G-94)}$$

the cross-wind integrated scalar concentration distribution, in an analytical form, can be presented as:

$$c_y(x,z) = \frac{r}{U\Gamma(\mu)}\left(\xi\frac{1}{x}\right)^{\mu} \exp\left[-\xi\frac{z^r}{x}\right]$$

Examining equation (G-63) reveals that the cross-wind integrated footprint can be thus derived as:

$$f_y(x,z) = -K(z)\frac{dc_y(x,z)}{dz}$$

$$= -\kappa z^n \frac{r}{U\Gamma(\mu)}\left(\xi\frac{1}{x}\right)\exp\left(-\xi\frac{z^r}{x}\right)\left(-\xi\frac{rz^{r-1}}{x}\right) \quad \text{(G-95)}$$

$$= \frac{1}{\Gamma(\mu)}\xi^{\mu}\left(\frac{z^{m+1}}{x^{\mu+1}}\right)\exp\left(-\xi\frac{z^r}{x}\right)$$

G.5 Upwind Locations at Inflection Points of Footprint in Kormann and Meixner (2001)

As described previously, integration segment boundaries should be determined by the upwind inflection points of the footprint. Since the footprint is known to be a bell-shaped function, there is one maximum point (x_{max}) and two inflection points (x_{IL} and x_{IR}) on both sides of the maximum, respectively. Accordingly,

x_{max} may be found by setting the first order derivative of the footprint function to zero. Similarly, x_{IL} and x_{IR} may be found by setting the second order derivative to zero. The following section shows derivations for these points.

G.5.1 Footprint Model

The cross-wind integrated footprint [$f_y(x, z)$] in Kormann and Meixner (2001) is given by:

$$f_y(x,z) = \frac{1}{\Gamma(\mu)} \xi^{\mu} \left(\frac{z^{m+1}}{x^{\mu+1}} \right) \exp\left(-\xi \frac{z^r}{x} \right) \tag{G-96}$$

where x is the upwind distance to the measurement station; z is measurement aerodynamic height; m is the exponent of the vertical profile of horizontal wind velocity; and r, μ, and ξ are composite variables, given by:

Shape factor:

$$r = 2 + m - n \tag{G-97}$$

where n the exponent of vertical profile of eddy diffusivity.

μ:

$$\mu = \frac{m+1}{r} \tag{G-98}$$

ξ:

$$\xi = \frac{U}{\kappa r^2} \tag{G-99}$$

where U is the wind constant.

G.5.2 Upwind Location of Maximum Footprint

Differentiating (G-96) with respect to x generates:

$$\frac{df_y(x,z)}{dx} = \frac{\xi^{\mu} z^{m+1}}{\Gamma(\mu)} \frac{d}{dx} \left[\frac{1}{x^{\mu+1}} \exp\left(-\xi \frac{z^r}{x} \right) \right] \tag{G-100}$$

$$= \frac{\xi^{\mu} z^{m+1}}{\Gamma(\mu)} \exp\left(-\xi \frac{z^r}{x} \right) \left[\frac{\xi z^r - x(\mu+1)}{x^{\mu+3}} \right]$$

The marginal stream-wise footprint [$f_y(x,z)$] is a bell-shape function with respect to x, with the maximum found at x_{max}, which follows that:

$$\left.\frac{df_y(x,z)}{dx}\right|_{x=x_{\max}} = 0 \tag{G-101}$$

All terms except for the term in the square bracket in (G-100) are greater than zero for any real-world case in the field, and therefore setting that term equal to zero results in the solution for x_{max}:

$$x_{\max} = \frac{\xi z^r}{\mu+1} \tag{G-102}$$

G.5.3 Upwind Location of Inflection Points in Footprint Curve

Differentiating both sides of (G-100) with respect to x generates:

$$\frac{d^2 f_y(x,z)}{dx^2} = \frac{\xi^\mu z^{m+1}}{\Gamma(\mu)} \frac{d}{dx}\left\{\exp\left(-\xi\frac{z^r}{x}\right)\left[\frac{\xi z^r - x(\mu+1)}{x^{\mu+3}}\right]\right\} \tag{G-103}$$

$$= \frac{\xi^\mu z^{m+1}}{\Gamma(\mu)} \exp\left(-\xi\frac{z^r}{x}\right)\left\{\xi\frac{z^r}{x^2}\left[\frac{\xi z^r - x(\mu+1)}{x^{\mu+3}}\right] - \frac{(\mu+3)\xi z^r}{x^{\mu+4}} + \frac{(\mu+1)(\mu+2)}{x^{\mu+3}}\right\}$$

Because the footprint is a bell-shaped function, it has two inflection points. One is to the left of x_{max} (x_{IL}), and the other is to the right of x_{max} (x_{IR}. Equation (G-103) must equal zero at the inflection points. In this equation, the term ahead of the curly bracket is never zero. Therefore we can simply set the terms in the curly brackets to zero to find the inflection points:

$$\xi\frac{z^r}{x^2}\left[\frac{\xi z^r - x(\mu+1)}{x^{\mu+3}}\right] - \frac{(\mu+3)\xi z^r}{x^{\mu+4}} + \frac{(\mu+1)(\mu+2)}{x^{\mu+3}} = 0 \tag{G-104}$$

Rearranging the terms in this equation yields:

$$\xi^2 z^{2r} - 2(\mu+2)\xi z^r x + (\mu+1)(\mu+2)x^2 = 0 \tag{G-105}$$

Solving the quadratic equation results in:

$$x = \frac{\xi z^r\left(\mu+2\pm\sqrt{\mu+2}\right)}{(\mu+1)(\mu+2)} \tag{G-106}$$

Substituting x_{max} [see equation (G-102)] into (G-106) and then taking the point to the left results in:

$$x_{IL} = x_{\max}\left(1-\frac{1}{\sqrt{\mu+2}}\right) \tag{G-107}$$

and taking the point to the right gives:

$$x_{IR} = x_{\max}\left(1 + \frac{1}{\sqrt{\mu + 2}}\right) \tag{G-108}$$

G.6 References

Gash J.H.K. 1986. A note on estimating the effect of a limited fetch on microclimate evaporation measurements. Boundary-Layer Meteorology 35: 409-413.

Hsieh, C.I., G. Katul, T.W. Chi. 2000. An approximation analytical model for footprint estimation of scalar fluxes in the thermal stratified atmospheric flows. Boundary-Layer Meteorology 35: 409-413.

Horst, T.W., J.C. Weil. 1992. Footprint estimation for scalar flux measurements in the atmospheric surface layer. Boundary-Layer Meteorology 59: 279-296.

Huang, C.H. 1979. A theory of dispersion in turbulent shear flow. Atmospheric Environment 13: 453-463.

Jarvis, P.G. G.B. James, J.J. Landsberg. 1976. Coniferous forest. In vegetation and the atmosphere, Vol 2, Monteith J.L. ed, Academic, London, pp 171-240.

Kaimal, J.C., J.J. Finnigan. 1994 Atmospheric Boundary Layer Flows: Their structure and Measurement. Oxford University Press, Oxford, p. 3-31.

Kljun, N, P. Calanca, M.W. Rotach, H.P. Schmid. 2004. A simple parameterization for flux footprint predictions. Advances in Water Resources 23: 765-772.

Kormann, R, F.X. Meixner. 2001. Analytical footprint model for non-neutral stratification. Boundary-Layer Meteorology 99: 207-224.

Nemes, G. 2010. New asymptotic expansion for the Gamma function. Archiv der Mathematik 95: 161–169

Raupach, M.R., R.A. Antonia, S. Rajagopalan. 1991. Rough-wall turbulent boundary layers. Appl Mech Rev. 44: 1-25.

Rosenberg, N.J., B.B. Blad, S.B. Verma. 1983. Microclimate: The Biological Environment, 2nd ed. John Wiley & Son, New York, p. 135.

Schmid, P.H. 1994. Source areas for scalar and scalar fluxes. Boundary-Layer Meteorol 67: 293-318.

Schuepp, P.H., M.Y. Leclerc, J.I. MacPherson, R.L. Desjardins. 1990. Footprint prediction of scalar from analytical solution of diffusion equation. Boundary-Layer Meteorol 50: 355-373.

Szeicz, G., G. Endrodi, S. Tajchman. 1969. Aerodynamic and surface factors in evaporation. Water Resource Research 5: 380-394.

Stanhill, G. 1969. A simple instrument for the field measurements of turbulent diffusion flux. J Appl Meteorol 8: 509.

Stull, R.B. 1988. An Introduction to Boundary Layer Meteorology. Kluwer Academic Publishers, Netherlands, 666p.

Tanner, C.B. W.L. Pelton. 1960. Potential evapotranspiration estimates by the approximate energy balance method of Penman. J Geophys Res 65:3391.

van Ulden A.P. 1978. Simple estimates for vertical diffusion from sources near the ground. Atmospheric Environment 12: 2125-2129.

Appendix H. Surface Energy Flux

Calculation of the soil surface heat flux is done only if all necessary measurements are available, which includes soil heat flux, soil temperature, and soil volumetric water content.

The soil surface heat flux, *G,* typically reported in units $W \cdot m^{-2}$, is found by summing the average soil heat flux measured at some depth and the change in heat storage in the layer of soil above that depth over some interval of time:

$$G = G_{Depth} + \Delta_{storage}$$

G_{Depth} in the program is found by averaging the heat flux measurements from soil heat flux plates over the averaging interval, e.g., 30 minutes. If there are multiple heat flux plates, an average of the temporal averages of each plate is used.

In the datalogger program calculation of the change in storage is done as follows:

$$\Delta_{storage} = \frac{\left[c_s \rho_s \left(T_{soil,f} - T_{soil,i}\right) + c_w \rho_w \left(T_{soil,f} q_{v,f} - T_{soil,i} q_{v,i}\right)\right] D}{\Delta t}$$

where:

c_s = the specific heat of dry mineral soil at the site in $J \cdot kg^{-1} \cdot K^{-1}$. This value is among the station configuration variables (see *C_dry_soil* in TABLE 4-1*)* entered by the user. If no value was entered, a default of 870 is used.

ρ_s = the soil bulk density at the site in $kg \cdot m^{-3}$ and is entered by the user (see *Bulk Density* in TABLE 4-1). If no value was entered, a default of 1300 is used.

$T_{soil,f}$ = the soil temperature averaged over the last minute of the current flux averaging interval.

$T_{soil,i}$ = the soil temperature averaged over the last minute of the previous flux averaging interval.

c_w = the specific heat of liquid water in $J \cdot kg^{-1} \cdot K^{-1}$. A value of 4210 is used, which is the specific heat of liquid water at 0 °C.

ρ_w = the density of liquid water in $kg \cdot m^{-3}$. A value of 1000 is used.

$q_{v,f}$ = the volumetric water content averaged over the last minute of the current flux averaging interval (e.g., 30 minutes).

$q_{v,i}$ = the volumetric water content averaged over the last minute of the previous flux averaging interval.

D = the depth in m below the surface at which the soil heat flux plates are buried and is entered by the user (see *HFP Depth* in TABLE 4-1). If no value was entered, a default of 0.08 is used.

Δt = the length of time of the flux averaging interval (e.g., 30 minutes.

NOTE TCAV and CS65X sensors both make soil temperature measurements. However, if they are both being used, the TCAV measurements will be used preferentially for $T_{soil,f}$ and $T_{soil,i}$, as the TCAV provides a greater spatial average.

NOTE The program supports either CS616s or CS65Xs for measurements of soil water content. It won't support both types of sensors at the same time.

NOTE If a CS616 is used, outputs for water content are corrected for temperature as detailed in the CS616 manual. The temperature measurement from the TCAV sensor assumed to be closest to the CS616 is used for this correction.

It is assumed that soil sensors are installed in a manner similar to that presented in the figure below. In many applications, the setup shown in the figure (two heat flux plates, one TCAV, and one CS616) is replicated for better spatial averaging at the site. Accordingly, the program supports up to four soil heat flux plates (HFP01 or HFP01SC), two soil temperature sensors (TCAV or CS65X), and two water content sensors (CS616 or CS65X).

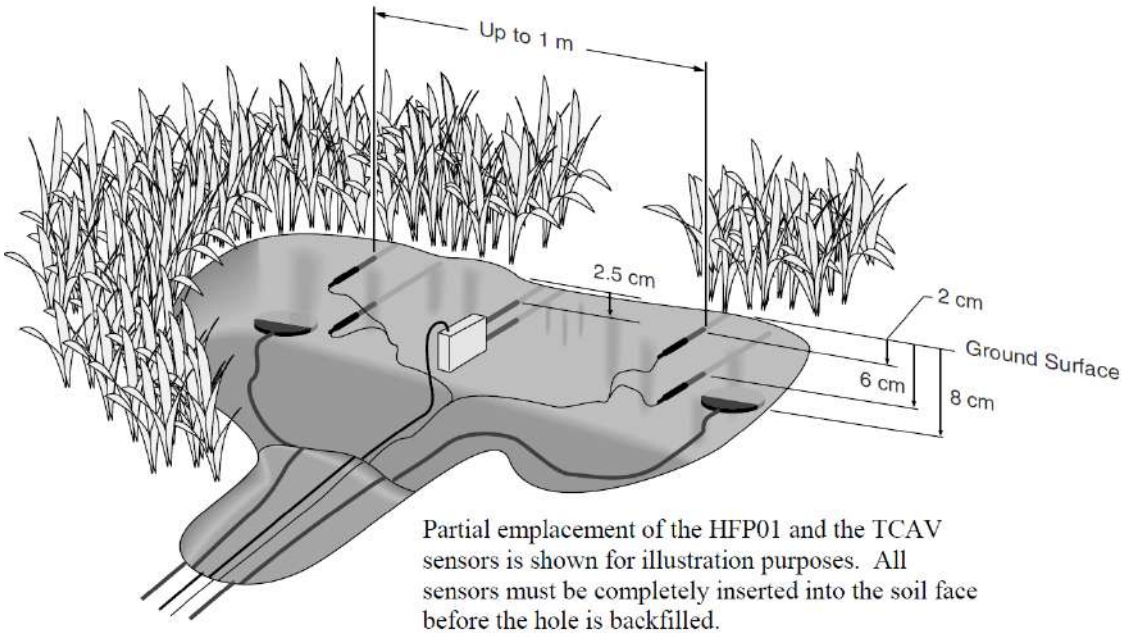

Partial emplacement of the HFP01 and the TCAV sensors is shown for illustration purposes. All sensors must be completely inserted into the soil face before the hole is backfilled.

Finally, if a measurement of average net radiation over the flux averaging interval is available, energy closure may be calculated as follows:

$$E_{closure} = \frac{LE + H}{R_n - G}$$

Where all variables are in $W \cdot m^{-2}$ and LE is latent heat flux, H is sensible heat flux, and R_n is net radiation.

Appendix I. EasyFlux DL Process Flow Diagram

Sequence of Program Functions

Every SCAN_INTERVAL (default 100 ms)

Collect raw data from gas analyzer, sonic anemometer, FW (if applicable), and panel temp

⇩

Align data, accounting for electronic delays

⇩

Parse out diagnostic flags from gas analyzer and sonic data

⇩

Calculate various variables (e.g., e, rho_d, rho_a, Td, CO2_mixratio, H2O_mixratio, RH)

⇩

Store raw data in multiple datasets, each dataset with a different lag applied to gas analyzer data relative to sonic data (to be used later in cross correlation; lags from -MAX_LAG to +MAX_LAG are used; MAX_LAG default is 2)

⇩

If using FW, store raw data in multiple datasets, each dataset with a different lag applied to FW data relative to sonic data (to be used later in cross correlation; lags from -MAX_LAG to +MAX_LAG are used; MAX_LAG default is 2)

⇩

Write a record to ts_data and diagnostic output tables

Every SLOWSEQUENCE_SCAN_INTERVAL (default 5 s)

Measure battery voltage

⇩

Measure biomet and energy balance (slow response) sensors

⇩

If station variables have changed, save new values to memory

Every 5 Minutes

Do coordinate rotations and find the 5-minute covariances for u with w, v with w, Ts with w, CO2 with w, and H2O with w (used later for steady state test for quality grading; see appendix F on Data Quality Grading).

Every AVERAGING_INTERVAL (default 30 minutes)

Filter out data with diagnostic flags or signal strengths or measurements outside of acceptable ranges, do coordinate rotations (use double coordinate rotation method unless planar fit angles have been entered by user), and recalculate all covariances with rotated wind components. (See Appendix B on Double Coordinate Rotation and Appendix C on Planar Fit Rotation.)

⇩

Use rotated wind components to find turbulent kinetic energy, friction velocity, and preliminary values of Obukhov length and stability

⇩

Calculate frequency correction factors for wTs, wu, and vw to account for block averaging and line averaging. If conditions are stable, iteratively calculate Obukhov length, cospectral equations, and correction factors until factors change by <0.0001 or until 10 iterations have completed. (See Appendix D on Frequency Corrections.)

⇩

Calculate value for steady state test using the 30-minute momentum covariances and the 5-minute momentum covariances. (see Appendix F on Data Quality Grading.)

⇩

Calculate the overall quality grade for momentum flux. (See Appendix F on Data Quality Grading.)

⇩

Calculate and use a new roughness length if 1) user didn't enter a fixed value, 2) there is neutral stability, and 3) wind speed is >3 m/s. (See Appendix G on Footprint.)

⇩

Calculate footprint characteristics using the Kljun et al (2004) model if conditions are appropriate, else use Kormann and Meixner (2001) model. (See Appendix G on Footprint.)

⇩

Calculate the covariance of CO2 and rotated wind components for each lagged dataset.

⇩

Find the effective lateral separation distance between gas analyzer and sonic (to use in frequency correction) and the effective separation scan lag (used to constrain which lagged datasets are physically possible). (See Appendix D on Frequency Corrections.)

⇩

Find the dataset with the physically possible lag that maximizes the covariance of CO2 and vertical wind. Use this dataset for the FLUX output table. If any results are invalid, continue with lag of zero. (See Appendix D on Frequency Corrections.)

⇩

Assume the same lag found for CO2 will also maximize covariance of H2O and vertical wind. Calculate covariances of appropriately lagged H2O and rotated wind components.

⇩

Calculate cospectra functions and frequency correction factors for covariances of CO2 and rotated wind components, taking into account attenuation from block averaging, line averaging, and spatial separation. (See Appendix D on Frequency Corrections.)

⇩

Calculate cospectra functions and frequency correction factors for covariances of H2O and rotated wind components, taking into account attenuation from block averaging, line averaging, and spatial separation. (See Appendix D on Frequency Corrections.)

⇩

Calculate final momentum flux from rotated and frequency corrected covariances of u with w and v with w.

⇩

Apply SND correction to the rotated and frequency corrected covariance of w and Ts.

⇩

Calculate specific heat of ambient (moist) air and calculate final sensible heat flux.

⇩

Calculate scaling temperature (used for data quality grading). (See Appendix F on Data Quality Grading.)

⇩

Apply WPL correction to rotated and frequency corrected covariance of CO2 and vertical wind for final CO2 flux. (See Appendix E on WPL correction.)

⇩

Apply WPL correction to rotated and frequency corrected covariance of H2O and vertical wind. Then multiply result by calculated latent heat of vaporization for final latent heat flux. (See Appendix E on WPL correction.)

⇩

Calculate Bowen Ratio

⇩

Calculate the overall quality grades for fluxes of sensible heat, latent heat, and CO2. (See Appendix F on Data Quality Grading.)

⇩

If FW05, FW1, or FW3 is used

Calculate the covariance of FW temperature and rotated wind components for each lagged dataset.

⇩

Find the effective lateral separation distance between FW and sonic (to use in frequency correction) and the effective separation scan lag (used to constrain which lagged datasets are physically possible). (See Appendix D on Frequency Corrections.)

⇩

Find the dataset with the lag that maximizes the covariance of FW temperature and vertical wind. Use this dataset for the FLUX output table. If any results are invalid, continue with lag of zero.

⇩

Calculate the time constant for the FW (to be used in frequency corrections). (See Appendix D on Frequency Corrections.)

⇩

Calculate frequency correction factors for covariances of FW temperature and rotated wind components, taking into account attenuation from block averaging, line averaging, spatial separation, and the FW time constant. (See Appendix D on Frequency Corrections.)

⇩

Calculate final fine-wire sensible heat flux

⇩

If energy balance sensors are used

Calculate soil surface energy flux. (See Appendix H on Surface Flux.)

⇩

Calculate energy closure

⇩

Write a record to the Flux and Flux_Notes output tables

Campbell Scientific Worldwide Offices

Australia
Location: Garbutt, QLD Australia
Email: *info@campbellsci.com.au*
Website: *www.campbellsci.com.au*

Brazil
Location: São Paulo, SP Brazil
Email: *andread@campbellsci.com.br*
Website: *www.campbellsci.com.br*

Canada
Location: Edmonton, AB Canada
Email: *dataloggers@campbellsci.ca*
Website: *www.campbellsci.ca*

China
Location: Beijing, P. R. China
Email: *info@campbellsci.com.cn*
Website: *www.campbellsci.com.cn*

Costa Rica
Location: San José, Costa Rica
Email: *info@campbellsci.cc*
Website: *www.campbellsci.cc*

France
Location: Antony, France
Email: *info@campbellsci.fr*
Website: *www.campbellsci.fr*

Germany
Location: Bremen, Germany
Email: *info@campbellsci.de*
Website: *www.campbellsci.de*

South Africa
Location: Stellenbosch, South Africa
Email: *sales@csafrica.co.za*
Website: *www.campbellscientific.co.za*

Southeast Asia
Location: Bangkok, Thailand
Email: *info@campbellsci.asia*
Website: *www.campbellsci.asia*

Spain
Location: Barcelona, Spain
Email: *info@campbellsci.es*
Website: *www.campbellsci.es*

UK
Location: Shepshed, Loughborough, UK
Email: *sales@campbellsci.co.uk*
Website: *www.campbellsci.co.uk*

USA
Location: Logan, UT USA
Email: *info@campbellsci.com*
Website: *www.campbellsci.com*

Please visit *www.campbellsci.com/contact* to obtain contact information for your local US or international representative.